7-1983

Modeling Surface and Subsurface Stormflow on Steeply-Sloping Forested Watersheds

Digital Object Identifier: https://doi.org/10.13023/kwrri.rr.142

Patrick G. Sloan
University of Kentucky

Ian D. Moore
University of Kentucky

George B. Coltharp
University of Kentucky

Joseph D. Eigel
University of Kentucky

Research Report No. 142

MODELING SURFACE AND SUBSURFACE STORMFLOW ON STEEPLY-SLOPING FORESTED WATERSHEDS

By

Patrick G. Sloan
Research Assistant

Ian D. Moore
Principal Investigator

George B. Coltharp
Co-Investigator

Joseph D. Eigel
Agricultural Engineer

Project Number: A-085-KY (Completion Report)

Agreement Numbers: 14-34-0001-1119 (FY 1981)
14-34-0001-2119 (FY 1982)

Period of Project: October 1980 - March 1983

Water Resources Research Institute
University of Kentucky
Lexington, Kentucky

The work upon which this report is based was supported in part by funds provided by the United States Department of the Interior, Washington, D.C., as authorized by the Water Research and Development Act of 1978. Public Law 95-467.

July 1983

DISCLAIMER

The contents of this report do not necessarily reflect the views and policies of the United States Department of the Interior, Washington, D.C., nor does mention of trade names or commercial products constitute their endorsement or recommendation for use by the U.S. Government.

ABSTRACT

A simple conceptual rainfall-runoff model, based on the variable source area concept, was developed for predicting runoff from small, steep-sloped, forested Appalachian watersheds. Tests of the model showed that the predicted and observed daily discharges were in good agreement. The results demonstrate the ability of the model to simulate the "flashy" hydrologic behavior of these watersheds.

Five subsurface flow models were evaluated by application to existing data measured at Coweeta on a reconstructed homogeneous forest soil. The five models were: Nieber's 2-D and 1-D finite element models (based on Richards' equation), the kinematic wave equation, and two simple storage models developed by the authors, the Boussinesq and kinematic storage models. All five models performed reasonably well on this homogeneous soil. The coupled infiltration model had a large effect on the simulation results. The cost of running the computer models and the computer memory requirements increased as their complexity increased.

Field soil-water and precipitation measurements were made on a small test plot in Robinson Forest, in Eastern Kentucky. These data were used to calculate runoff during four precipitation events and to test three of the subsurface flow models on a natural watershed. Of the models tested, the simple kinematic storage model performed the best. Flow from the test plot was dominated by macropore flow during storm events, and by flow through the soil matrix during baseflow or recession periods. No surface runoff was observed on the test plot during the period of field observations, except on the saturated near-channel source areas; all runoff was initiated by subsurface flow.

Descriptors: Forest watershed*; forest hydrology; mathematical models; model testing; subsurface flow*; subsurface water; runoff.

Identifiers: Macropore flow; stormflow; steeply-sloping forested watersheds; watershed models; process models.

ACKNOWLEDGMENTS

The authors wish to extend their sincere appreciation to the following:

Mr. W. Smith for his assistance in conducting the seismic survey of the test plot.

Mr. C. Shaw and Mr. G. Mohammad for their assistance in collecting the research data.

Dr. B. J. Barfield for reviewing the manuscript.

Ms. N. Rotter for the excellent job she has done in typing this manuscript under very short time constraints.

Mr. J. Weber and Mr. R. White for preparing the figures and diagrams.

Appreciation is also expressed to the University of Kentucky Computing Center and the College of Agriculture Computing Center for processing the computer runs. Thanks is also expressed to the College of Agriculture for providing supplementary financial support for this project.

TABLE OF CONTENTS

Table of Contents (Continued) Page

Table of Contents (Continued) Page

Table of Contents (Continued) **Page**

LIST OF TABLES

LIST OF FIGURES

List of Figures (Continued) **Page**

List of Figures (Continued) **Page**

List of Figures (Continued) **Page**

List of Figures (Continued) **Page**

List of Figures (Continued) **Page**

CHAPTER 1

INTRODUCTION

The hydrologic response of a watershed is dependent on many highly interrelated and complex factors. The major components of the hydrologic cycle are precipitation inputs, evapotranspiration, interception, surface storage, infiltration, surface runoff, subsurface flow and groundwater discharge, and total water yield or streamflow. Land use changes which may influence one or more of these components on a given watershed could have significant impacts on the hydrologic environment at the watershed outlet and at points downstream. Before the effects of land use changes can be modeled, the governing flow processes on natural undisturbed watersheds must be well understood. The hydrologic processes that occur on steep-sloped forested watersheds are generally less well defined (quantitatively) that those occurring on milder slopes such as in agricultural and urban areas.

Steeply sloping forested watersheds, such as those found in the Appalachian region of eastern Kentucky, are important sources of wood fiber products and coal. The latter is becoming more and more important as an energy source. There is a growing awareness of the need to protect the quality of the environment and this is reflected in part by Public Law 95-87, the Surface Mine Reclamation Act of 1977. This legislation requires a hydrologic study on all areas to be surface mined. Furthermore, it recognizes that a sound understanding of the hydrologic balance of affected watersheds is required and recognizes that this balance should be modified as little as possible so as not to damage the fragile ecosystem. Though not subjected to the same legislative control, the forestry industry should, and for the most part does, operate under the same general principles. The hydrologic effects of clear-cut logging are especially important in this case. Of all forestry practices, clear-cut logging has perhaps the greatest potential for harming the hydrologic environment. With knowledge of hillslope hydrology so poorly developed,

it is doubtful whether physically accurate hydrologic (and hence environmental studies) can be performed at this time. The focus of this report is to examine quantitative methods of describing the hydrologic response of steep-sloped forested watersheds in the Appalachian region.

The Hortonian concept of infiltration and runoff (Horton, 1933) has traditionally been used to predict storm runoff. The essence of this widely used concept is that storm runoff is rainfall that has not penetrated the soil and baseflow is produced by seepage from the water table. It is represented in mathematical terms as

$$R = P - I - E \qquad \ldots (1)$$

where R is runoff, P is precipitation, I is infiltration, and E is evaporation.

Precipitation and evaporation can be measured with limited accuracy, but estimates of infiltration are often subjective because of the variability of infiltration characteristics over even small areas. However, the major drawback to the concept is that it does not allow for lateral saturated/unsaturated subsurface flow (Zaslavsky and Sinai, 1981). When using the Hortonian concept in areas other than agricultural lands or urban areas, where it may be most accurate conceptually, gross errors can result in predicting runoff.

Lateral subsurface flow has often been observed in field studies on steep-sloped forested watersheds (Mosley, 1979; Kirkby and Chorley, 1967; Whipkey, 1965; Dunne and Black, 1970; and others). It has also been recognized that the various runoff processes have greater heterogeneity than originally believed. The variable source area concept has evolved as a result, being first proposed by Hewlett (1961).

The specific objectives of this project were:

(1) To identify the major mechanisms of stormflow on steeply sloping watersheds, characteristic of eastern Kentucky, and quantify the principal components.

(2) To test and develop computer-based models for predicting stormflow on steeply-sloping forested watersheds. Two types of models were examined: (a) daily-based continuous simulation models of an entire watershed's hydrologic response; and (b) event process models of hillslope hydrologic response.

Chapter 2 presents a review of the literature dealing with runoff processes (qualitative) and runoff models (qualitative). Field studies were conducted on a steep-sloped watershed and a test plot in Robinson Forest, Eastern Kentucky, to determine what runoff processes are dominant on these types of watersheds. The watersheds and the field studies are described in Chapter 3. These studies provided the precipitation and runoff records for developing and testing the daily-based continuous-simulation and the event process models.

A simple conceptual, lumped-parameter, continuous, daily-based, rainfall-runoff model, based on the variable source area concept, was developed and tested using $6\frac{1}{2}$ years of record from the Little Millseat watershed in Robinson Forest. The model is briefly described in Chapter 4, together with the testing and evaluation procedures and results.

Existing field data, measured at the Coweeta Experimental Station by Hewlett (1961) and Hewlett and Hibbert (1963), were used to compare existing subsurface flow process models. The models tested include a two-dimensional finite element saturated-unsaturated flow model (Nieber, 1979; Nieber and Walter, 1981), a one-dimensional finite element saturated-unsaturated stormflow model (Beven, 1981, 1982). Two simplified storage models were also developed and compared, using the Coweeta data. These results are presented in Chapter 5.

Chapter 6 presents the analysis of the test plot data (instrumentation described in Chapter 3) and the method of calculating the runoff using a hydrologic water balance approach. This chapter also presents the results of the comparison of three of the subsurface flow models using the instrumented test plot data. Finally, Chapter 7 presents the conclusions stemming from this study.

CHAPTER 2
LITERATURE REVIEW

2.1 MECHANISMS OF RUNOFF GENERATION

Knowledge of the processes involved in runoff generation and the conversion of rainfall to stream flow has slowly evolved since Horton first identified the relationship between infiltration and overland flow in 1933 (Horton, 1933). We now understand that Horton's infiltration theory of surface runoff represents one extreme of the spectrum of processes involved. Hursch (1936) identified the other extreme as subsurface stormflow. Since that time many field studies have been conducted where both of these extremes were observed individually and in combination to varying degrees.

The classical description of the runoff process was first proposed by Horton (1933) with his infiltration theory. It was assumed that infiltration occurred uniformly throughout a watershed. During a precipitation event the infiltrability decreases (as the soil saturates from above) until the rainfall intensity exceeds the infiltrability at which time surface runoff begins in the form of overland flow. This rainfall excess, the water that does not infiltrate, was thought to produce overland flow over the entire watershed at once. It was believed that only overland flow exhibits the quick response times necessary to generate stormflow and that infiltrated water becomes the source of long-term baseflow. Therefore, in the Horton conceptualization of the runoff process all storm flow is water that never infiltrates the soil. The concept has persisted, been modified, and incorporated into many sophisticated computer models such as the Stanford Watershed Model IV (Crawford and Linsley, 1966). It is easy to visualize and use, especially if the unit hydrograph method is used for predicting the timing of runoff (Sherman, 1932). Overland flow due to surface saturation from above does occur as Horton found, but the concept has been widely misused. Some examples of areas of occurrence are unvegetated surfaces, deserts, farm lands, urban areas, and areas exhibiting low infiltrabilities. Application

to steep-sloped forested watersheds in humid climates is often inappropriate since observance of overland flow in these areas is extremely rare (Mosley, 1979; Kirkby and Chorley, 1967; Whipkey, 1965).

Realization that overland flow does not occur uniformly over a watershed as originally thought brought about the development of the partial source area concept and the variable source area concept. The partial source area concept has been widely supported by field studies including those by Betson and Marius (1969), Dunne and Black (1970), and Corbett (1979). A source area is that part of the watershed where precipitation is converted to runoff. The process may be by saturation from above as Horton envisioned or saturation from below as the water table rises to the soil surface (Dunne and Black, 1970; and Pilgrim et al., 1978). These areas are often near the stream channel and quickly become saturated during a rainfall event. They may also be wetlands with shallow water tables that rise as they are fed by infiltration and/or subsurface flow from upslope areas. Being adjacent to the channel, the time lag is very short for overland flow (Freeze, 1972; Hewlett and Hibbert, 1967). Freeze (1972) found topography and the physical configuration of the basin to be important for the development of near channel source areas. Betson and Marius (1969) found that the depth of the soil surface is important in the generation of stormflow and that source areas do not necessarily have to be adjacent to the stream. In their studies they found source areas in places where the upper soil horizon was thin and the lower horizon had a significantly lower permeability. They also found a more heterogeneous runoff pattern than had previously been reported and upslope source area runoff did not always reach the channel because deeper soils downslope absorbed the water.

The field study of Dunne and Black (1970) provided evidence of the partial source area concept. One of their study areas had well drained slopes and poorly drained soils at the base of these slopes. They found significant runoff occurred only from the small wet

area at the base of the slope. Its low storage capacity was quickly filled, the water table intersected the surface and then the partial source area behaved as an impervious area. The runoff was very sensitive to rainfall, which confirmed their other observations. The rest of the watershed seemed to maintain the wet area which only dried up in the summer. Under most rainfall and natural antecedent conditions, the runoff hydrograph was controlled by precipitation that fell on the channel and wet areas along the stream. For these areas the conversion of rainfall to runoff was almost 100%. They were also extremely sensitive to rainfall intensity fluctuations.

In the early 1960s, Hewlett (1961) conducted a number of field studies at Coweeta and was the first to propose the concept of dynamic watershed source areas (i.e. variable source areas), which he believed had important implications on headwater hydrology. As he studied the drainage of water downslope in soil troughs, moisture gradients were observed that increased downslope, as shown in Figure 2.1. It was proposed that rain falling after drainage had set up these hydraulic gradients quickly satisfied the soil water deficits near the channel, saturating the soil, and thus set up conditions for stormflow generation. The deficits upslope would take longer to satisfy, but as rainfall continued the contributing area would expand. His concept was that stormflow is generated from precipitation over saturated areas which begin to contribute as deficits are satisfied. Upslope rain subsequently recharges the soil for sustained base flow and the maintenance of the channel wet areas.

When soil moisture levels are high and the water table is close to the surface, only a small input is needed for the relaxation of tension in the soil pores and the rapid rise of the water table. The rate of runoff to the channel then accelerates for several reasons. The saturated thickness of soil is thicker allowing greater subsurface flow. As the water table rises the zone of saturation moves upward into the loose permeable surface layer which may be highly structured

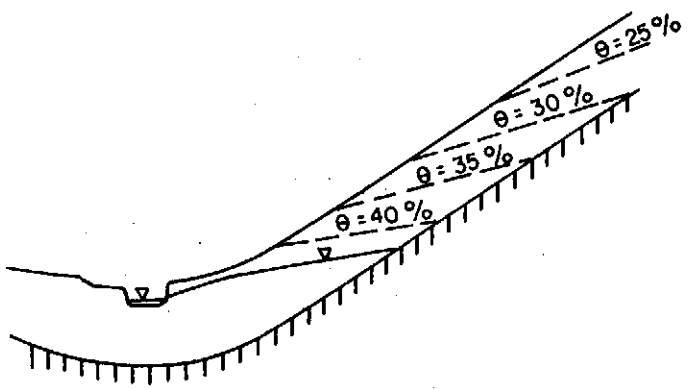

Figure 2.1 Idealized Water Content Distribution on a Hillslope After Drainage

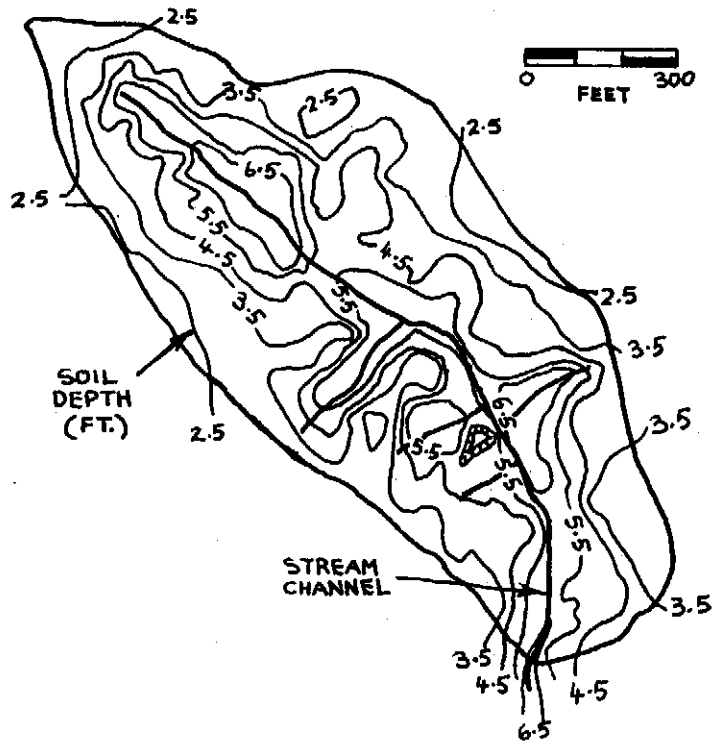

Figure 2.2 Measured Soil Depths (in feet) on a Small Forested Watershed in Pennsylvania with an Average Slope of 36% (from Corbett, 1979).

by biological activity. Seepage in this highly structured layer occurs at higher velocities and may even approach turbulent flow. Finally, if the precipitation input is great enough, the water table will rise to the surface and overland flow will occur.

Dunne and Black (1970) also applied artificial storms of high return periods to their watersheds. Similar mechnaisms to those in the natural storms were observed. In one test, rain was applied only to the channel area and a hydrograph similar to natural storms was observed. As the durations were increased the source areas expanded. In the watershed which contained the wet area, the source area expanded when a perch water table developed in the A horizon and rose to the surface. It was not able to extend very far up the steep slopes, but additional water was contributed by water returning to the surface. They concluded that the response of the variable source areas depends on the season and proposed an antecedent precipitation index to predict response.

Corbett (1979) studied a small forested watershed in Pennsylvania with an average slope of 36% and soil depths varying from 0.45 to 2.55 m. After extensive experimentation with the application of artificial rainfall, he concluded that the variable source area concept provided the best framework with which to evaluate the watershed's response. The front portion of the watershed had shallow soils draining to the channel while the back portion had to drain through deep soils to reach the stream (Figure 2.2). He observed a delay between the response of the front and back halves of the watershed. For dry antecedent moisture conditions he observed that the rising limb and the peak of the hydrograph were produced by contributions from precipitation on the channel and the base of the slope only. The lower and middle slopes provided the major portion of runoff during the recession. For a 4.88 cm storm the conversion efficiency of rainfall to runoff was 19% for the channel zone, 9% for the base slope and 4.4% for the middle and upper slopes.

For wet antecedent moisture conditions Corbett (1979) observed

peak flow rates two to three times greater than those for the dry antecedent conditions and a substantial increase in the amount of rainfall converted to quick and delayed flow. Temporary zones of saturation developed during the storm and the development of these areas had an important bearing on how efficiently a particular area responded to rainfall. The saturated zone developed within the soil profile and there was not a general rise of the water table. Surface runoff did not occur on the side slopes and Corbett considered saturated overland flow to be only a minor contributor even in wet conditions. Under dry antecedent conditions direct surface runoff was practically nonexistent.

2.2 SUBSURFACE STORMFLOW

Subsurface stormflow (i.e. quick response interflow) can be distinguished from true groundwater flow in that it enters the stream before reaching the groundwater zone (Whipkey, 1965). Over the range of antecedent moisture conditions tested, Corbett (1979) estimated that subsurface stormflow provided 75 to 97% of the stormflow volume. Saturated overland flow was a minor factor under wet conditions and practically nonexistent for dry conditions. For dry antecedent conditions the peak was produced by channel precipitation and precipitation at the base of the slope adjacent to the stream. With wet antecedent conditions a temporary zone of saturation built up and travelled as a wave with the crest discharging into the channel to produce the hydrograph peak. Of all the variables investigated, the antecedent flow rate had the greatest correlation with quickflow. It is probably the best overall indicator of the extent of the saturated variable source areas. Tischerdorf (1969) observed similar mechanisms in his study of an Appalachian watershed in Georgia. The upper soil zone (0.9 to 1.2 m) responded to rainfall quite rapidly (which is discussed later).

Undisturbed forest soils are likely places to look for subsurface stormflow. The organic litter protects the mineral soil and maintains high surface permeabilities that promote high percolation rates

to the A and B horizons. The upper soil profile can be interlaced with roots, decayed root holes, animal burrows, worm holes, and structural channels (i.e. macropores) making a highly permeable medium for the rapid movement of water in all directions (Figure 2.3). When a relatively impermeable layer is reached percolating water moves laterally towards the stream (Mosley, 1979; Pilgrim et al., 1978; Weyman, 1970, 1973; Whipkey, 1965, 1967; Corbett, 1979). Water can therefore move in the subsurface regime by moving either through the soil matrix, or through macropores in the soil profile. The rates of water movement through these two zones are likely to be vastly different.

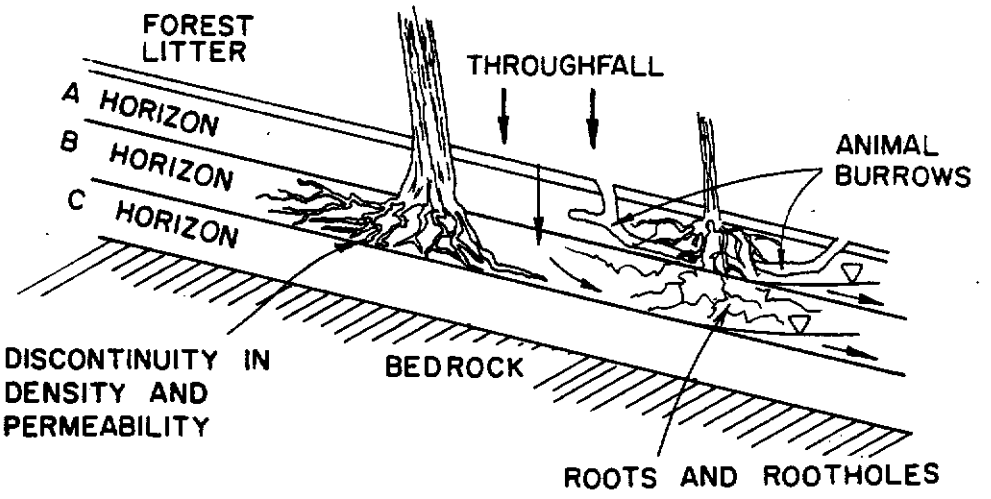

Figure 2.3 Vertical and Lateral Subsurface Flow on a Forested Hillslope.

2.2.1 Subsurface Stormflow Through the Soil Matrix

Where there is not a well-developed system of macropores, Hewlett and Hibbert (1967) proposed the process of displacement to account for the rapid response of subsurface flow to rainfall (translatory flow). They proposed that if the soil is at or above field capacity, precipitation input thickens the water films surrounding the soil particles, causing the release of previously stored water. This translatory flow enters the saturated zone, moves downslope as a pulse and if it emerges at the surface, contributes to storm-flow. This contribution then is previously stored water and not new water. Hewlett and Hibbert (1967) also proposed that subsurface flow, not surface flow, is the major process causing the extension of perennial channels into intermittent and ephemeral channels by returning to the surface as return flow.

If the stream channel is deeply incised as proposed by Freeze (1972), subsurface flow can discharge directly into the stream. As precipitation continues, the zone of saturation increases in depth and extent. Lateral subsurface flow accelerates because of the increased saturated layer thickness and the increased hydraulic gradient caused by extension of the zone upslope.

The temporary zones of saturation are critical for the subsurface flow mechanism (Corbett, 1979). As the zones of saturation expand, flow through the capillaries accelerates because of the increased saturated thickness and hydraulic gradient, as discussed above in connection with translatory flow. More important though, is the effect on the macropores. More soil pipes (macropores) become saturated and flow full and the hydraulic gradients are greater for them also. The macropores found in forest soils can therefore be very important.

2.2.2 Subsurface Stormflow Through Macropores

Whipkey (1967) postulated that interconnected macrochannels formed by roots and animal burrows can provide the means for rapid subsurface flow from upper slopes to stream channels. With advanced

growth, roots can become major soil forming agents compressing the soil causing local changes in porosity and bulk density (Corbett, 1979). When they decay they leave openings, resulting in a large increase in noncapillary porosity (Retzer, 1963). As trees move in the wind, their roots will loosen the soil and open the structure in surface and deeper horizons. Stem flow at the base of trees then becomes important. Animal burrows, which can be extensive in natural watersheds, can also act like subsurface pipe networks and can rapidly transport water through the soil profile. Beasley (1976) and Corbett (1979) supposed that if subsurface stormflow is to occur in macrochannels they must be open to the surface and be under a positive head at the openings. This could occur at the base of trees, in depressions formed by uprooted trees, in decaying stumps, and where animal activity is found. Such conditions are common in forested environments (Beasley, 1976).

Barcelo and Nieber (1982) used a computer model to study the influence of soil pipe networks on watershed hydrology. They showed that a conduit system in the soil increases the overall response to precipitation (Figure 2.4). Soil pipes also accelerate the contribution to streams by short-circuiting the slope between productive source areas and source areas adjacent to the stream (Figure 2.5). Such source areas were observed by Betson and Marius (1967) and Pilgrim et al. (1978). Jones (1975) estimated that 25% of stream flow was contributed by pipe flow for the watershed he studied. The lag time for discharge from the soil pipes also suggested that the flow must have entered the pipe through cracks and holes that connected directly to the surface. Barcelo and Nieber (1982) found that soil pipes can increase the peak discharge of the watershed, increase the volume of water removed during the storm flow period, and significantly affect moisture distribution on the hillslope. The contribution of a single pipe is dependent on the antecedent moisture conditions surrounding the pipe. Their overall conclusion was that soil pipes act as a collective network to accelerate drainage

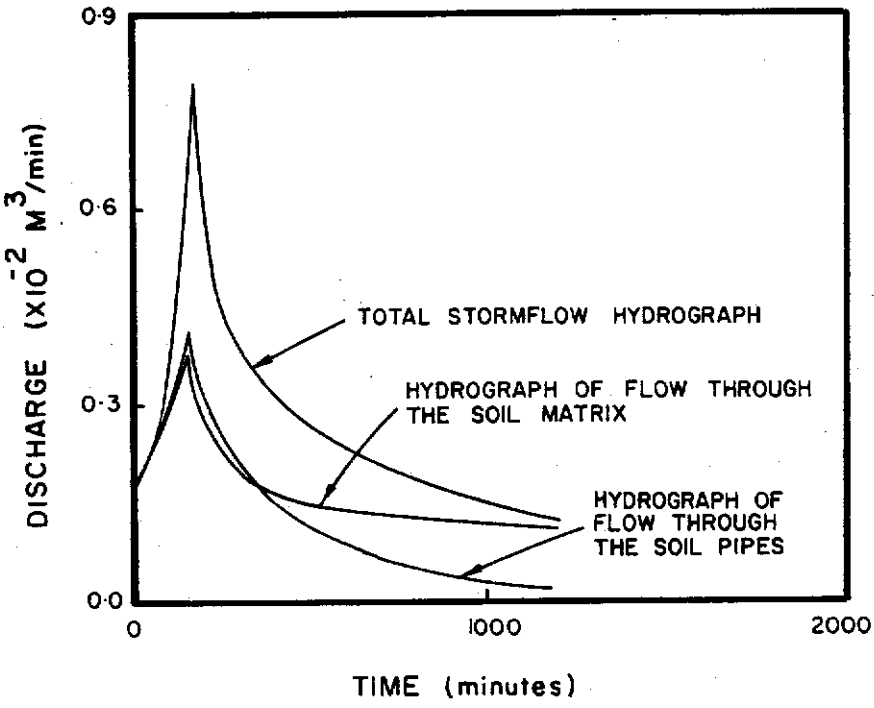

Figure 2.4 Contributions of Matix Flow and Pipe Flow to the Total Stormflow Hydrograph on an Idealized Hillslope (from Barcelo and Nieber, 1982).

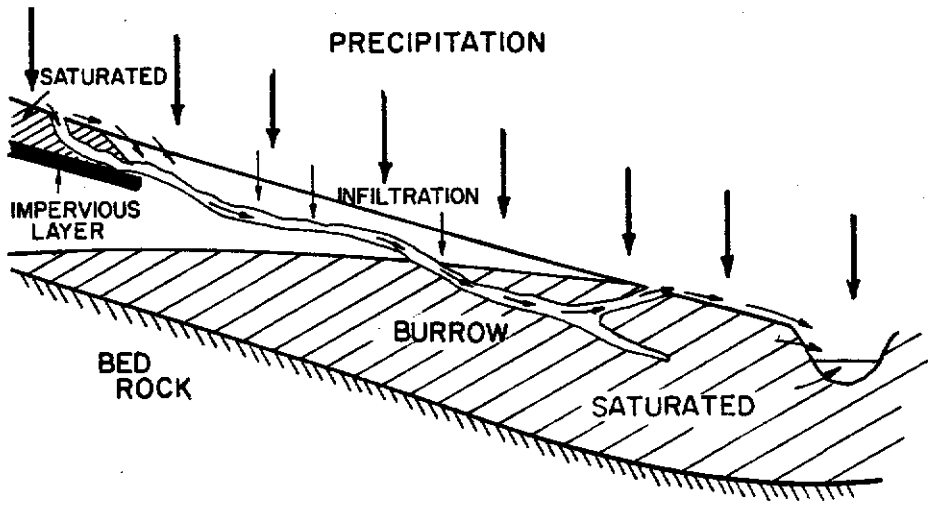

Figure 2.5 Short-Circuiting of Source Areas by Flow in Soil Pipes.

and reduce the potential for moisture storage in the soil matrix. Field studies indicate that rapid flow is more likely to occur through macropores than by the process of displacement and capillary flow.

Pilgrim et al. (1978) used specific conductance and the concentration of dissolved solids to show that there was a short flushing effect and then both surface and subsurface flows were composed almost entirely of new water. This confirmed that rapid subsurface flow must be occurring through macropores and not the soil matrix. Suspended sediments were transported by subsurface water which must have come through macropores. They believed that the sediments were entrained by the falling raindrops.

2.2.3 Topographic and Geologic Influences on Subsurface Stormflow

A watershed can be divided into valley basisn and interbasins. Valley basins and interbasins can have either concave or convex slopes, but the valley basin will have concave contours, while the interbasin has convex contours (Figure 2.6a). The valley basin is water-gathering because the topography brings about the convergence of soil water towards the center of the basin (Figure 2.6b). The interbasin is water-spreading, indicated by its divergent flow line pattern (Nieber, 1979).

Research by Zaslavsky and Sinai (1981) brings together the concepts of rainfall distribution, lateral subsurface and the variable source area concept with considerable insight. They found topography to be the controlling factor in the mechanisms of lateral subsurface flow and moisture distribution in a basin. In particular, they found curvature to be the most important parameter. They measured soil water content in a field after a rainfall which produced no surface runoff or water table. Figure 2.7 shows moisture content plotted as a function of curvature. A strong linear relationship can be seen. They believed that lateral flow in a case like this was a result of effective anistropy caused by soil layering in the surface transition layer. They further believed that soils with root holes and other macropores near the surface and/or those covered with forest litter could be classified

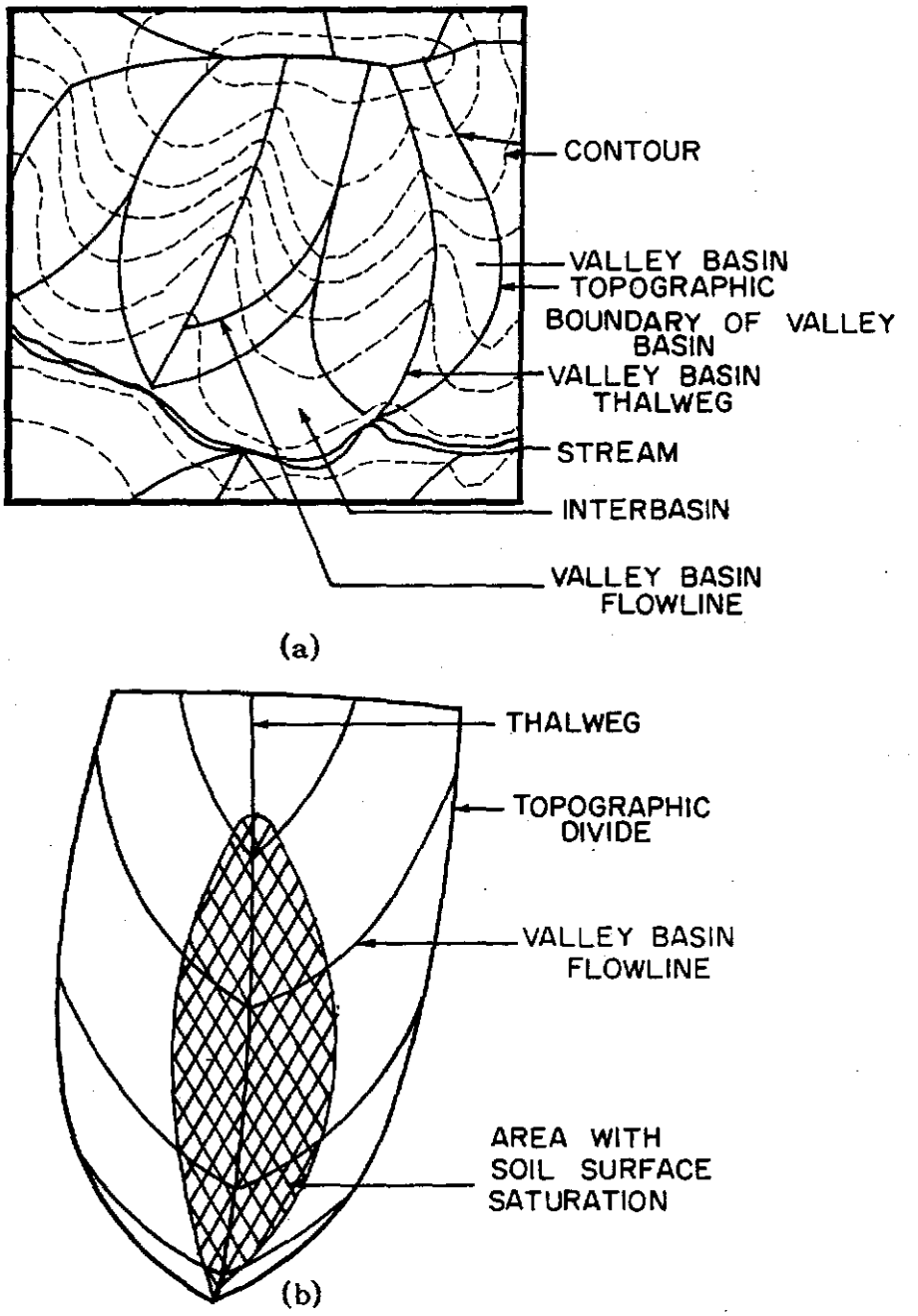

Figure 2.6 The Effect of Topography on Subsurface Flow Lines and Source Areas (from Nieber, 1979).

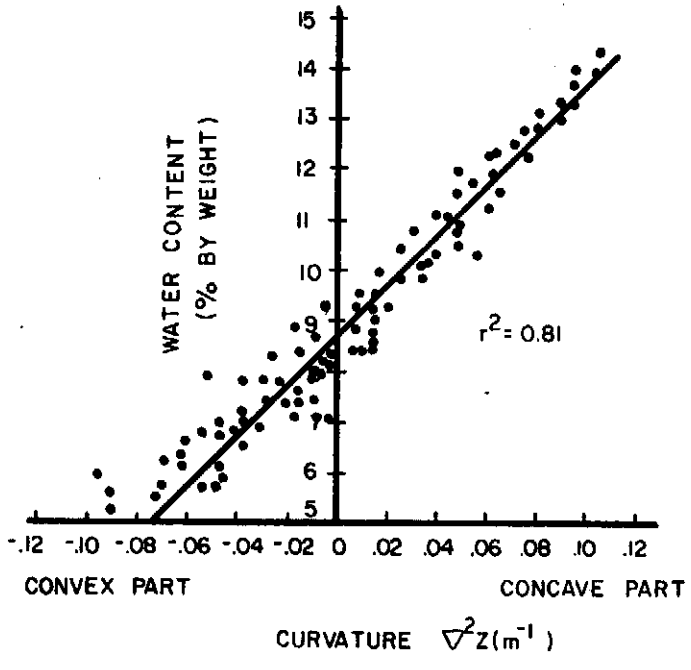

Figure 2.7 Measured Correlation Between Water Content and Curvature on a Sloping Watershed (from Zaslavsky and Sinai, 1981).

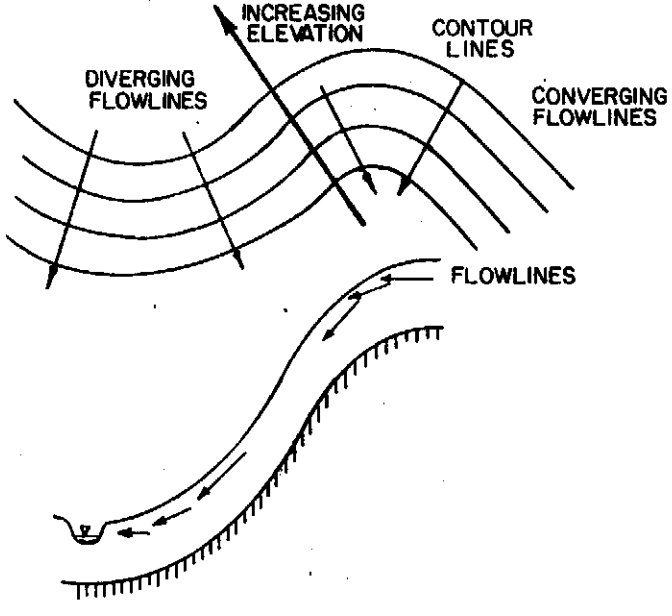

Figure 2.8 Plan and Side-Elevation Views of Convergence and Divergence of Subsurface Flow.

as having a significant surface transition layer. They also investigated other mechanisms of lateral flow and moisture accumulation such as splashing of raindrops, flow in layered soils, and the bending of streamlines near a water table. For all of these mechanisms topography was the most important parameter.

Zaslavsky and Sinai (1981) found that the relative amount of moisture accumulation depended on the total rainfall, not the intensity. Accumulation due to lateral flow continues long after rainfall ceases. Using numerical simulation they found that saturation occurs initially in the transition layer at the most concave location, regardless of rainfall intensity. Zaslavsky and Sinai (1981) also believed that lateral flow in the transition layer was roughly proportional to both the slope and rainfall intensity.

Freeze (1972) used a three dimensional saturated-unsaturated subsurface flow model coupled with a one dimensional stream flow model to investigate the topographic and hydrologic configuration effects on mechanisms of runoff in a basin. Unfortunately, he investigated slopes of only 7.5 and 15%. The results at these slopes showed that subsurface stormflow is only significant for convex hillslopes feeding deeply incised channels and having high hydraulic conductivities (at least 36 cm/hr).

Kirkby and Chorley (1967) believed that the evidence of small contributing areas strongly favored subsurface flow as a major factor controlling the flood hydrograph. In hollows and concave slopes discharge increases because of convergence of flow. Convexity in either direction has the opposite effect (Figure 2.7). For thinner and less permeable soils moisture content and flow per unit area would be higher thus allowing for overland flow at lower intensities. The results of Freeze's (1971, 1972) numerical studies support these proposals. He found that on concave slopes and convex slopes with low permeabilities direct runoff was dominated by overland flow on transient near channel saturated areas. Freeze found that saturation occurred by infiltration rather than subsurface flow from upslope.

Whipkey (1965) studied the flow of water through the soil

profile of a forested watershed with a slope of 28%. Infiltrated water essentially flowed vertically through the soil until a compacted layer of silt was reached and then lateral flow was initiated. The majority of the flow emerged from the layer just above the compact silt. The discharge began quickly after rainfall began and peaked near the end of the storm. The discharges from the lower depths were stable and uniform long after the storm ceased. Not only did the structural discontinuity initiate lateral flow, but there was evidence that a quasi-impermeable layer formed in front of the wetting front as it moved deeper into the soil profile initiating lateral flow just above the wetting front. For dry conditions flow started from the highest layer and then worked down suggesting that the reduction of hydraulic conductivity with moisture content started lateral flow. Weyman (1973) also measured the downslope flow of water and reached similar conclusions. That is, in general, either distinct restricting soil horizons or impermeable bedrock are essential for the initiation of lateral flow.

Dunne and Black (1970) observed that subsurface flow originated in the top soil of their concave watershed, as proposed by Kirkby and Chorley (1967). This lateral flow in the A Horizon was initiated by the presence of an impeding layer underneath. When there was no impeding layer subsurface flow was negligible. In any case, they believed that subsurface flow was too small and too late to contribute significantly to the rapid rise and fall of the stream hydrograph. However, in some storms when the water table rose to the surface, this water would return to the surface and its velocity would increase by a factor of 100 to 500. When perched water tables developed, Dunne and Black observed that channel precipitation, direct precipitation on saturated areas and return flow over saturated areas as being the prime contributors to stormflow.

In the studies conducted by Pilgrim et al. (1978) the great variability of runoff processes was their most significant observation. The principal variable affecting the runoff processes was the depth of the soil. Their instrumented slope had a uniform grade of 30%

with a surface soil of silty loam 0.31 to 0.76 m in depth, underlain by an essentially impermeable layer. Maximum infiltration occurred on deeper soils. Horizontal overland flow occurred on part of the plot where the rainfall intensity exceeded the infiltrability. At the bottom of the plot saturated overland flow occurred when the saturated A Horizon reached the surface. The source areas increased during the storm, and some were isolated, not adjacent to the channel, as Betson and Marius (1969) observed. Subsurface stormflow occurred through the extensive network of macropores, emerged as return flow and was directly discharged into the stream. Pilgrim et al. (1978) concluded that Hortonian runoff (due to saturation from above) and saturated overland flow (includes direct precipitation on saturated source areas and return flow) were the major contributors to stormflow and about equal in magnitude (this may differ for large storms). Subsurface flow was a small component of storm runoff but the major contributor to recession flows. During the storm period subsurface flow was important in that it contributed water to the saturated areas.

2.2.4 Timing and Flow Velocities Associated with Subsurface Stormflow

In order for discharge of subsurface flow to occur there must be saturation at the outlet (Weyman, 1970, 1973). Whipkey (1965) observed a buildup of a mound of soil water that occurred at the base of his plot during storms. After the event it would gradually decrease in length and depth. The apparent hydraulic conductivity of the subsurface flow, the primary flow contributor, was 28.6 cm/hr. Considering the physical properties of the media this was much higher than expected. However, a large number of root holes, cracks, decayed root channels, and earthworm holes were observed and must have been interconnected to some extent to account for this. Actual discharge in the form of pipe flow was observed from many of these openings. The observed short lag times for the initiation of individual discharges led the researchers to believe that some of these openings were open to the surface and became

locally saturated by the channeling of water from the canopy and fauna, which allowed pipe flow. Their conclusion was that turbulent flow was occurring and that the porous media flow equations may be difficult to apply to heterogeneous forest soils. Findings by Weyman (1970) on a watershed in England support Whipkey's study. He also found a strong similarity with respect to time between the subsurface flow hydrograph and the control section hydrograph (one weir was just above his study area and another below - the control section hydrograph was generated by subtracting the upstream hydrograph from the downstream hydrograph) from which he deduced that subsurface stormflow was the major mechanism of runoff on his plot. However, the stream hydrograph differed and he concluded that the headwater zone had faster runoff characteristics and generated the peak.

Field studies of subsurface stormflow have shown that the direct application of Darcy's law to these situations may not be realistic (Whipkey, 1965, 1967; Weyman, 1970; Pilgrim et al., 1978; Mosley, 1979). At present there are at least three deterministic approaches to representing the turbulent nature of subsurface stormflow. Barcelo and Nieber (1982) used pipe flow equations coupled with Richards' equation to model the contribution from the soil pipe network and that from the soil matrix. The difficulty in this approach arises in defining the soil pipe network, which is very heterogeneous in the forest environment. Another approach is to modify Darcy's equation for turbulent flow. Whipkey (1967) cited several of these attempts. The first is to add a second-order term to Darcy's equation,

$$\frac{dH}{dx} = aq + bq^2 \qquad \ldots .(2.1)$$

where dH/dx is the pressure gradient, q is the seepage velocity, and a and b are constants. In the same manner, a third-order term may be added,

$$\frac{dH}{dx} = aq + bq^2 + cq^3 \qquad \ldots .(2.2)$$

where c is an additional constant. Another equation that has been postulated is

$$\frac{dH}{dx} = aq^m \qquad \ldots .(2.3)$$

where m is an exponent between 1 and 2. Equation 2.3 reduces to Darcy's equation when m equals 1. The constant, a, then becomes 1/K, where K is the hydraulic conductivity. All of these attempts of adding additional terms or modifying Darcy's equation have not been entirely successful. Most were developed using laboratory data and apply only to specific porous conditions. Therefore, general application to highly permeable, shallow forest soil is not realistic (Whipkey, 1967). Attempts have also been made to represent turbulent flow in porous media based on the correlation between Reynold's number and friction factor. However, Whipkey (1967) quotes Scheidegger (1957) as placing little value on this concept.

The last approach to modeling subsurface stormflow to be discussed here uses Darcy's equation and effective soil parameters. For example, if hydraulic conductivity is measured using soil cores, the result can be assumed to be the lower limit because the actual soil profile is interlaced with macropores and soil pipes, that will increase the overall hydraulic response. Soil parameters, in effect, are averaged over the soil profile, removing the heterogeneous nature of forest soils and soil structure.

In this light, the findings by Freeze (1971, 1972) are understandable considering the slopes and the hydraulic conductivities for porous medium flow used. Pilgrim et al. (1978) noted that if the porous media flow equations, based on Darcy's equation, are used to predict flow, then the appropriate parameters may be radically different than those obtained from laboratory tests or what is expected for the soil. On a slope twice as steep as Freeze's model, Pilgrim et al. (1978) observed apparent hydraulic conductivities 25 times greater than Freeze's highest conductivity. Tracer studies confirmed that this rapid flow was through cracks, root holes, and

animal burrows (i.e. not flow through the soil matrix). Their instrumented slope was no longer forested but many animal and insect holes, and decayed root holes of trees and other vegetation were observed.

Mosley (1979) carried out a similar study to that of Pilgrim et al. (1978) on a forested watershed in New Zealand with 35% slopes. Overland flow did occur in small areas next to the channel, but he thought the performance of the whole watershed was controlled by subsurface flow. The stream flow and subsurface flow hydrograph peaks coincided closely in time. He observed an increase of subsurface peak flow with distance from the water divide and concluded that this water was moving considerable distances downslope. Subsurface flow was extremely sensitive and responsive to rainfall intensity. Using tracer techniques, dye travel velocities were observed to be three orders of magnitude greater than the matric hydraulic conductivity. Discharge emerged from the base of the humus and B Horizon layers. Flow above the mineral layer was at a velocity between free overland flow and porous medium flow. In the A and B Horizons many root holes were observed to provide pathways for the movement of water. When these macropores are greater than 3 mm in diameter capillary forces are negligible and pipe flow results. The subsurface stormflow was new water, not translatory flow, a finding similar to that of Pilgrim et al. (1978). Slow drainage by saturated and unsaturated flow through the soil matrix accounted for delayed flow and hydrograph recession. Storms having small amounts of quick flow were dominated by channel precipitation, but for heavier storms subsurface stormflow was observed throughout entire watersheds. Mosley's watershed had a deeply incised channel and only a limited amount of area next to the channel where wetlands could develop, so this was a good area to study the subsurface flow mechanism.

2.3 MODELS OF FORESTED WATERSHED RUNOFF

There are three classes of models that have been used to

study hydrologic processes and systems: physical, analog, and mathematical. With the advent of computers and the rapid improvement in memory capacity and computation speed, mathematical models are now the most commonly used class of models. Mathematical models have been classified in a variety of ways. For example, Clarke (1973) divided mathematical models into four groups: stochastic-conceptual, stochastic-empirical, deterministic-conceptual, and deterministic-empirical. Fleming (1979) proposed the classification and subdivisions shown in Figure 2.9. Models of watershed response may also be classed as either continuous or event type models.

Broadly speaking, deterministic models treat processes as if they are part of a determinant system, with no attempt to represent the random process that may be present (e.g. Stanford Watershed Model); statistical models treat the interrelationships between processes as governed by the theory of statistics (e.g. Markov Models); and optimum search models attempt to maximize an objective function subject to specified constraints (e.g. multiple reservoir operation models). These types of mathematical models are described more completely by Fleming (1979) to whom the interested reader is referred for more details.

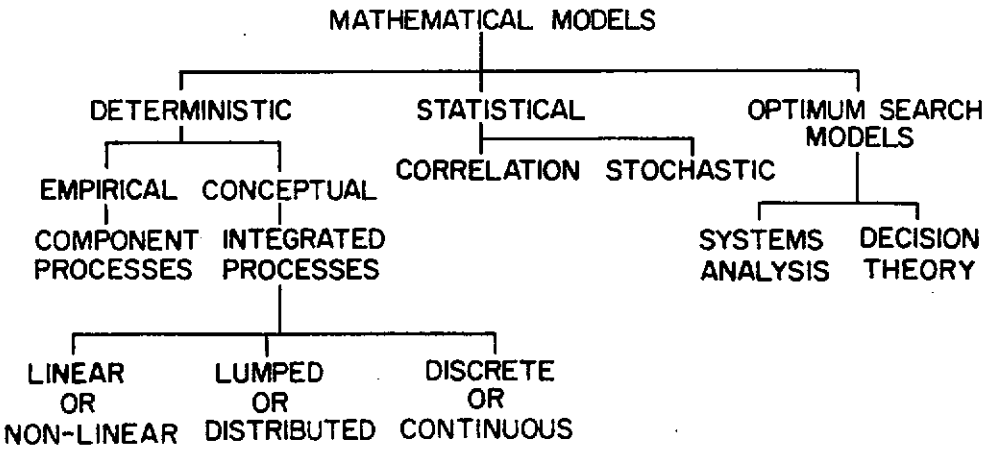

Figure 2.9 Classes of Mathematical Models (from Fleming, 1979).

In recent years the statistical and deterministic type models are to some degree being combined. The input parameters of deterministic models are being characterized stochastically, producing a range of responses as output from the deterministic model. This approach is better able to model the physical heterogeneity of many watersheds.

2.3.1 Conceptual Models of Watershed Response

Conceptual watershed models that predict the response of an entire watershed range from complex general purpose models such as the Stanford Watershed Model (Crawford and Linsley, 1966) and its many subsequent modifications, to models with simple soil water storage and evaporation relationships. The simple models, based on Thornthwaite's (1948) soil-water budgeting concept, for example, usually have monthly time periods (Federer and Lash, 1978). An example of this type of model is Haan's (1972) water yield model.

2.3.1.1 Stanford Watershed Model

The Stanford Watershed Model (SWM) was the first complex, process oriented, general purpose digital simulation model developed (Carwford and Linsley, 1966). At the time of its development, Horton's theory of runoff generation was generally accepted. The soil surface was the primary control in runoff generation by the process of infiltration. Cawford and Linsley realized that evidence was beginning to show the importance of small source areas in determining watershed runoff, but believed it was due to variations in infiltration. Their approach then was to develop a cumulative frequency distribution of infiltration capacity for a watershed that would simulate the variations in infiltration and runoff. Crawford and Linsley recognized that determining a distribution for forested watersheds would be difficult, but thought it could be inferred from simulation studies. As was discussed earlier, this approach is not appropriate for steep-sloped forested watersheds, where infiltrability is so great it is not a controlling factor.

In the Stanford Watershed Model the channel hydrograph is the result of the overland flow hydrograph, the interflow hydrograph and the groundwater hydrograph. Interception storage is filled before precipitation is added to any other storage. Precipitation on impervious areas is routed directly to the stream, while on the rest of the watershed it is subject to the cumulative infiltration functions. Water is divided into three storages; upper zone, interflow, and overland flow. Water that does not infiltrate moves toward the stream. The interflow component which is added to storage, is simply proportional to the local infiltration capacity. Discharge from interflow storage is empirically based on a daily recession value and a 15 minute time interval. Overland flow is also modeled using an empirical relationship for unsteady flow. Water in the upper zone storage is routed to the lower zone or ground water storage which is in turn routed to the stream. Evapotranspiration is handled in the same manner as infiltration, that is, using a cumulative frequency distribution.

An example of the infiltration capacity function is shown in Figure 2.10. The ratio of an increment added to interflow detention to an increment added to surface runoff detention was determined to range from 0.5 to 3.0. This parameter affects the time distribution of runoff and Crawford and Linsley used optimization to determine it.

2.3.1.2 BROOK Model

Models having a daily time interval lie between the complex models, such as SWM and simple models. The Brook model, developed for hydrological simulation of eastern forests is one example (Federer and Lash, 1978). It is a continuous lumped parameter model for watersheds less than 200 hectares in area. There are five storages which are for intercepted snow, snow on the ground, water in the root zone, water in unsaturated soil below the root zone, and groundwater. Potential evaporation is determined by using a form of Thorntwaite's (1948) empirical relationship. Federer and Lash used

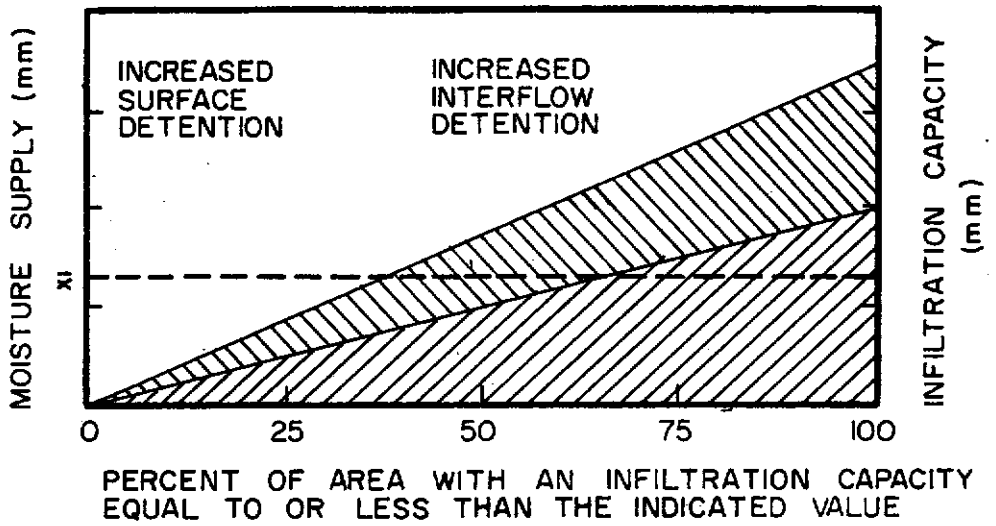

Figure 2.10 Infiltration Capacity Function Used in the Stanford Watershed Model (from Crawford and Linsley, 1966).

a modification by Hamon (1963) that allowed evaporation at temperatures below 0°C. Evaporation is also corrected for the slope and aspect of the watershed. Leaf area and stem area indices were used to model the effect of trees on interception, evaporation, transpiration and snowmelt. For hardwood trees the leaf area index varies over the year. A constant temperature (-2.8°C) was used to determine whether precipitation fell as rain or snow. The following empirical function was used by Federer and Lash to simulate the contribution from variable source areas:

$$y = m + ne^{r\theta} \qquad \ldots .(2.4)$$

where y is the fraction of precipitation converted to direct runoff, m is the fraction of stream area in the watershed, θ is the soil water content in the root zone, and n and r are constants.

Drainage from the root zone and below the root zone was simplified by assuming homogeneity and ignoring hysteresis. Then, if the soil is well above a water table and the gravitational potential controls the flow rate, Darcy's equation becomes,

$$Q = K(\overline{\theta}) \qquad \ldots .(2.5)$$

where Q is the drainage rate, and $K(\overline{\theta})$ is the hydraulic conductivity at the mean water content of the soil, $(\overline{\theta})$. Davidson et al. (1969) and Black et al. (1970) found this approximation to be valid under field conditions. Campbell's equation (Campbell, 1974) was used to represent the unsaturated hydraulic conductivity - water content function. If the soil moisture characteristic can be described in the form proposed by Gardner et al. (1970),

$$h = - g \theta^{b} \qquad \ldots .(2.6)$$

then the relationship proposed by Campbell (1974) is valid,

$$K_r = \theta^{2b+3} \qquad \ldots .(2.7)$$

where h is the pressure head, θ is the volumetric water content, K_r is the relative hydraulic conductivity, and g and b are constants determined from the soil water characteristic. Drainage from the root zone contributes to the unsaturated zone below, that extends to the depth of the permanent water table or an impermeable layer. Drainage from this zone is modeled in the same manner as the root zone. Drainage is divided between interflow and groundwater accretions by a constant. In watersheds without permanent water tables, such as Hubbard Brook where the model was developed, the constant is zero - all drainage becomes interflow. To prevent the soil water flow equations from failing, time intervals of less than one day were required.

Federer and Lash tested the model on the Hubbard Brook watershed in New Hampshire and the Coweeta watershed in North Carolina. Six years of record on each watershed was used for

development and calibration. The poorest monthly correlation coefficients, as low as 0.1, occurred for high flows in the spring and low flows in the summer. Coweeta was easier to simulate because there was not as much snow, which removed some error in the spring, and the large storage below the root zone contributed to stream flow throughout the summer removing some of the low flow error. However, biases did occur at Coweeta for interflow due to the crude nature of the interflow and ground water algorithms (Federer and Lash, 1978). The model was tested on one large watershed but did not give good results.

The most sensitive parameter in the Brook model on these two watersheds was the exponenet of the hydraulic conductivity equation: (Equation 2.7) 2b + 3. This constant was determined from measured soil properties and was very close to the optimum because a 20% increase or decrease lowered the correlation coefficients. At Hubbard Brook a 20% decrease in the constant caused an 11% increase in the stream flow. Response at Coweeta was similar. The exponent of the variable source area equation (Equation 2.4) was also somewhat sensitive. Both the depth of the unsaturated zone and the fraction of water going to ground water storage affected the timing of runoff (but not the volume significantly).

2.3.1.3 Variable Source Area Simulator (VSAS) Model

In an effort to meet the need of a hydrological model that reflected the actual physical runoff process involved, Troendle and Hewlett (1979) developed a Variable Source Area Simulator (VSAS) for small forested watersheds. Their concept was that instantaneous streamflow is the sum of subsurface flow, precipitation on channel and saturated area and overland flow from virtually impervious areas.

$$q(t) = A_1(t)K_s \frac{dH}{dx} + A_2(t)P(t) + A_3P(t) \quad \ldots (2.8)$$

where q is the instantaneous discharge, A_1 is the saturated area along channels where subsurface water exfiltrates to the stream, $A_2(t)$ is the horizontal projected area of saturated areas, A_3 is the

virtually impervious area where Hortonian flow occurs, P(t) is precipitation, K_s is the saturated hydraulic conductivity, and H is hydraulic head.

Equation 2.8 is applied by dividing the watershed into segments and the segments into increments, as shcwn in Figure 2.11. The soil profile is then divided into layers according to soil properties. A finite difference scheme with a 15 minute time interval was used to solve the subsurface flow equations:

$$\text{Darcy's equation: } q = -K(h)\,\nabla H \qquad \ldots .(2.9)$$

$$\text{Richards' equation: } d\theta/dt = \nabla[K(h)\nabla H] \qquad \ldots .(2.10)$$

where ∇ is $\partial/\partial x + \partial/\partial y + \partial/\partial z$.

The unsaturated hydraulic conductivity - water content equation used was Green and Corey's (1971),

$$K(\theta) = a e^{b\theta} \qquad \ldots .(2.11)$$

where a and b are constants. Subsurface water is redistributed in this manner: If a lower element cannot accept the flux from an element because it is saturated, the water stays in the upper element and this element increases in water content. When gravity forces flow into a saturated element water flows into the element above or onto the soil surface. At the end of each interval A_1 and A_2 are redetermined. Hysteresis was neglected in the above equations. Interception was based on the work of Helvey and Patrick (1965) and varied from 1.27 to 2.54 mm for their forested watershed. Since Troendle and Hewlett were only concerned with storm events, they assumed that evapotranspiration losses were zero.

Troendle and Hewlett's simulation analysis indicated that the greatest water movement occurs in the A and B Horizons and that the storm hydrograph is largely controlled by the upper 2-4 m of soil. Normally three layers were sufficient to model discontinuities in the soil water characteristics and initial water contents. A 38.4 ha watershed in north-central West Virginia was used to test the model. Bore holes and seismic measurements were used to define

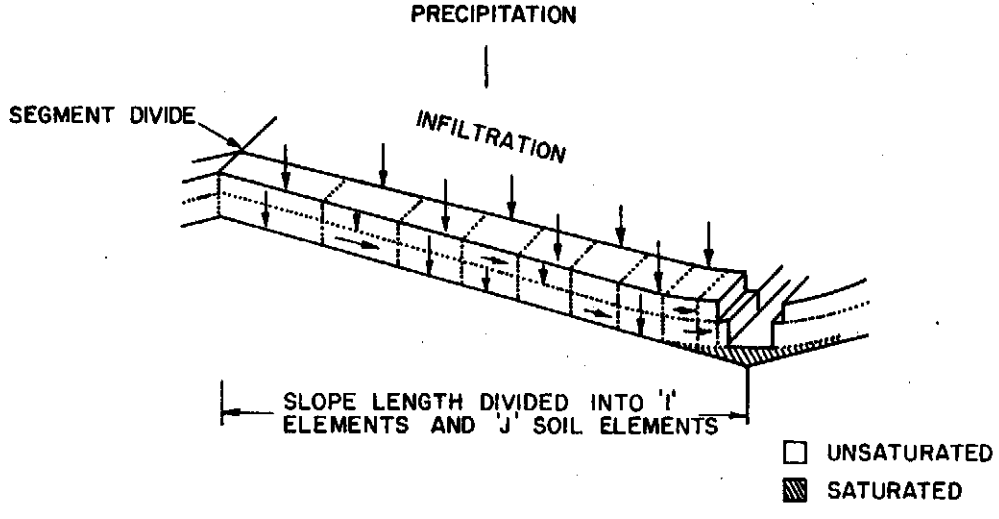

Figure 2.11 Division of Watershed Segments into Increments for the VSAS Model (from Troendle and Hewlett, 1979).

the soil layers. The major task was in describing the soil configuration adequately to represent the expanding and shrinking source areas for rapid flow generation. The most important initial condition was the distribution of soil water in the hillslope. Troendle and Hewlett found that water contents in the lower 25% of the slope controlled the rise to peak and that the recession limb reflected moisture conditions in the middle quarter. The upper half of the slope made only minor contributions unless daily rainfall was greater than 100 mm.

2.3.2 Process Models of Subsurface Flow

Process models deal with a specific process in the overall picture of watershed response, such as overland flow, infiltration, stream flow, etc. The following discussion focuses on subsurface flow since it is a primary contributor to runoff from the steep forested watersheds with which we are concerned.

2.3.2.1 A Three-Dimensional Flow Model Using Richards' Equation and Finite Difference Techniques

The results of the mathematical study of Freeze (1971) were discussed earlier. He developed a model for this study which could handle three-dimensional, heterogeneous, isotropic, saturated-unsaturated, confined-unconfined flow. Richards' equation, the governing equation for saturated-unsaturated flow can be derived from Darcy's equation and continuity and is presented in Equation 2.10. Freeze solved this nonlinear parabolic partial differential equation by using an iterative implicit finite difference formulation and the line successive over-relaxation technique. In the case of a two-dimensional problem a block centered nodal grid is defined and the appropriate boundary and initial conditions imposed. Closer spacing of the nodes is required at the flux surface and near a stream. The nature of the equations causes some problems with convergence.

2.3.2.2 Two-Dimensional Flow Models Using Richards' Equation and Finite Element Techniques

Finite element methods were first applied in other areas such

as structural analysis and only recently has their usefulness in subsurface hydrology been exploited. Neuman (1973) was one of the first to develop a working model using these techniques. The model, UNSAT2, was further modified to handle layered hillslopes. Mohsenisaravi (1981) used this model to investigate subsurface flow on an Idaho watershed. He found saturated hydraulic conductivity to be the most sensitive parameter while the unsaturated properties did not make much difference. To duplicate the measured hydrographs the saturated hydraulic conductivity had to be calibrated for each year of record. The conductivities varied by up to a factor of eight. There was some disturbance on the watershed during the time of study by logging and fire. Mohsenisaravi believed that for steep forested watersheds with highly permeable shallow soils nonlaminar flow theory may need to be incorporated to properly model the processes. He found that saturated hydraulic conductivities determined from some samples would most likely underestimate the actual value. These findings are consistent with those of Pilgrim et al. (1978), and others, described earlier.

Nieber (1979, 1982) also developed a finite element model for predicting hillslope runoff. Making the assumptions of Darcian flow, a homogeneous and isotropic soil, that air in the soil is at atmospheric pressure, noncapillary pores are absent, and deep percolation is absent; one arrives at Richards' equation:

$$\frac{\partial \theta}{\partial t} = C(h) \frac{\partial H}{\partial t} = \frac{\partial}{\partial x} [K(h) \frac{\partial H}{\partial x}] + \frac{\partial}{\partial z} [K(h) \frac{\partial H}{\partial z}] \qquad \ldots .(2.12)$$

where h is the capillary pressure, θ is volumetric water content, $C(h) = \partial \theta / \partial h$ (the specific water capacity), $H = h + e$, e is the gravity head, and x and z are distances in the horizontal and vertical directions, respectively. C and K are strongly dependent on h, for which Nieber used expressions proposed by Verma and Brutsaert (1971):

$$C(h) = \frac{mABh^{B-1}}{(A+h^B)^2} \qquad \ldots .(2.13)$$

$$K(h) = K_s\left[\frac{A}{A+h^B}\right]^N \qquad \ldots .(2.14)$$

where m is the effective porosity, K_s is the saturated hydraulic conductivity, and A, B, and N are constants determined from the soil moisture characteristics of the soil.

For his simulations, Nieber (1979, 1982) used drainable porosity for m, where drainage was assumed to cease at some arbitrary point, i.e. field capacity. Since he was simulating drainage from a laboratory soil trough using mason sand as soil, this assumption may be appropriate. However, for this study m is defined as the effective porosity,

$$m = \theta_s - \theta_{res} \qquad \ldots .(2.15)$$

where θ_s is the saturated water content and θ_{res} is the residual water content at which further water cannot be removed by suction. It is assumed that $\theta_{res} = 0$ for the remainder of this study. When effective porosity, rather than drainable porosity is used, the Verma and Brutsaert equations are compatible with other approximations, such as those of Campbell (1974) and Gardner et al. (1970).

The finite element approach was applied to the space domain and a fully implicit backward finite difference scheme was used to descretize the time domain. The global function residual was minimized by using the Galerkin procedure which is a method of weighted residuals. Nieber used linear triangles as finite elements, whereas Neuman used linear rectangles. When boundary and initial conditions are applied the equations can be solved. At each time step the flux nodes are checked to see if the saturated zone has reached the surface causing a Dirichlet boundary condition.

Nieber tested his model against previous mathematical solutions and laboratory data. Adequate representation of transient saturated-unsaturated flow in the laboratory was achieved only after hysteresis was taken into account. The model did best under wet conditions, in which the soil water content was greater than about 30% by volume.

2.3.2.3 A Flow Model Using the One-Dimensional Richards' Equation

Mulitdimensional finite difference and finite element subsurface flow models such as those developed by Freeze, Neuman, and Nieber are rather expensive to operate and detailed data is required to describe an actual watershed. Thus, these models are limited largely to research applications and are beyond the range suitable for most practical problems. Simple models for routine solutions would be more appropriate, while the more exact solutions could be used to test these approximate solutions (Nieber, 1982). To meet the need of simpler solutions Nieber (1982) developed a one-dimensional model using Richards' equation.

If it is assumed that there is no flow normal to the hillslope gradient, Equation 2.12 becomes one-dimensional and reduces to:

$$C(h)D\frac{\partial H}{\partial t} = \frac{\partial}{\partial x}\left[K(h)D\cos^2\alpha\frac{\partial H}{\partial x}\right] \quad \ldots .(2.16)$$

where α is the angle of the impermeable bed, and D is the soil depth. The boundary and initial conditions are:

Seepage boundary: h=0 and H=e

No flow boundary: $\partial H/\partial x = 0$

Initial condition: $H_o = H(x,t=0)$

Because of the one-dimensional assumption, infiltration cannot be handled directly. Nieber used the concept of piston flow to model the delay in lateral flow caused by the available storage in the soil profile. Water infiltrating at a constant rate, I , increases the water content so that,

$$K(\theta_I) = I \quad \ldots .(2.17)$$

where θ_I is the water content in the transmission zone behind the wetting front. θ_I is calculated using Equation 2.17 and the known soil water characteristic curve. The available water storage in the profile is then $\theta_I - \theta$. An advance rate of the wetting front, V, can be calculated,

$$V = I/(\theta_I - \theta) \quad \ldots .(2.18)$$

Lateral flow is initiated when the impermeable base is reached which occurs at time T, where

$$T = D/v. \qquad \ldots .(2.19)$$

Since Nieber assumed no flow normal to the slope, hydrostatic conditions exist and thus the velocity of the wetting front increases with depth. Integration is required. After rainfall ceased, Nieber assumed that drainage occurred at the same rate until all or some of the storage was depleted. Another option would be to have the drainage rate a function of storage, as is often assumed in many conceptual watershed models.

Nieber used the same method of solution for the one-dimensional model that he used for his two-dimensional model. The one-dimensional solution was then compared to the two-dimensional model. He found that the one-dimensional model gave higher drainage rates at small times, but approached the two-dimensional solution at large times. Nieber believed that the difference was due to the violation of the hydrostatic pressure assumption. Figure 2.12 illustrates this point with results from the two-dimensional model.

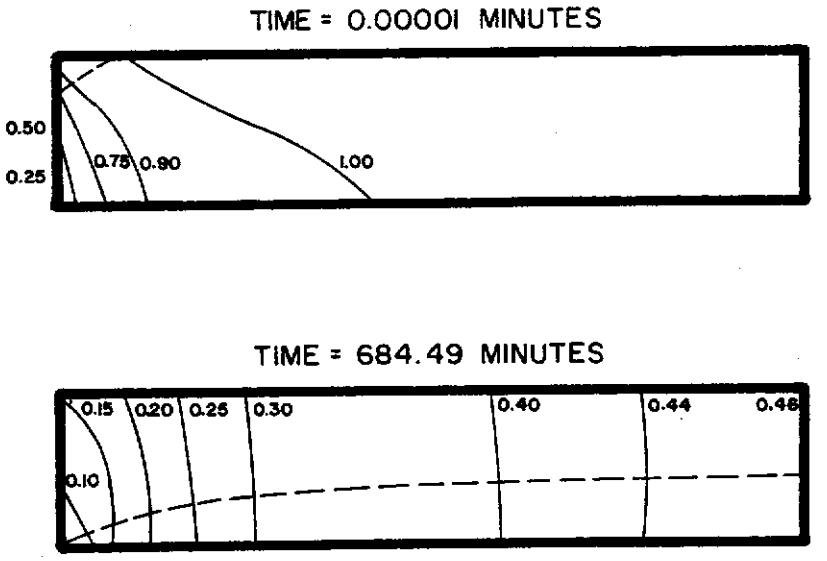

Figure 2.12 Hydraulic Pressure Head Distribution, for a Horizontally Draining Bed, Predicted by Nieber's 2-D Model (from Nieber, 1982).

This error decreases as the slope of the soil bed is increased. The one dimensional solution converges to the two dimensional case more quickly because the two dimensional effect near the outflow is not as great (Figure 2.13).

Figure 2.14 presents hydrographs predicted by the different models. The effect of the infiltration model is shown. Delay A allowed drainage to occur at the same rate as q until all stored water was depleted. Delay B allowed only 63% of the stored water to drain. This proportion was estimated from the two dimensional results.

2.3.2.4 One-Dimensional Flow Using the Modified Boussinesq Equation

Nieber (1982) also evaluated a simpler model that used the familiar Boussinesq equation. Flow in the unsaturated zone was neglected and it was assumed that the flow lines were parallel to the impermeable bed and that the flux rate was proportional to the slope of the free water surface. After modifications are made for a sloping bed the modified Boussinesq equation results,

$$\frac{m}{K_s}\frac{\partial H}{\partial t} = \frac{\partial}{\partial x}\left[(H - z)\cos^2\alpha \frac{\partial H}{\partial x}\right] \qquad \ldots .(2.20)$$

The results of Nieber's simulation are shown in Figure 2.13. The flow rate is significantly affected by the drainable porosity and capillarity. Nieber believed the major problems were that unsaturated flow was neglected and that the Dupuit - Forchheimer assumptions were violated.

Henderson and Wooding (1964), and Childs (1971) also studied the Boussinesq equation and the modified equation, also known as the extended Dupuit - Forchheimer equation. They found the extended or modified equation to give a better approximation than the original Boussinesq equation for slopes greater than 20%. By using a coordinate system with axes parallel and normal to the impermeable bed, Equation 2.20 becomes,

$$C\frac{\partial h}{\partial t} = K_s\cos\alpha \frac{\partial}{\partial x}\left[h\frac{\partial h}{\partial x}\right] - K_s\sin\alpha\frac{\partial h}{\partial x} + i \qquad \ldots .(2.21)$$

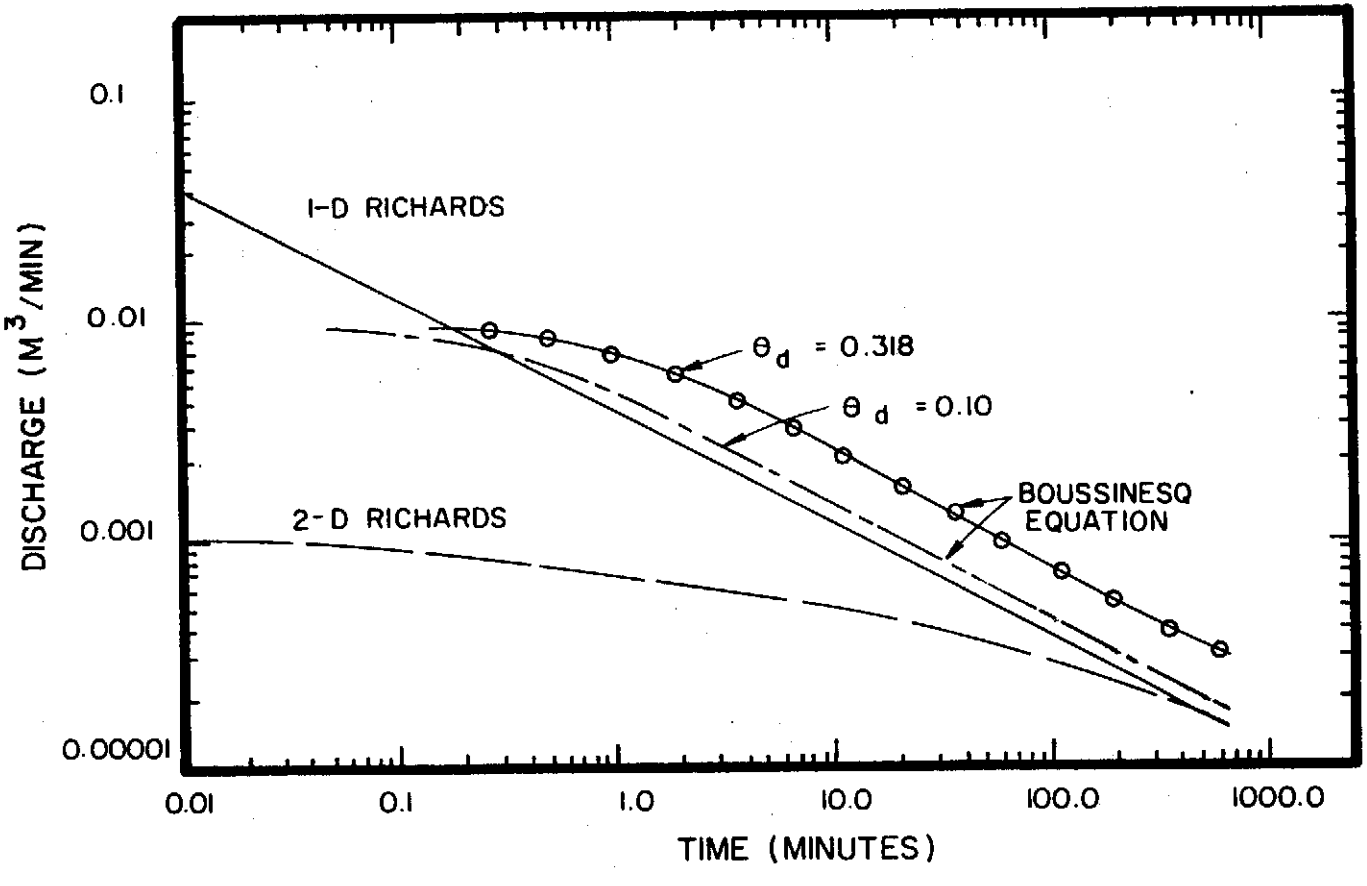

Figure 2.13 Drainage Hydrographs, for a Horizontally Draining Bed, Predicted by Nieber Using the 1-D Richards', 2-D Richards', and the Boussinesq Equations (from Nieber, 1982).

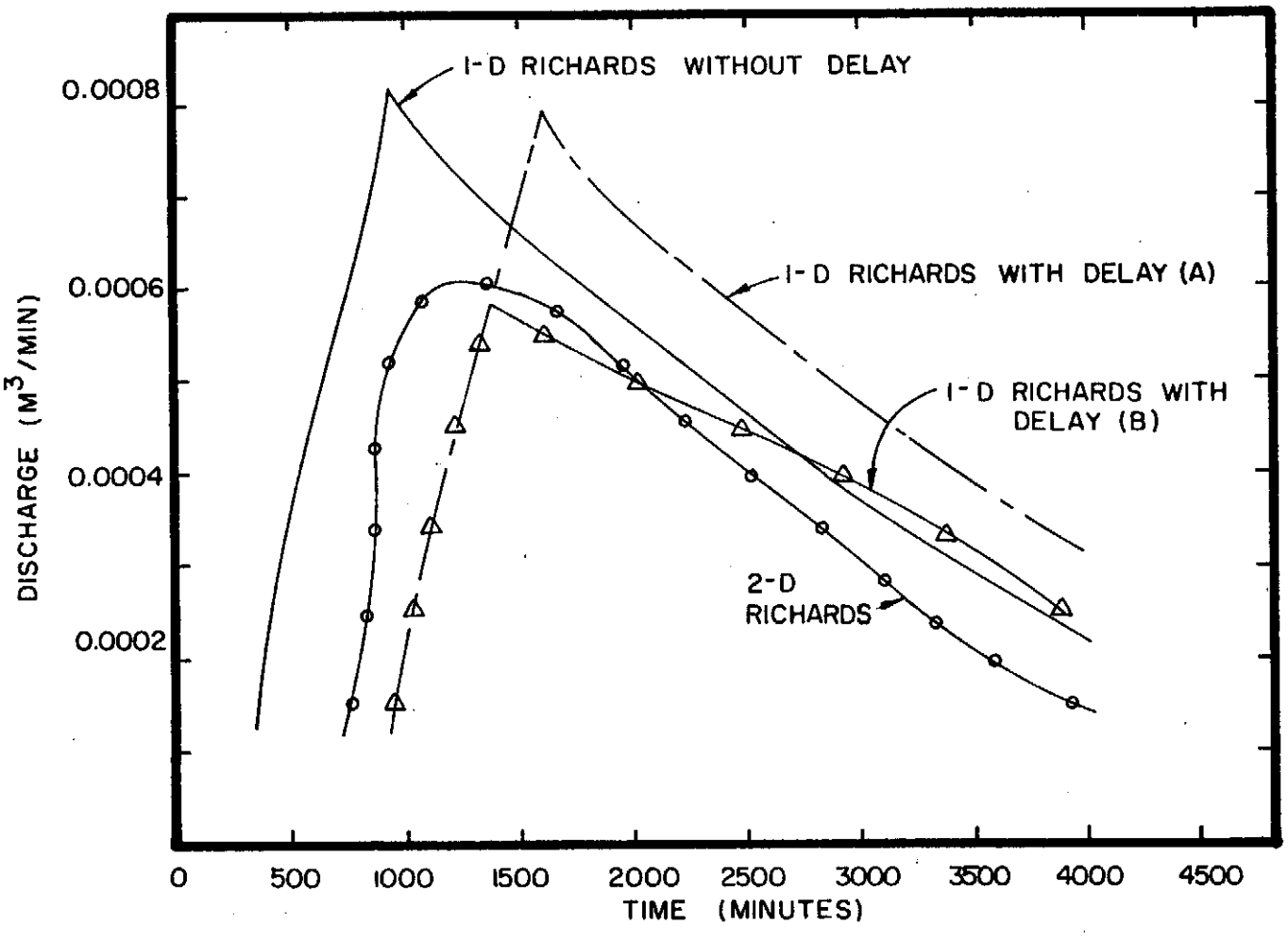

Figure 2.14 Hydrographs Predicted by Nieber Using the 1-D and 2-D Richards' Equations, With a Bed Slope of 50% (from Nieber, 1982).

$$q = K_s h \left[\frac{\partial h}{\partial x} \cos \alpha - \sin \alpha \right] \quad \ldots .(2.22)$$

where i is the rainfall input.

2.3.2.5 One-Dimensional Flow Using the Kinematic Wave Equation

The Boussinesq equations assume that the hydraulic gradient is equal to the slope of the free water surface. A further approximation is to assume that the hydraulic gradient at any point is equal to the bed slope. Then,

$$q = K_s h \sin \alpha \quad \ldots .(2.23)$$

$$C \frac{\partial h}{\partial t} = - K_s \sin \alpha \frac{\partial h}{\partial x} + i \quad \ldots .(2.24)$$

The form of the approximation is of the linear kinematic wave equation.

Beven (1981) evaluated these approximations with the results shown in Figures 2.15 and 2.16. He found the kinematic wave solution to be acceptable for the rising limb of a hydrograph for $\lambda < 1.0$; λ being a dimensionless parameter and defined as,

$$\lambda = \frac{4 \, i \cos \alpha}{K_s \sin^2 \alpha} \quad \ldots .(2.25)$$

Beven calculated λ for 27 field studies and compared them to a $\lambda = 0.75$ (Figure 2.17). For a rainfall rate of one cm/hr, 12 of the studies met the criteria.

Beven (1982) extended this solution to include vertical flow in the unsaturated zone (i.e. wetting and drying fronts) and non-homogeneous, but uniformly varying, soil conditions. This extension is discussed more fully in Section 5.2.3.

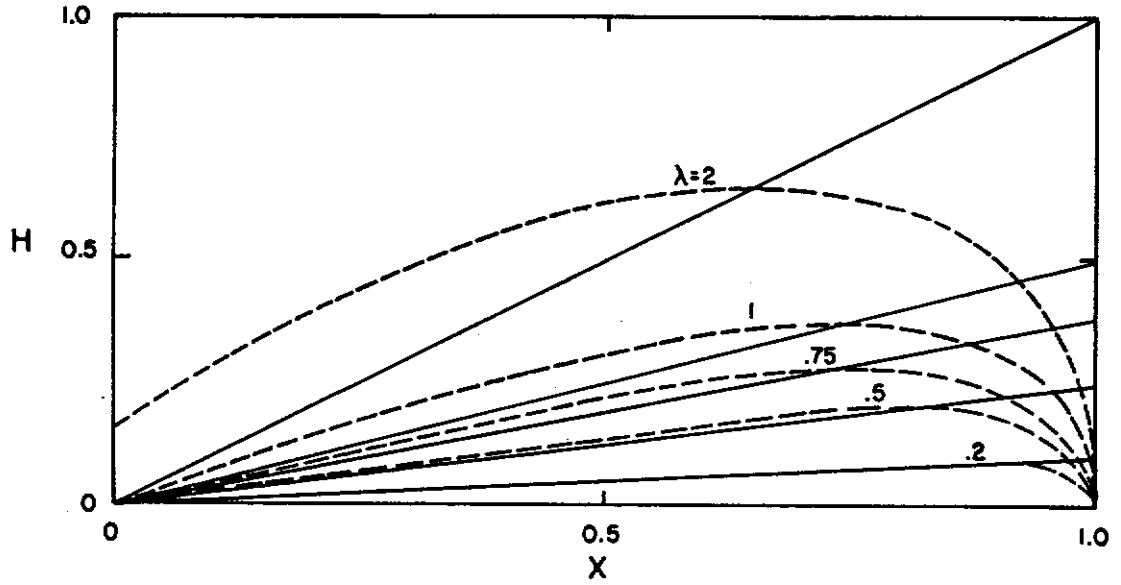

Figure 2.15 A Comparison of Steady State Water Table Profiles Predicted by the Dupuit-Forchheimer (broken lines) and Kinematic Wave (solid lines) Equations for Different Values of λ , Where X is the Dimensionless Distance in the Upslope Direction and H is the Depth of Flow Relative to the Impermeable Bed (from Beven, 1981).

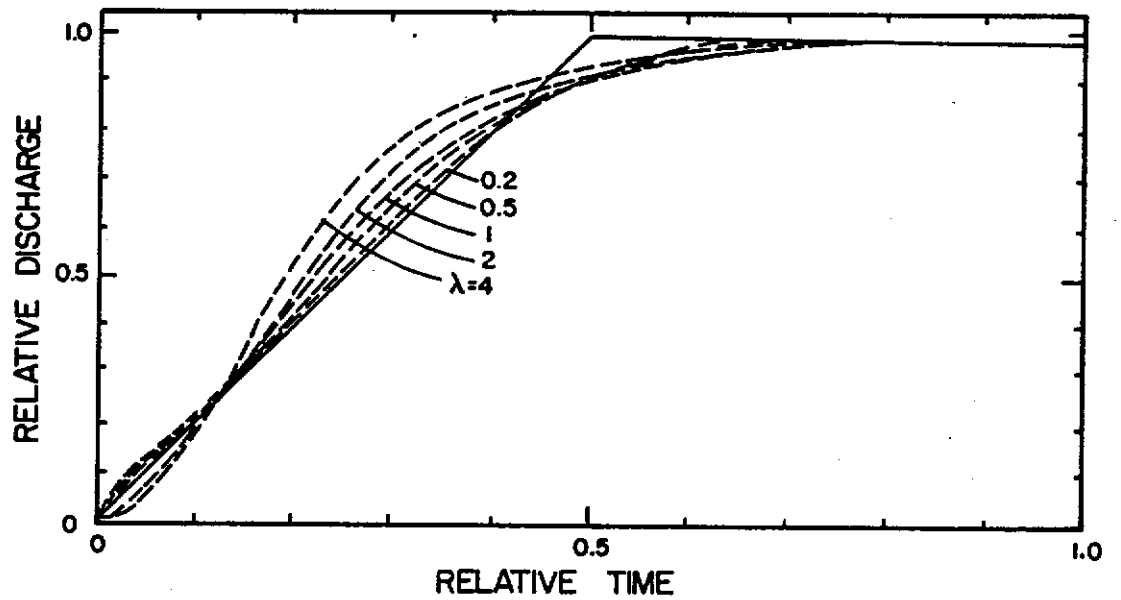

Figure 2.16 Rising Hydrographs Predicted by the Extended Dupuit-Forchheimer (broken lines) and Kinematic Wave (solid line) Equations for Different Values of λ (from Beven, 1981).

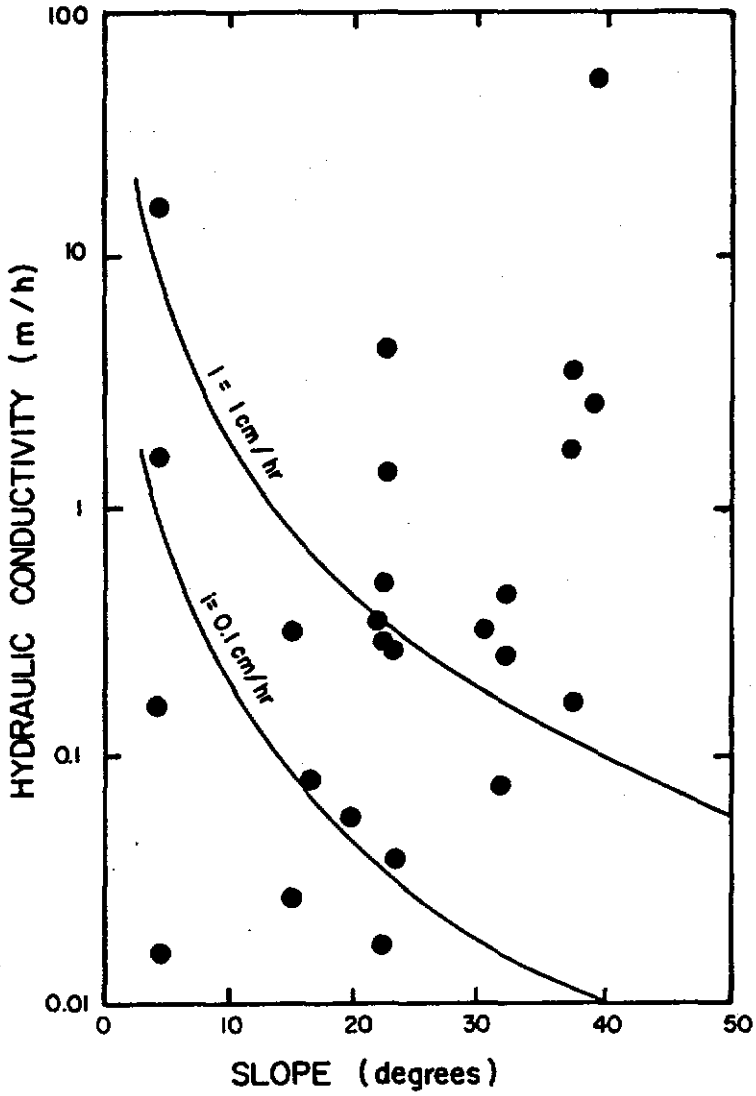

Figure 2.17 Saturated Hydraulic Conductivity Versus Slope Angle for 27 Subsurface Stormflow Field Studies Reported in the Literature. The Solid Lines Represent the Limit of Acceptability of the Kinematic Wave Equation for Different Input Rates i (cm/hr), Assuming a Critical Value of =0.75 (from Beven, 1981).

CHAPTER 3

EXPERIMENTAL SITE DESCRIPTION AND DESIGN

In steep-sloped forested watersheds animal burrows, root holes, and nonuniform and layered soils can significantly alter the response of a watershed over what would be expected from a uniform "ideal" watershed. Subsurface flow for the ideal case is considered in Chapter 5 of this report. The objectives of the field study were to:

(1) identify the primary mechanisms of runoff generation on a steep-sloped forested watershed;

(2) quantify the principal components of runoff generation;

(3) develop and test a continuous conceptual model of watershed runoff from steep-sloped forested watersheds; and

(4) compare three subsurface flow models based on their ability to predict storm flow for individual precipitation events on a steep-sloped forested watershed.

3.1 DESCRIPTION OF STUDY AREA

The study was conducted at the University of Kentucky's Robinson Forest Substation in the Eastern Mountain and Coal Field region of Kentucky (Figure 3.1). The research forest consists of approximately 6,000 hectares (15,000 acres) of reforested land, and is located primarily in Breathitt County, Kentucky. The forest was logged prior to being donated to the University of Kentucky in 1923, and since then has remained virtually undisturbed. The study was conducted using data obtained from the Little Millseat and Field Branch watersheds, and a small test plot located near their confluence (Figure 3.2).

The Little Millseat and Field Branch watersheds are 81.7 ha and 40.5 ha in area, respectively, and are characterized by steep slopes and narrow valleys (Figure 3.2). For example, the hillslopes and the channel slope of the Little Millseat watershed average about 42% and 6%, respectively (Nuckols, 1982). The soils of these two watersheds consist mostly of the Shelocta, Gilpin, DeKalb, Sequoia and Cutshin soil types (Smith, 1982) and have moderately rapid to rapid permeabilities (USDA, 1965). The Shelocta-Cutshin series, a cove

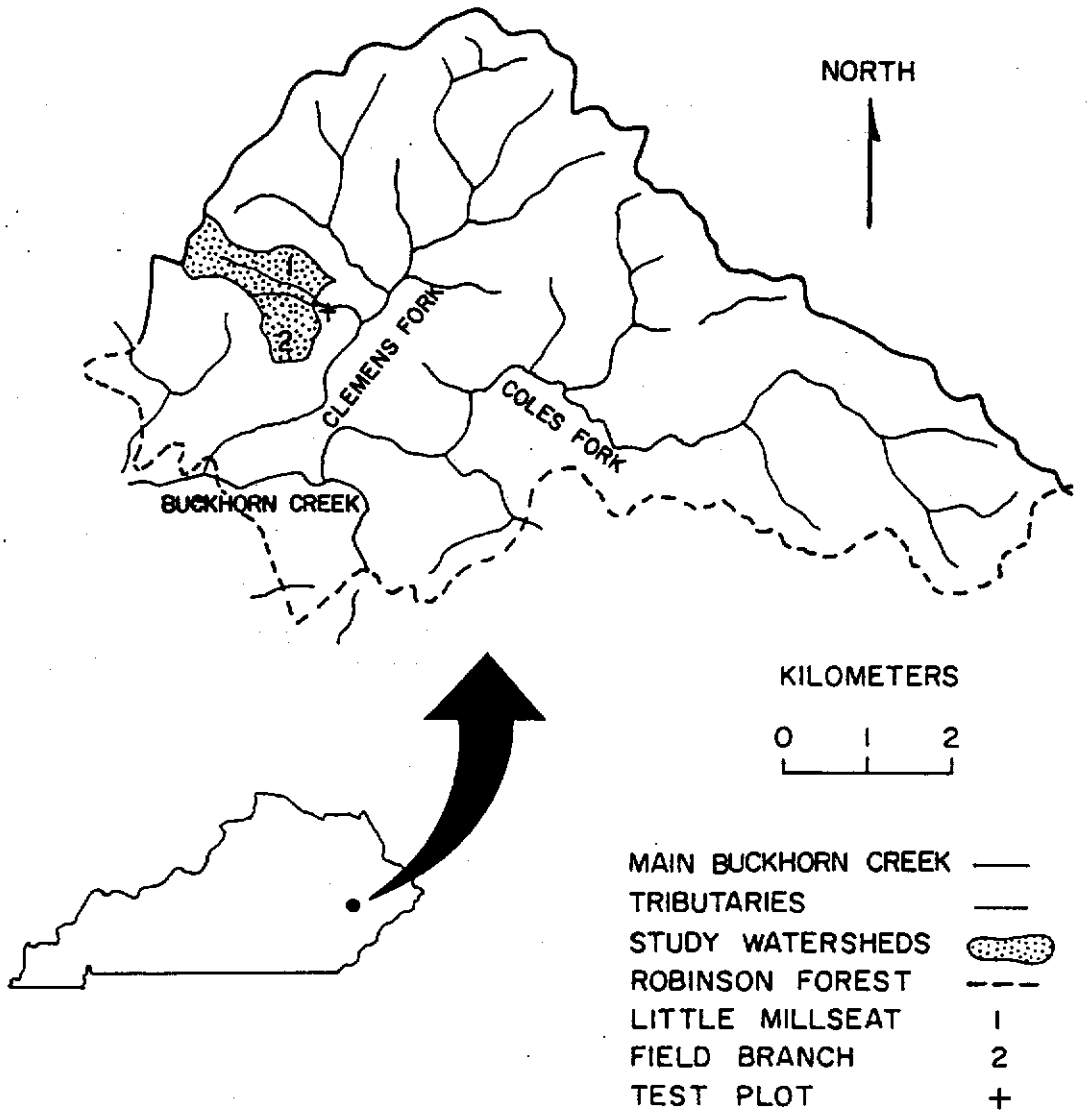

Figure 3.1 Location of the Experimental Site at the University of Kentucky's Robinson Forest Substation.

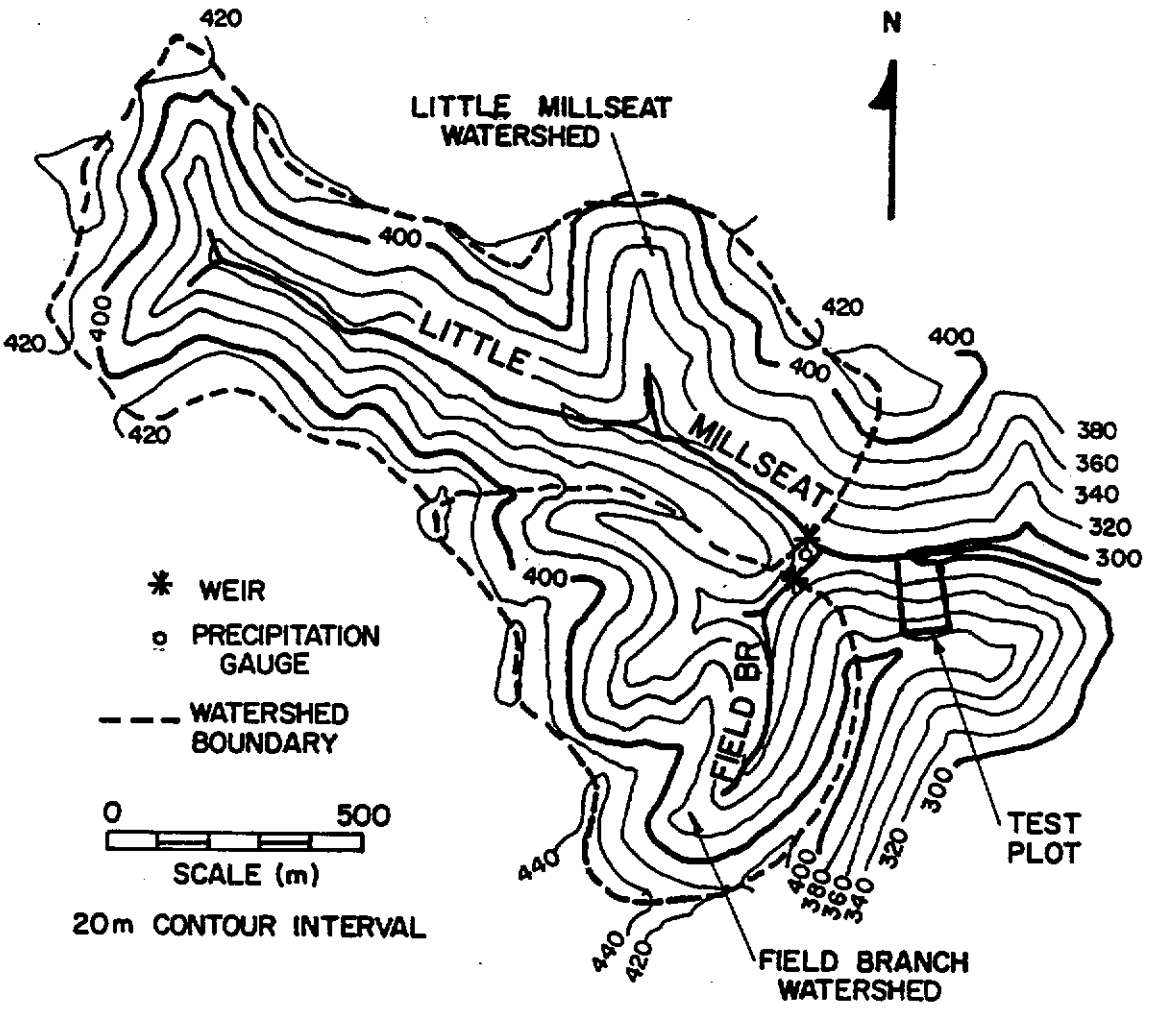

Figure 3.2 Topographic Map of the Little Millseat and Field Branch Watersheds and the Test Plot.

association, varies in depth from about 1.22 m to 1.83 m; the Shelocta-Gilpin association averages 1.40 m deep; and the DeKalb-Sequoia series, a ridge top association, is the shallowest with a 1.00 m average depth (Smith, 1982). Smith (1982) estimated the average weighted soil depth in the Field Branch watershed to be about 1.07 m, and the average wilting point and field capacity water contents to be 12 and 30% by volume, respectively. The average total porosity is about 46% by volume. The deepest soils occur along the upslope sides of benches and in cove sites, while rock outcrops are common along slopes and outslope edges of benches (Springer and Coltharp, 1978). The bedrock is composed of alternating layers of sandstones, siltstones, shales, and interbedded layers of coal from the Breathitt formation of the Pennsylvanian Age (Hutchins et al., 1976; Hanson, 1977).

The vegetation on the two watersheds is dominated by the oak - hickory type. Cove sites consist of the yellow poplar type and ridge tops and upper southwest exposures are classified as shortleaf pine - oak type (Shearer, 1976). Carpenter and Rumsey (1976) have compiled a complete list of tree species found in Robinson Forest.

3.1.1 Precipitation

The precipitation pattern for the watershed is typical for this area of the United States. Low-intensity, long duration storms predominate during the winter, and high-intensity, convectional storms occur in the summer. Precipitation as snow is insignificant and its contribution is neglected in this study. The average precipitation is 1143 mm and is fairly evenly distributed throughout the year with March receiving the greatest and October the least amounts (Hanson, 1977; Springer, 1978; Nuckols, 1982).

A weighing-bucket type rain gauge, shown in Figure 3.3, is located near the confluence of the two watersheds and the instrumented test plot (Figure 3.2). It has been operated by the University of Kentucky Forestry Department since 1971.

Figure 3.3 Seven-Day Continuously Recording Weighing-Bucket Type Precipitation Gauge Located Near the Confluence of the Little Millseat and Field Branch Watersheds.

3.1.2 Runoff

Curtis (1972) observed that the hydrograph peaks from forested watersheds near Robinson Forest were sharp, rather than the more rounded peaks that have been observed from most forested watersheds where subsurface stormflow controls runoff. He believed this was due to shallow soils, steep slopes, and horizontal, impervious bedrock. The "flashy" nature of watersheds in this area was also reported by Springer and Coltharp (1978), who used the ratio of annual quickflow to total streamflow volume and flow duration curves from the Falling Rock watershed, also located in Robinson Forest, as evidence of this behavior.

Runoff is less evenly distributed than precipitation, with winter and spring having the greatest runoff. Quickflow volumes follow essentially the same pattern as streamflow. On the Little Millseat watershed mean annual streamflow and mean annual quickflow are about 65 and 25% of mean annual precipitation, respectively (Nuckols, 1982; Coltharp, 1982, personal communication). On the Little Millseat watershed quickflow volumes account for almost one-half of the precipitation occurring in the winter, while in the fall and summer only 13 to 16% of precipitation is converted to quickflow. Nuckols (1982) believed that during the spring, summer, and fall the major portion of precipitation was routed through the terrestrial system (subsurface flow). In all seasons quickflow runoff consistently accounts for nearly one-half of the total runoff volume per season, indicating that channel precipitation and the near-channel precipitation-runoff processes must be the primary contributors to stream flow for the watershed (Nuckols, 1982).

Streamflow from the Little Millseat and Field Brnach watersheds is measured using permanent 3:1 sideslope, broad-crested V-notched weirs, such as the one shown in Figure 3.4. The weirs have a 0.9 m rated head, which allows a flow capacity of 4.83 m^3/s.

3.2 DESCRIPTION OF THE TEST PLOT

Rainfall, soil water content, soil water potential, and water

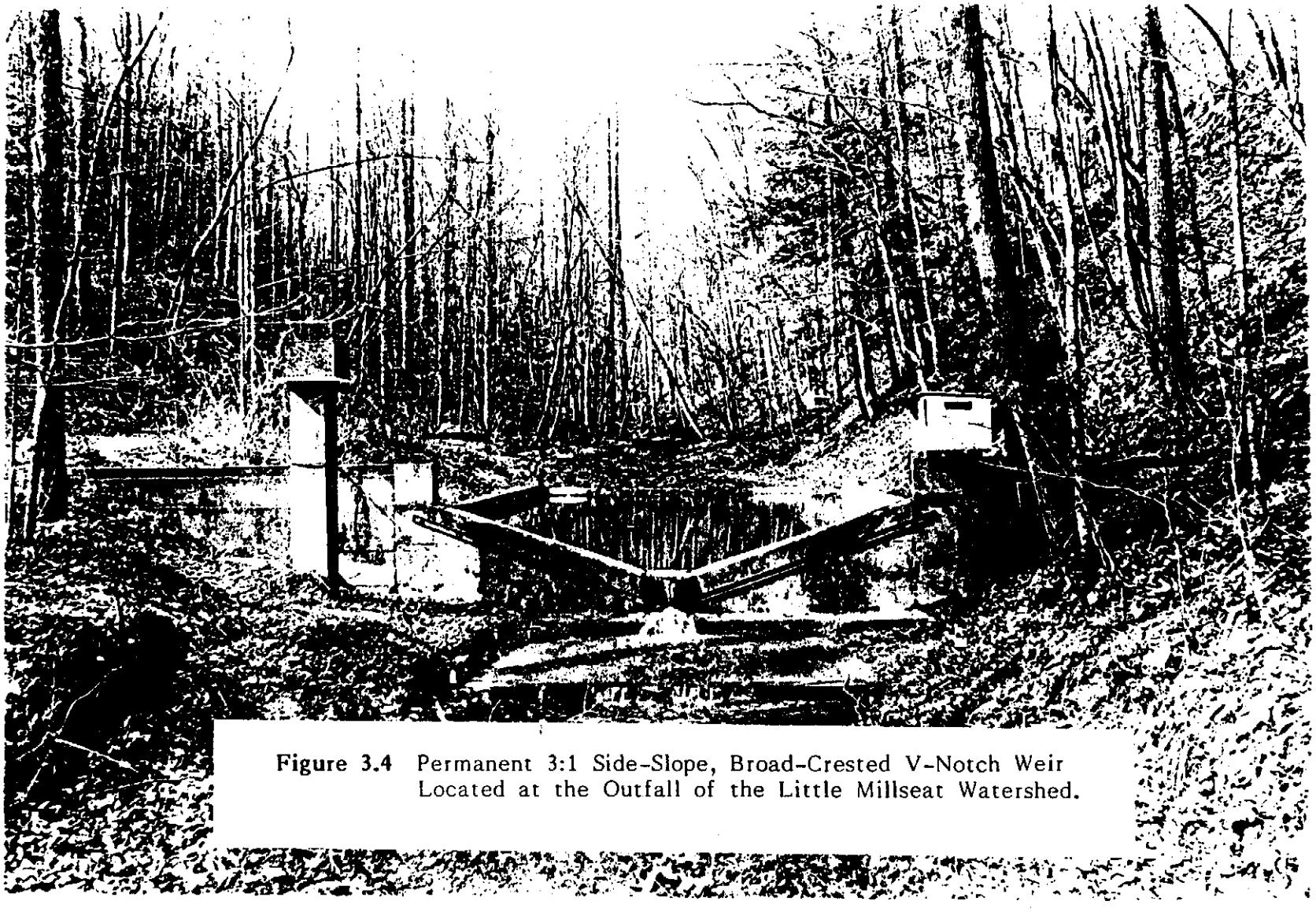

Figure 3.4 Permanent 3:1 Side-Slope, Broad-Crested V-Notch Weir Located at the Outfall of the Little Millseat Watershed.

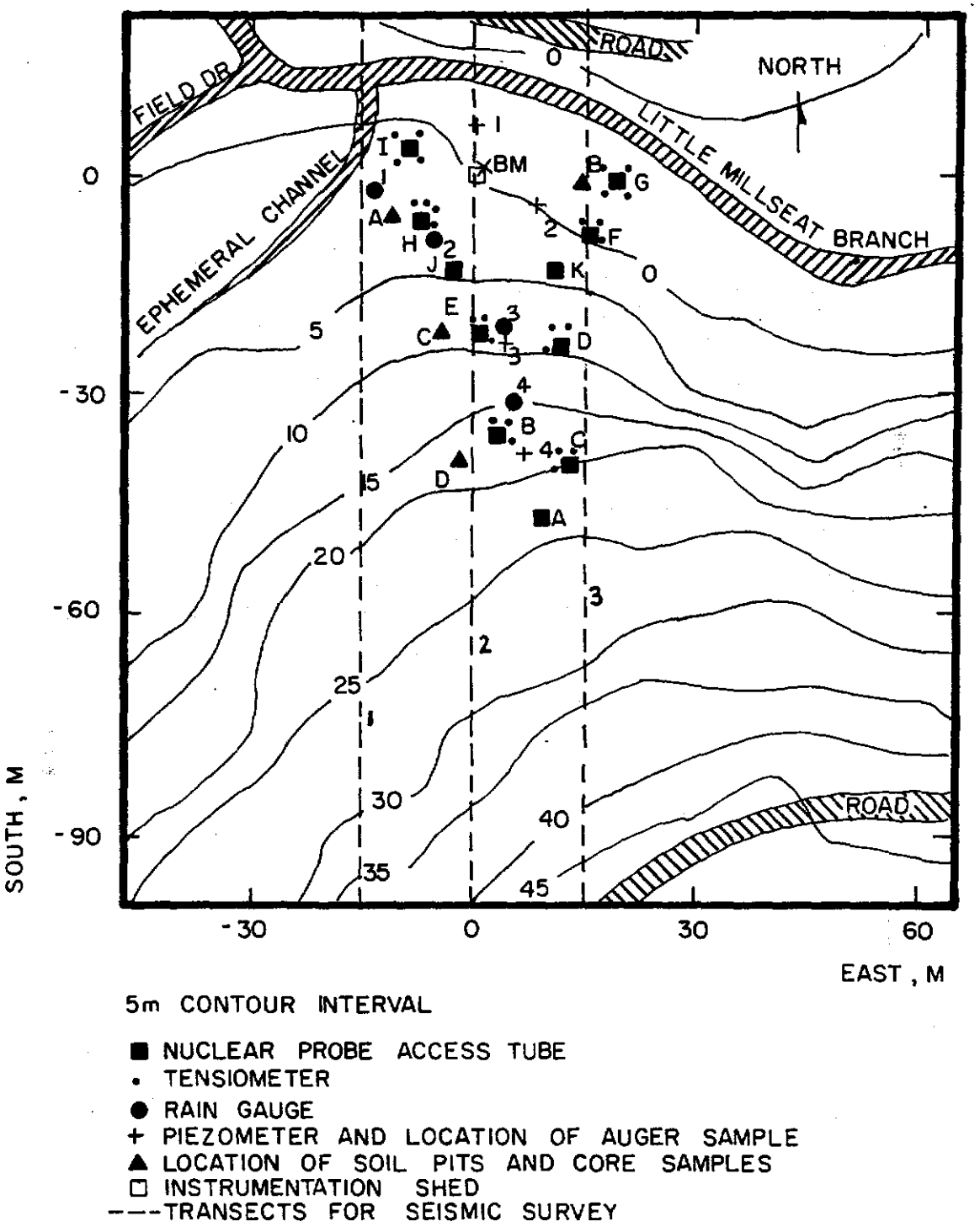

Figure 3.5 Topographic Map and the Location of the Instrumentation and Sampling Sites on the Test Plot.

table levels were measured on a regular basis on a hillslope near the confluence of the Little Millseat and Field Branch watersheds (Figure 3.2). Location of the instruments and a topographic map (surveyed by the authors) of the plot are shown in Figure 3.5.

Preliminary testing of the instrumentation took place in November, 1981. The analysis of data only includes the period of record from October 27, 1982 through December 1, 1982, because the tensiometer system was not completely debugged until then.

3.2.1 Soil Depths

The depth of the soil profile on the test plot was determined using a portable Bison Signal Enhancement Seismograph, Model 1575B. The seismic survey method depends on the principle of seismic refraction, that elastic waves travel at unique velocities through different materials. Time of travel for these seismic waves can be related to the thickness and density of the material (Smith, 1982; Hobson, 1970; Dobrin, 1960). In order for seismic waves to be refracted, velocity must increase with depth, and the layers of transmission must be thick enough to allow the wave to be transmitted horizontally (Hobson, 1970; Bison, 1974; Smith, 1982). Typical velocities are 244 ± 49 m/s for the weathered zone, and 792 ± 183 m/s for an intermediate layer, that could consist of alluvium, clay or similar unconsolidated material. Bedrock velocities are greater than 3050 m/s (Smith, 1982; Mangum et al., 1981).

Smith (1982) conducted a seismic survey of the Field Branch watershed as part of a hydrological study there. He compared his seismic results to soil depths measured in 21 soil pits and the correlation coefficient was 0.76. The deepest soils were at bench and cove sites. Shallower soils were found on the ridge tops and steeper slopes. Smith (1982) found the average initial velocity to be 244 m/s (73-520 m/s range). On 23 plots an intermediate velocity was found that averaged 463 m/s (215-812 m/s range). The average final velocity was 1615 m/s and ranged from 662 to 4572 m/s.

Soil depths for the instrumented test plot were measured using

the equipment and methods described by Smith (1982) in 1981. Three transects (Figure 3.5) were taken through the plot and the resulting soil depth profiles are shown in Figure 3.6. The average initial and final velocities were 109 ± 30.8 m/s and 913 ± 734 m/s, respectively.

The soil pits and the installation of the access tubes and tensiometers showed that the depth to bedrock was greater than that measured by the seismic survey. Insufficient spacing of the hammer and geophone was the primary cause of this underestimation. The depths given by the seismic survey are useful, however, since they represent the depth to an increase in the bulk density. These levels also correspond to levels with significant reductions of hydraulic conductivity and are therefore hydrologically important. The soil pits tended to show that the depth to bedrock decreased upslope, while the seismic survey showed that the depth to a major increase in density (after the surface layer) did not have the same trend, but was fairly uniform for the section surveyed.

3.2.2 Soil Water Characteristics

The soil water characteristic, which describes the relationship between water content and pressure head of the soil, is required for the solution of Richards' equation and the water balance equations. Equations for soil water capacitance, C(h), can be developed once these characteristics are known.

A pressure plate apparatus with compressed nitrogen was used to determine the soil water characteristic. A 5 bar and a 15 bar chamber were used along with 1, 3, and 15 bar ceramic plates. Samples were saturated for 24 hours and then the required pressure applied for 48 hours (until equilibrium was achieved). Water content was then determined gravimetrically.

Disturbed samples were collected at the four locations shown in Figure 3.5 using a 37.5 mm diameter auger. The samples, divided into 15 cm increments, were taken to the depth where bedrock, hard clay or rock was encountered. Soils of the same type were mixed together, clods broken by hand, and sieved through a #8

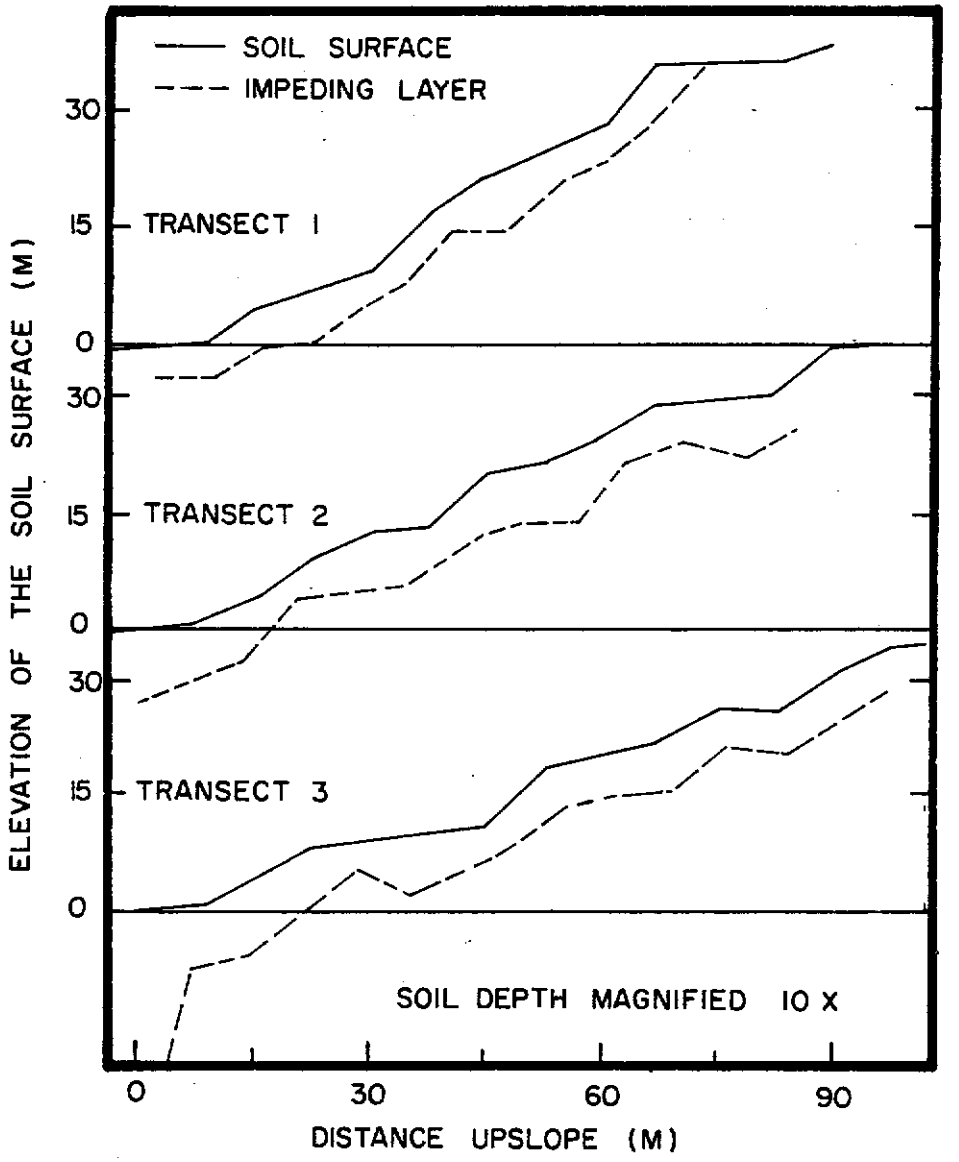

Figure 3.6 Profile of the Soil Surface and the Depth to an Impeding Layer Measured Along Three Transects Through the Test Plot (seismic survey results).

sieve. Water content determinations were then made at pressures of 1, 3, 5, 10 and 15 bars.

It was desired to have the soil water characteristics on a rock-free basis. Since the measured water contents were gravimetric, conversion to a rock-free volumetric water content required multiplication by the rock-free bulk density. This information was determined using the overall bulk densities and rock content values found using core samples (Section 3.2.4). The plots of volumetric water content versus pressure head were essentially linear on a log-log scale. Therefore, Equations 2.6 and 2.7 were used to define the soil water characteristic (Moore, 1981). From the pressure plate data on the ten soil samples, three slopes and seven intercepts were determined (b and g in Equations 2.6 and 2.7), for a total of seven different soil water characteristics (Table 3.2).

Smith (1982) also investigated the soil water characteristics of soil on the Field Branch watershed. He determined field capacity, which he defined as the water content at 1/3 bar, and wilting point, defined at 15 bars, for 21 plots. For the Field Branch watershed, Smith (1982) found the rock-free soil water content at 1/3 bar was on the average 0.339 for the A Horizon (upper 20 cm), and 0.291 to 0.370 for the B Horizon. Using the soil water characteristics estimated for the test plot, the corresponding water contents are 0.290 for the A Horizon, and 0.242 to 0.480 for the B Horizon.

3.2.3 Saturated Hydraulic Conductivity

In a study of subsurface stormflow the hydraulic conductivity is very important. Saturated hydraulic conductivity can be measured in the laboratory and then if certian assumptions are made, the soil water characteristic and saturated hydraulic conductivity can be used together to arrive at the unsaturated hydraulic conductivity as a function of water content (Equation 2.7).

Eighty soil samples were taken using a Uhland-type sampler. The cores were 76 mm in diameter and 76 mm long. Four soil pits were dug to obtain the cores. Their location is shown in Figure

3.5. For reasons of practicality, samples were only taken to a depth of 1.10 m. By this depth a fairly impermeable layer was encountered (which is consistent with the findings from the seismic survey), thus making the depth adequate for this study. The cores were placed in waxed containers to keep from drying out, and brought back to the laboratory to be tested on a contstant head permeameter. Depending on the soil's hydraulic conductivity, different hydraulic heads were used, and deionized distilled water was used for all the tests. The head was applied so that water flowed vertically upwards through the samples.

Table 3.1 summarizes the results of the hydraulic conductivity tests. The surface layer, the uppermost 15 cm, has the greatest hydraulic conductivity, as was expected. Discontinuities in the hydraulic conductivity were seen for all the pits. Impermeable layers were observed in Pits C and D.

The 76 mm diameter cores are somewhat limited as far as obtaining representative estimates of the hydraulic conductivity. Samples were taken at specific points in a very heterogeneous system and the effect of larger soil pipes cannot be measured with these small cores. The sampler introduces bias by selecting the easiest place to sample, i.e., where there are no, or few, rocks, roots or burrow holes. For these reasons, the saturated hydraulic conductivities determined using the cores and the permeameter can be viewed as the lower limit of saturated hydraulic conductivities in the field.

Smith (1982) reported similar values of saturated hydraulic conductivities for the Field Branch watershed. He used 54 mm diameter cores and a constant head permeameter, similar to the one discussed above. For the 11 plots included in the Shelocta soil series (the type most similar to that of the test plot), he measured the permeabilities in the A Horizon to average 21 cm/hr (0.76 to 43 cm/hr range) and 3.05 cm/hr (0 to 8.9 cm/hr range) for the B Horizon.

Table 3.1 Soil Properties Measured Using Core Samples

Soil Pit	Number of Cores	Depth (m)	Saturated Water Content (vol./vol.)	Bulk Density (g/cm^3)	Rock Content (%)	Saturated Hydraulic Conductivity (cm/hr)
A	4	0- .15	.534±.033	1.186±.010**	0.313	9.29 ± 4.37
	3	.15- .30	.452±.017	1.451±.050	2.73	3.24 ± 4.71
	3	.30- .46	.419±.010	1.535±.017	0.572	4.10 ± 4.14
	3	.46- .61	.434±.024	1.486±.074	0.842	5.40 ± 5.40
	3	.61- .76	.363±.021	1.724±.053	0.650	1.17 ± 1.03
	3	.76- .91	.392±.038	1.673±.098	18.1	3.65 ± 2.13
	3	.91-1.07	.449±.022	1.526±.049	0.676	2.57 ± 1.29
B	5	0- .15	.561±.021	1.188±.020	0.911	7.81 ± 0.88
	4	.15- .30	.502±.026	1.310±.045	1.61	0.841 ± .513
	3	.30- .46	.448±.012	1.540±.049	0.399	0.310 ± .446
C	4	0- .15	.549±.047	1.133±.077	17.1	32.10 ± 22.95
	3	.20- .41	.408±.014	1.551±.032	8.08	13.86 ± 13.94
	3	.41- .56	.386±.014	1.577±.028	20.8	16.90 ± 7.17
	3	.61- .76	.354±.008	1.720±.044	22.9	3.81 ± 3.14
	3	.76- .91	.455±.084	1.636±.070	18.7	2.56 ± 2.38
	3	.91-1.02	.413±.010	1.717±.027	14.7	0.0637± .0654
	2	.99-1.09	.406±.024	1.727±.054	10.5*	0
D	4	0- .15	.496±.055	1.353±.091	17.2	6.35 ± 6.66
	3	.15- .33	.432±.053	1.529±.127	5.75	2.95 ± 3.05
	3	.38- .51	.385±.021	1.609±.016	7.85	3.44 ± 2.48
	3	.46- .61	.391±.027	1.613±.052	21.0	3.36 ± 1.29
	3	.61- .76	.388±.016	1.594±.010	19.3	1.96 ± 1.87
	3	.71- .91	.374±.013	1.770±.052	18.2*	0.0592± .0683
	3	.89-1.07	.407±.068	1.812±.106	17.0	0.137 ± .233

* An impermeable layer
** ± one standard deviation

3.2.4 Bulk Densities

The same cores used to determine the saturated hydraulic conductivities were also used to determine the bulk densities. After three replications had been run on the permeameter, the saturated core was weighed, oven dried and weighed again, giving bulk density, saturated water content, and rock fraction. These results are also shown in Table 3.1. It can be seen that densities and porosities correlate somewhat with the hydraulic conductivities. The data can also be used to differentiate between soil layers with different physical properties.

3.2.5 Significance of Soil and Plot Physical Properties in Relation to Subsurface Flow on the Test Plot

All measured physical properties of the soil and the hillslope were translated to an imaginary cross section along a flowline passing through the center of the test plot. The cross section was divided into 11 elements (Figure 3.7) having the soil properties presented in Table 3.2.

The saturated hydraulic conductivities measured in the laboratory (Table 3.2) show that the upper 15 cm has the highest permeability. They are sufficiently high that one would not expect saturation from above, Hortonian-type flow, to occur, especially since these are the lower limits of hydraulic conductivities. In the bottom area hydraulic conductivity decreases to 2-3 cm/hr and is fairly uniform for the depth sampled. Three cores in the bottom were impermeable (Table 3.1), so thin impermeable layers may be present that do not show up in the overall hydraulic conductivities. On the hillslope, however, saturated hydraulic conductivities decrease with depth (Table 3.2), and an impermeable base was encountered (Table 3.1).

When digging the soil pits, roots and animal burrows were seen that would increase the hydrologic response above that which the measured saturated hydraulic conductivities suggest. In the bottom area many soil pipes were encountered, such as the one shown in Figure 3.8, which was under positive head, since water flowed

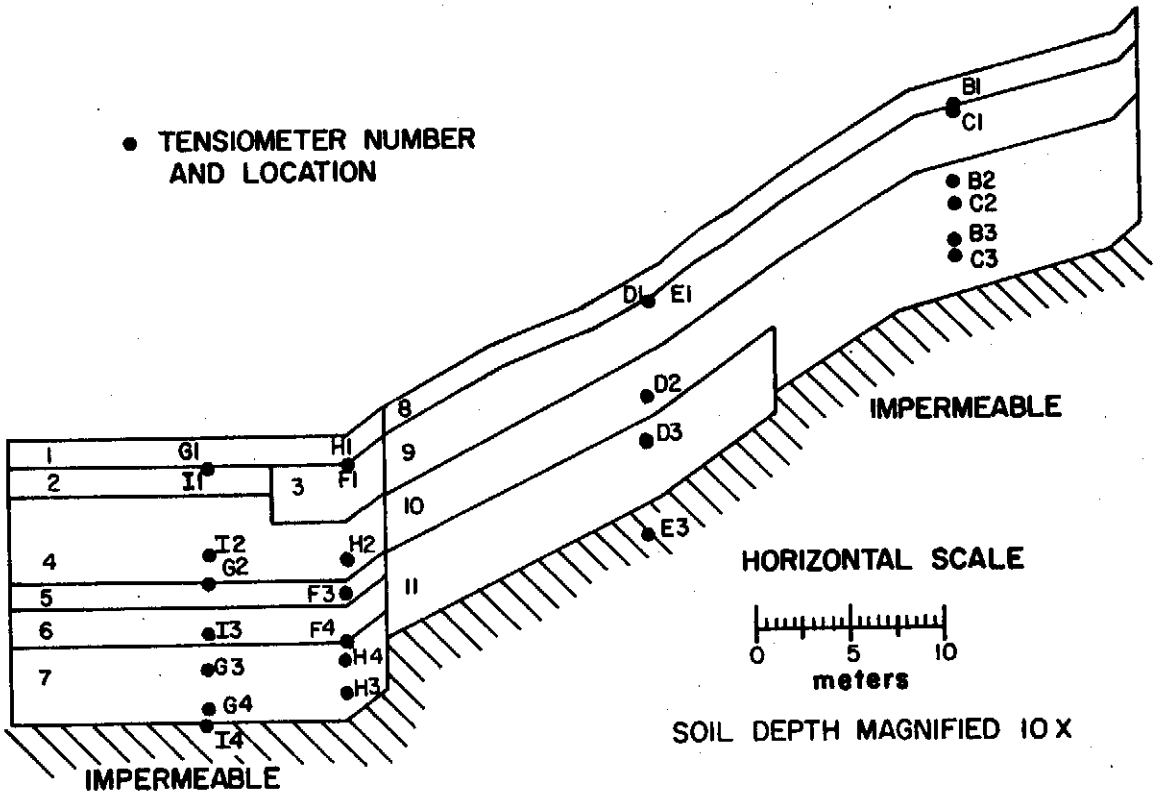

Figure 3.7 Hillslope Cross-Section Divided Into 11 Elements on the Basis of the Measured Soil Properties.

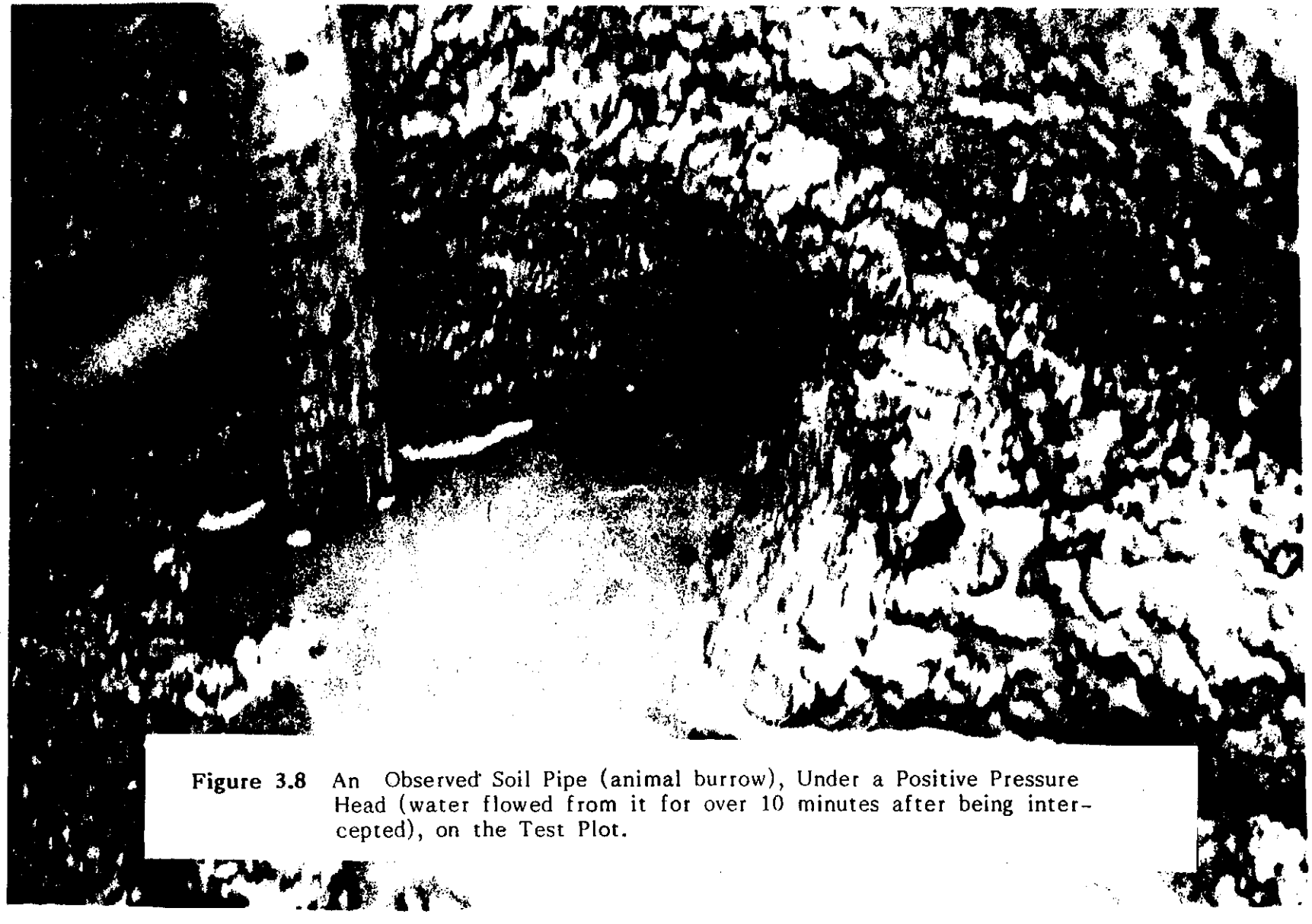

Figure 3.8 An Observed Soil Pipe (animal burrow), Under a Positive Pressure Head (water flowed from it for over 10 minutes after being intercepted), on the Test Plot.

Table 3.2 Soil Properties by Elements

Element	Rock Free Bulk Density (g/cm^3)	Rock Content (%)	g*	b*	Rock Free Saturated Water Content	Saturated Hydraulic Conductivity (cm/hr)	Number of Cores
1	1.147±.112	.61	.0812	3.015	.551±.040**	8.47 ± 2.86	9
2	1.353±.069	2.17	.0108	4.115	.487±.032	2.11 ± 3.25	6
3	1.443±.086	1.33	.0454	3.015	.461±.036	2.16 ± 3.15	12
4	1.541±.166	.64	.0318	3.404	.427±.041	2.36 ± 3.14	12
5	1.673±.098	18.1	.0318	3.404	.478±.046	3.65 ± 2.13	3
6	1.541±.166	.64	.0318	3.404	.427±.041	2.36 ± 3.14	12
7	1.518±.049	.67	.0833	4.115	.452±.022	2.57 ± 1.29	3
8	1.147±.122	17.2	.0812	3.015	.631±.088	19.2 ±20.8	8
9	1.459±.222	7.23	.1131	3.015	.440±.062	6.75 ± 8.99	10
10	1.459±.222	19.9	.1131	3.015	.479±.098	4.37 ± 6.57	18
11	1.526±.110	14.6	.1663	4.115	.499±.108	.984± 1.82	11

* Constants in Equations 2.6 and 2.7
** ± one standard deviation

from it for at least 10 minutes. In all pits many tree roots were seen in the upper 30 cm layer (Figure 3.9), which appear to break up the soil and make it more permeable. After digging through the root zone layer for the soil pits on the hillslope, water was observed running along the roots and dripping into the pit (Figure 3.9). This photograph was taken in the fall and there had been a light rain approximately 36 hours previously.

Smith (1982) observed similar properties while digging 21 pits in the nearby Field Branch watershed. He believed that the way in which these soils responded to precipitation was best described by the variable source area concept, and that water movement towards the stream was primarily by lateral subsurface flow. The A Horizon with its high noncapillary porosity and permeability is a major medium for this rapid lateral movement, while the less permeable B Horizon may initiate the lateral flow (Smith, 1982). The extent of macropores in all horizons and the extensive areas of fractured bedrock suggested to Smith that

Figure 3.9 Extensive Root Network in the Upper 30 cm Layer of the Soil Profile on the Test Plot.

turbulent flow was also a major mechanism of stormflow. He also noted that at the outcroppings of horizontal layers of coal, clay, shale and sandstone, water flows and ice formations in the winter are often observed. This observation and the movement of leaves and rocks below these outcroppings after large storms with high antecedent moisture conditions, indicates the exfiltration of lateral subsurface flow and the formation of ephemeral stream channels. These mechanisms are sufficient to explain the "flashiness" of eastern Kentucky watersheds (Smith, 1982).

3.3 INSTRUMENTATION ON THE TEST PLOT

Rainfall, soil water content, soil water potential and water table levels were measured on the hillslope near the confluence of the Little Millseat and Field Branch (Figure 3.2).

3.3.1 Rain Gauges

Four rain gauges were used on the instrumented slope and were located at the sites shown in Figure 3.5, which represent sites with varying amounts of canopy coverage. Two gauges, RG-1 and RG-2, were at stream level, while the other two, RG-3 and RG-4, were upslope. The rain gauges, designed and constructed in the Agricultural Engineering Department shop, are of the tipping bucket type (Figure 3.10) and were interfaced with a Campbell CR5 data logger with four pulse counters. The data logger counted the tips at 30 minute time intervals.

Calibration of the rain gauges was carried out in the field be dripping one liter of water through the gauges and counting tips. The average depth per tip was 0.6 mm. Several times during the course of the study they became clogged with leaves and had mechanical or electrical failure, but for the most part produced a reliable record from April 14, 1982 through December, 1982.

3.3.2 Soil Water Content

Soil water content was measured at 15 cm depth intervals in access tubes on a weekly basis using a nuclear soil moisture probe.

Figure 3.10 One of Four Tipping-Bucket (approximately 0.6 mm/tip) Rain Gauges Used to Measure Rainfall on the Test Plot.

The instrument used was a Troxler Model 3222 Depth Moisture Gauge (Figure 3.11) which has a 10 mc radiation source containing Americium-241 and a Beryllium target. Four locations were at stream level and the rest were on the hillslope as shown in Figure 3.5. Readings were taken at depths ranging from 15 to 132 cm at 15 cm increments. Access tube depths varied from 71 to 132 cm. On two occasions the source became disconnected from the instrument causing incomplete records for those two weeks. In all, over 2600 readings were taken from March 26, 1982 through December, 1982.

Nuclear soil moisture probes should be calibrated for different soils to insure correct estimates of water content. To calibrate the probe, readings were taken in an access tube and then a soil pit was dug along-side the tube to take water content samples. The gravimetric water content samples were converted to a rock-free volumetric basis by using the bulk density and rock content data from nearby soil pits and appropriate data from Smith's (1982) study. For the calibration, volumetric water contents that included rock were used because the nuclear probe measures the amount of water in a sphere approximately 30 cm in diameter surrounding the probe.

The nuclear probe calculates water contents using an internal calibration already programmed into it. The calibration curve is of the form,

$$\theta = \theta_f + \mathcal{S}(A_0 + A_1X + A_2X_2^2 + A_3X_3^3) \qquad \ldots (4.1)$$

where θ is volumetric water content, θ_f is the offset, $\mathcal{S}$ is slope, X is the ratio of the count to standard count, and the A's are constants programmed into the machine. The offset is normally set to zero and the slope to one, unless changed by the user. The normal procedure for calibration is to perform a linear regression on the predicted (as measured by nuclear probe) versus the observed (as determined gravimetrically and converted to a volumetric basis) water contents and estimate the appropriate offset and slope. However, after plotting this data a fairly large scatter was seen. This is probably due to the heterogeneous nature of the soil and the inability of the soil cores to

Figure 3.11 Troxler Model 3222 Depth Moisture Gauge Used to Measure Soil Water Content on the Test Plot on a Weekly Basis.

adequately represent the average rock contents for the different depths. Large rocks near the access tube will cause the observed water content to be greater than the predicted, because the rock content used to calculate the volumetric water content does not account for the large rock. Similarly, large voids near the access tube will cause the predicted water content to be greater than the observed.

The distribution of the calibration points was fairly evenly distributed about the standard calibration curve (slope=1 and offset=0), so it was decided not to change the calibration. This was deemed appropriate since there did not seem to be any offset, which would introduce the most error.

3.3.3 Water Table Depth

The water table depth was measured at the four locations shown in Figure 3.5; two at stream level and two upslope. Readings were taken weekly in four 50 mm access holes from June 12, 1982 through December, 1982.

3.3.4 Soil Water Pressure Head

Twenty-eight tensiometers (Figure 3.12a) were used to measure the soil water pressure head (soil water potential) at the eight locations shown in Figure 3.5. Four locations on the hillslope had three tensiometers each. Depths for the 25 mm diameter 50 mm porous cup tensiometers varied from 15 to 150 cm below the soil surface. Mercury manometers connected to the tensiometers enabled measurements to be made visually or automatically using an arrangement described by Atkinson (1978) (Figure 3.12b). All tubing connections were kept as small as possible in order to minimize response times. A nichrome wire inserted in the manometer changed resistance as the mercury level varied. This variable resistance tansducer became part of a balanced circuit and the voltage drop across it was measured (Figure 3.12b). The output, varying form 0 to 10 mV, was linear for the manometer range. The campbell data logger scanned the tensiometers at 30 minute time intervals, the same time interval used with the rain gauges.

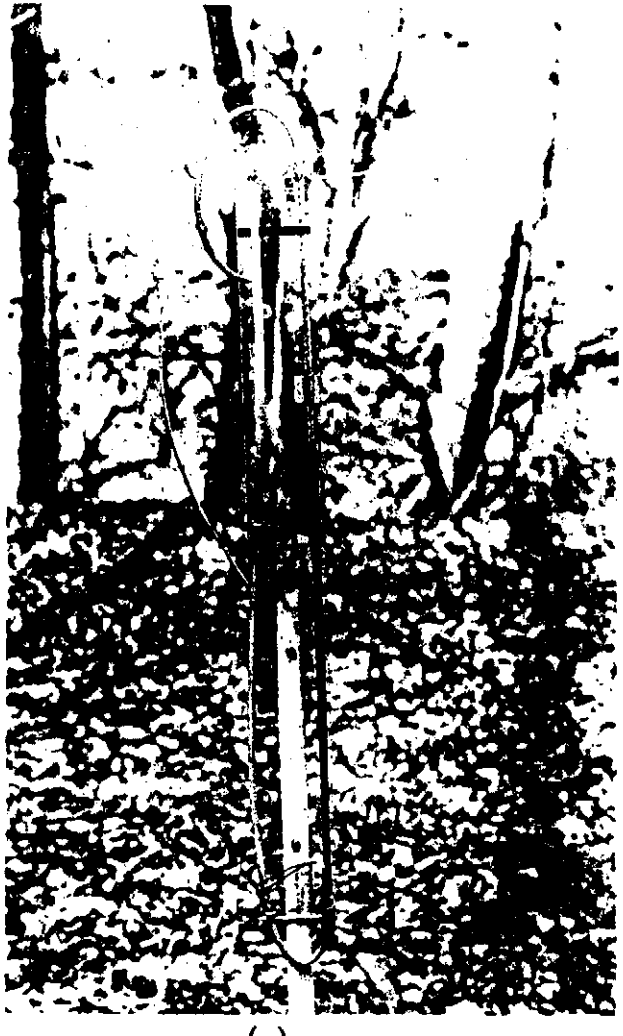

(a)

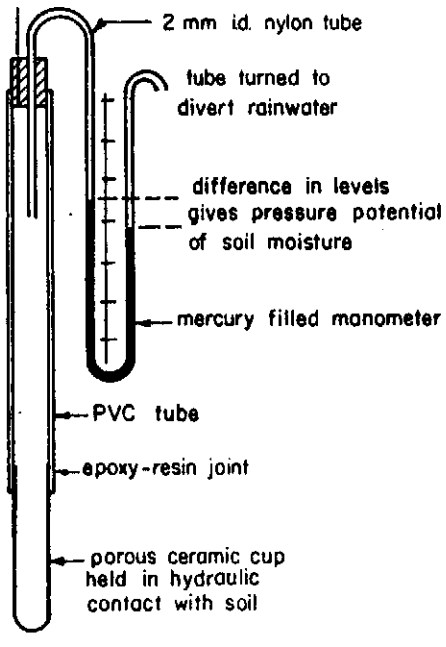

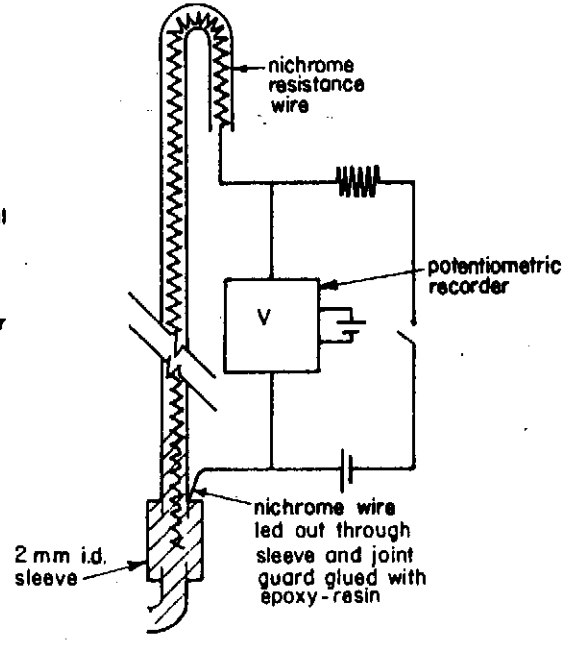

(b)

Figure 3.12 Tensiometers Used for Measuring the Soil Water Pressure Head on the Test Plot: (a) In Place in the Field; and (b) Schematic Diagram of the Recording Manometer (adapted from Atkinson, 1978).

A combination field and laboratory method was used to calibrate the tensiometers, with fairly good results. An example of one calibration curve is presented in Figure 3.13. The manometers were originally calibrated in the lab, determining a slope and intercept for each calibration curve. Once set up in the field, losses in the lines and instrumentation change the intercept, but not the slope. By simultaneously taking a manual reading of the difference in mercury levels and a reading of the voltage output, the correct intercept was calculated using the laboratory determined slope.

Instrument reliability varied greatly from tensiometer to tensiometer. Some would hold tensions for several months and others only a day or less. Poor reliability was caused in part by leaks in the tubing connections and the two access ports. Poor contact with the soil also caused problems, but was rectified by using a fine sand and silt material to seat the porous cups which were having difficulty. Electrical difficulties also plagued the tensiometers, including ground-loops in the system. Tensiometer data were collected from July 28, 1982 through December, 1982. Ground-loop errors were not fully removed until October 20.

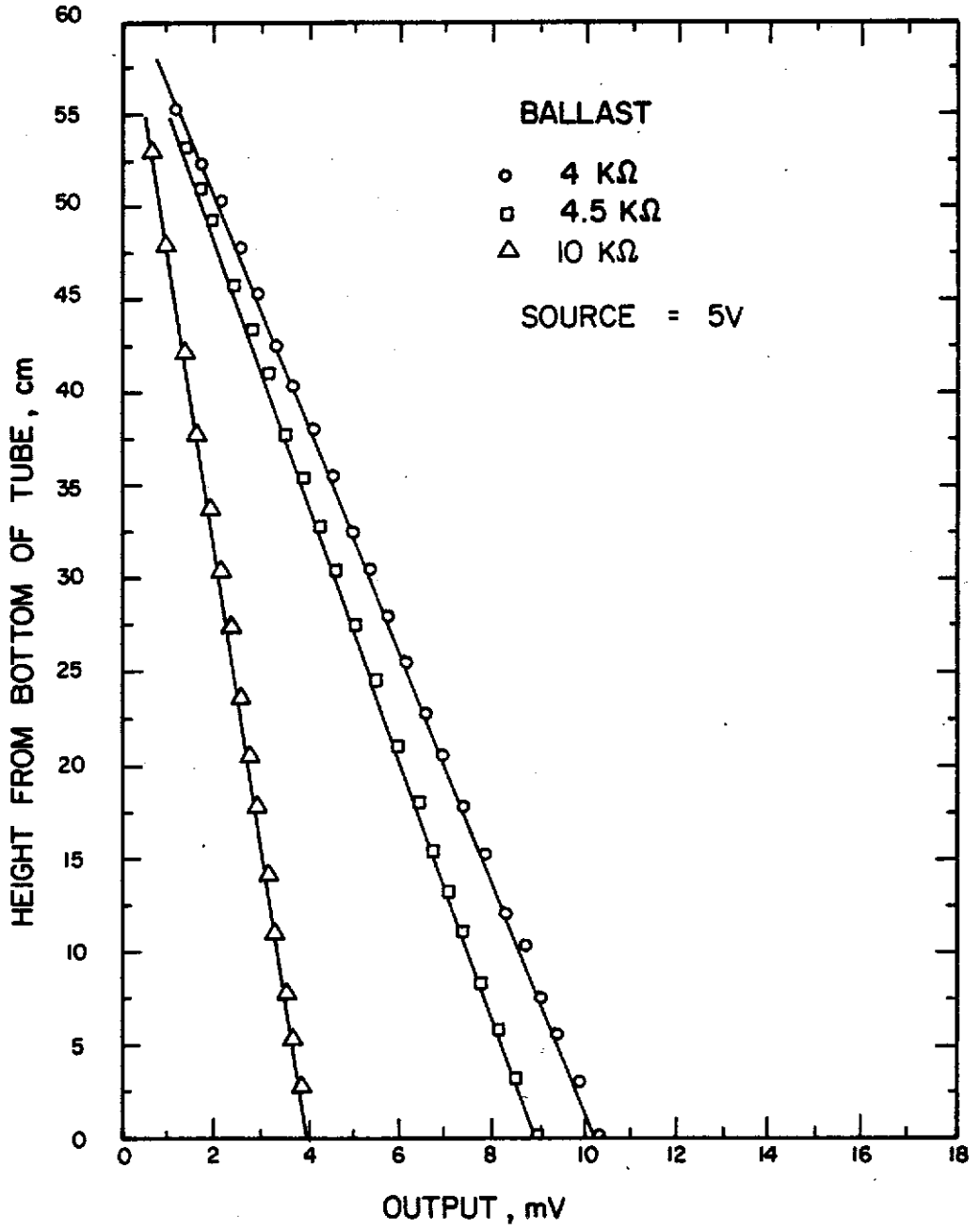

Figure 3.13 An Example of the Calibration Curves for the Recording Manometer Tensiometers Used on the Test Plot (showing the effect on the calibration curve of changing the balance resistance in the circuit).

CHAPTER 4

A DAILY MODEL FOR PREDICTING RUNOFF FROM SMALL APPALACHIAN WATERSHEDS

Within Kentucky, 116 daily-read stream-gauging stations, 123 crest stage, and 102 low-flow partial-record stations are maintained by the U.S. Geological Survey (1981) and other Federal and State agencies. In addition, a limited number of gauging stations are maintained for special purposes; for example, by the University of Kentucky for research. These gauging stations serve to monitor the flow of more than 16,000 km of flowing streams in Kentucky and are chiefly confined to larger streams and tributaries of the major river basins. It is economically impractical to gauge every stream, especially first, second, and third order streams.

One cost-effective method of determining the hydrological character of a watershed is via the use of continuous simulation models. These models predict watershed discharge (and quality) as either deterministic or stochastic functions of precipitation and other variables that are more readily and cost-effectively measured than discharge. In Kentucky, and many other parts of the United States, the majority of rainfall and runoff records are held as daily values. Many of the questions concerning the baseline hydrological behavior of watersheds can be answered using these daily data, or simple models that can predict daily streamflow.

The application and/or evaluation of a number of continuous deterministic rainfall-runoff models on watersheds in Kentucky has been reported, including Haan's Water Yield Model (Haan, 1976), the TVA Daily Streamflow Simulation Model (Nuckols and Haan, 1979), and the Stanford Watershed Model (Ross, 1970). The complexity of these rainfall-runoff models and their input data requirements vary, the internal time step in the model being an important factor. Generally, the smaller the time step, the greater the complexity of the model and the greater the input data requirements. Haan's model predicts

monthly watershed yield and is the simplest of the three models. The TVA model (TVA, 1972) predicts daily streamflow, while the Stanford model (Crawford and Linsley, 1966) predicts hourly streamflow. Nuckols and Haan (1979) reported poor results with the TVA Daily Streamflow Simulation Model in Kentucky. In tests of rainfall-runoff models of varying complexity, Haef (1981) showed that simple models can give satisfactory results. He could not prove that complex models give better results than simpler ones. However, he did demonstrate that neither the simple nor the complex models were free from failure in certain cases.

This chapter presents the development and validation of a simple continuous rainfall-runoff model, requiring a minimum of input data, that is suitable for predicting baseline streamflow from small steep-sloped forested Appalachian watersheds on a daily basis. The model was validated on the Little Millseat watershed.

4.1 DESCRIPTION OF THE MODEL

The model, schematically illustrated in Figure 4.1 and mathematically formulated in Table 4.1, is a conceptual lumped-parameter representation of the rainfall-runoff process. In this model, a watershed is idealized as consisting of a series of interconnected water storages with the in- and outflow representing actual physical processes. These processes are described using both physically and empirically based equations (Table 4.1). The concepts used in the model are common to many daily rainfall-runoff models including those of BROOK (Federer and Lash, 1978; Federer, 1982), BOUGHTON (Boughton, 1966, 1968), and MONASH (Porter and McMahon, 1971, 1976). These 3 models are the basis of the watershed model described herein.

The model consists of three conceptual water stores or zones - the Interception Zone; the Soil Zone; and the Groundwater Zone - and has 13 parameters and one function (FCAN) that characterize the watershed. Definitions of these parameters are given in Table 4.2.

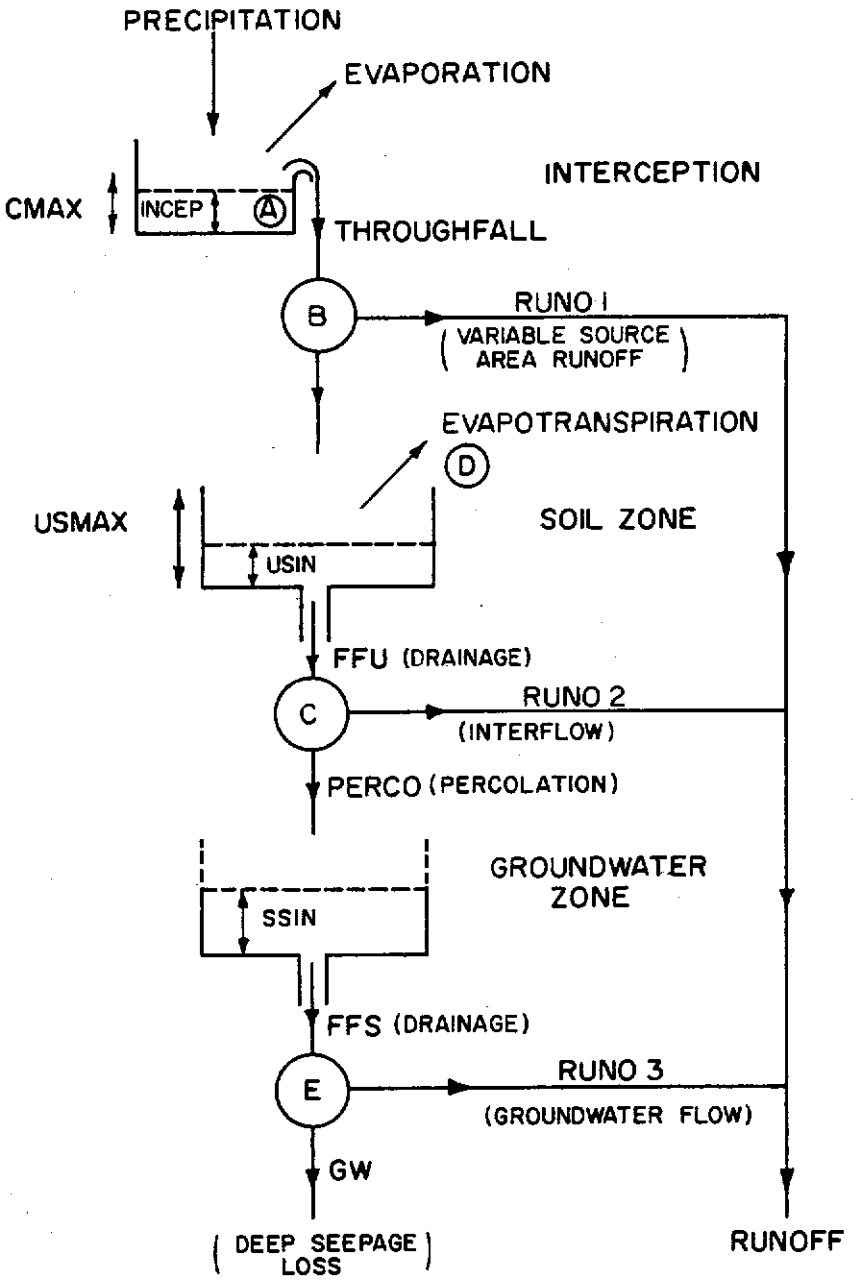

Figure 4.1 Schematic Flow Diagram of the Daily Watershed Model.

Table 4.1 Watershed Model Function Descriptions

FUNCTION	EQUATION	FUNCTION SCHEMATIC	PROCESS
A	CMAX = CEPMAX * FCAN	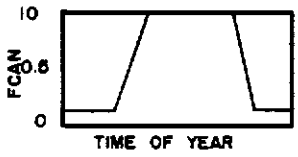	INTERCEPTION
B	RUNOI = PB * PRECIP INFIL = (I-PB) * PRECIP $PB = FSTP + PC\,e^{PAC * (USIN/USMAX)}$	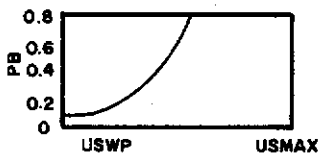	VARIABLE SOURCE AREA RUNOFF
C	RUNO2 = KI * FFU PERCO = (I-KI) * FFU $FFU = FU * \left(\frac{USIN}{USMAX}\right)^{KU}$	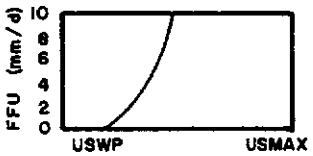	SOIL ZONE DRAINAGE & INTERFLOW
D	AEVAP = EVAP (EVAP < PE) = PE (EVAP > PE) $EVAP = \frac{(USIN - USWP)}{ERATE}$	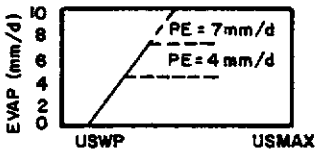	SOIL ZONE EVAPOTRANSPIRATION
E	RUNO3 = K2 * FFS GW = (I-K2) * FFS $FFS = FS * (SSIN)^{KS}$	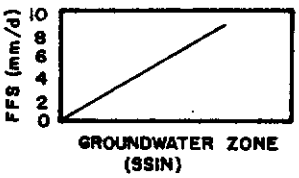	GROUNDWATER ZONE SEEPAGE & GROUNDWATER FLOW

Since snow is an insignificant form of precipitation in eastern Kentucky (Springer and Coltharp, 1978), the model does not account for snowfall or snowmelt runoff. However, the model could be easily modified to include a degree-day approach for representing this process.

Precipitation is added to the interception store, and any excess (throughfall) becomes available for infiltration or runoff from the saturated source areas. The capacity of the interception store (CMAX) is a function of the maximum interception storage capacity (CEPMAX) and the degree of canopy development (FCAN). CEPMAX is dependent on the type of vegetation and the maximum leaf- area and stem-area indices, and FCAN reflects the annual canopy growth characteristics and stem-area index. The form of the FCAN-time relationship is shown in Table 4.1. Evaporation from the interception store is assumed to occur at the potential rate.

The size of the saturated source area increases exponentially as the Soil Zone wets up (i.e., as USIN increases). This source area consists of the stream area (FSTR) and the near-stream saturated zones that expand and contract in response to precipitation. This process is represented by the empirical equation proposed by Federer and Lash (1978) and is represented by Function B (variable source area process) in Table 4.1. Overland flow from the saturated source area is subtracted from the precipitation excess, and the remainder represents the infiltration into the Soil Zone. Infiltration rates in steep-sloped forested watersheds of the Appalachian region are very high and traditional Hortonian infiltration (Horton, 1933) rarely occurs. The infiltration rates were therefore assumed to be infinite.

Drainage from the Soil Zone is dependent on the water content or water volume of the Soil Zone (USIN) and increases exponentially as the water content increases. Campbell (1974) proposed a simple method of determining the hydraulic conductivity as a function of water content from the soil water retention curve. The method assumes that, and is only valid if, the soil water retention function

Table 4.2 Model Parameter Descriptions and Values

Process/Zone	Parameter	Definition	Parameter Value (Little Millseat Watershed)
Interception	CEPMAX	Maximum interception capacity (mm)	2.02
	FCAN	Canopy development function: modifies CEPMAX for time of year (i.e. canopy development)	See Table 4.1
Variable Source Area Runoff	FSTR	Fraction of watershed always contributing to direct runoff (i.e. area of stream)	0.05 (0.05)
	PAC	Source area exponent	39.295 (40)**
	PC	Source area coefficient	4.11×10^{-6} (4.1×10^{-6})**
Soil Zone	USMAX	Soil zone thickness (mm)	1087 (1070)
	KU	Soil water conductivity exponent (KU=2b+3, where -b is the slope of a log-log plot of the soil water retention curve)	11.810 (11.467)
	FU	Soil water conductivity coefficient	1.49×10^{7}
	K1	Fraction of Soil Zone drainage becoming interflow	1.0 (1.0)
Evapotranspiration	USWP	Wilting point water content (input as % by volume, used as mm of water in program)	124 (130) 11.44% (12.14%)
	ERATE	Evapotranspiration rate coefficient	27.4
Groundwater Zone	FS	Groundwater exponent (1 for linear groundwater recession)	-*
	KS	Groundwater recession constant	-*
	K2	Fraction of groundwater drainage becoming baseflow	-*
OTHER VARIABLES			
	CMAX	Actual interception capacity (mm)	
	USIN	Actual soil water volume (mm)	
	SSIN	Actual groundwater volume (mm)	
	PB	Fraction of water contributing to direct runoff	

* Groundwater Zone does not exist in the Little Millseat watershed.

Values in parentheses are the initial parameter estimates prior to optimization

** Values used in BROOK model (Federer and Lash, 1978) for Hubbard Brook Watershed

can be described by the relationship:

$$h = a\,\theta^{-b} \qquad \ldots .(4.1)$$

where h is the pressure head, θ is the volumetric water content (USIN/USMAX), and a and b are constants. This form of the equation was proposed by Gardner et al. (1970). This relationship is only valid if the water retention function plots as a straight line on a log-log scale. If Equation 4.1 is a valid representation of the water retention curve, then Campbell's equation can be used to estimate the hydraulic conductivity. Campbell's equation is:

$$FFU = FU\,\theta^{2b+3} \qquad \ldots .(4.2)$$

where FFU is the hydraulic conductivity (Soil Zone drainage rate), FU is a coefficient, and the other variables are as previously defined. The function is the same as the function describing Function C in Table 4.1. The water draining from the Soil Zone is divided between interflow (Subsurface Storm Flow) and percolation to the Groundwater Zone. This division is assumed to be a fixed fraction, K1, of the total drainage, FFU.

Evapotranspiration from the Soil Zone is limited by either the atmospheric demand (potential evapotranspiration) or by the plant available water (USIN-USWP, where USWP is the wilting point water content). The evapotranspiration is equal to the lesser of either the available water divided by a rate constant (ERATE) or the potential evapotranspiration (Function D, Table 4.1). In the model potential evapotranspiration is estimated from the input daily pan evaporation. Many techniques for estimating potential evapotranspiration have been proposed (for example; Penman, 1963; Bowen, 1926; Jensen and Haise, 1963) and could be used if the required input data were available. The model is not sensitive to the natural daily variation of potential evapotranspiration, but it is sensitive to the long term average evapotranspiration rates over periods of months and years.

Groundwater movement is modeled by a groundwater store with no fixed capacity (SSIN). Groundwater recharge occurs by percolation from the Soil Zone to the Groundwater Zone. Water is subsequently lost from the store as baseflow to the stream (groundwater flow) or deep seepage. Deep seepage models the loss of water to underlying aquifers and the ungauged water flowing beneath the river bed. The normal groundwater storage-discharge relationship used in this type of rainfall-runoff model is linear, but Porter and McMahon (1976) argue that within many watersheds more than one groundwater source or storage exists, leading to nonlinear behavior of the groundwater flow component. A nonlinear discharge function is therefore used in the model (Function E, in Table 4.1). The groundwater drainage is linearly divided (K2) between baseflow and deep seepage.

A computer listing of the main computational algorithms of the model (subroutines CANOPY and WATER) is presented in Appendix A. A complete listing of the program, including input, output, summary, statistical analysis, and parameter optimization routines is available from the Principal Investigator.

4.2 RESULTS

A split-record technique was used to evaluate the rainfall-runoff model. One section of the 6½ years of available record was used to calibrate the model (August 1971 to December 1974), while the remainder was used to independently evaluate model performance (January 1975 to December 1977). The hydrological and meteorological data used by the model and used to validate the model included daily precipitation, daily pan evaporation and mean daily streamflow for the Little Millseat watershed. The characteristics of the Little Millseat watershed and the precipitation and streamflow measuring instrumentation were described in Chapter 3. Daily evaporation measurements, in the form of pan evaporation data, were obtained from Buckhorn Reservoir in Perry County, Kentucky, that is located about 30 km southwest of the watershed.

The input parameters of the model were first estimated from the physical characteristics of the watershed described earlier. These initial estimates are shown in parentheses in Table 4.2. Individual parameters and groups of parameters were then adjusted so that the predicted and observed hydrographs showed good agreement. It was found that a visual comparison of the observed and predicted hydrographs, although subjective in nature, was the most effective means of optimizing the model's parameters. Finally, the steepest ascent method of automatic optimization (Boughton, 1968) was used to refine the parameter set. The sum of squares of the errors in the daily flows was the objective function for this optimization. The final parameter set is presented in Table 4.2. From this table it can be seen that the limited optimization produced very little change in the parameter set. The main effect of the optimization was to modify the peak flows, and determine the appropriate values of CEPMAX and FU, for which little information was initially available. An example of the output from the computer program is presented in Appendix A. Included in this output is a summary of the input parameters, initial conditions, and the daily, monthly, and annual simulated and predicted discharges from the Little Millseat watershed for 1976.

Evaluation of the standard of simulation achieved by a watershed rainfall-runoff model is difficult because streamflow provides a large amount of data of a range of types (Weeks and Hebbert, 1980), and no one test will satisfactorily evaluate all types (e.g. peak flow, low flow, mean flow, etc). Therefore, a variety of statistical and graphical tests is presented so that the reader may evaluate the model's performance. Many of these statistical and graphical tests are described by Aitken (1973), WMO (1974), Moore and Mein (1976), and Weeks and Hebbert (1980), and the reader is referred to these citations for more complete details of the methods.

Tables 4.3 and 4.4 present the annual summary and the optimization/test period summaries, respectively, on a monthly and daily flow basis. Graphical comparisons of the observed and predicted

monthly runoff, the residual mass curves for the optimization and test periods, and the daily flow duration curves are presented in Figures 4.2, 4.3, and 4.4, respectively. Figure 4.5 presents the annual hydrograph of the observed and predicted daily flows for 1976. This example represents the worst simulation for the test period in terms of the coefficient of determination of the daily flows (r^2 = 0.724), and the predicted peak flows.

4.3 DISCUSSION OF RESULTS

The results show that there is no significant difference in the standard of simulation in the optimization and test periods of the record.

The mean flow and the standard deviations of the observed and predicted monthly flows are in good agreement on an annual basis (Table 4.3) and during the optimization and test periods (Table 4.4).

Table 4.3 Annual Observed and Predicted Flow Summary

Year		Mean Daily Flow (cms x 10^{-3})	Standard Deviation (cmsd x 10^{-3}) Monthly	Daily	Coefficient of Determination Monthly	Daily
Optimization Period						
1971**	1*	8.67	160.3	19.27	0.619	0.637
	2	11.88	138.9	11.77		
1972	1	26.81	907.3	61.55	0.920	0.719
	2	24.84	781.7	40.39		
1973	1	13.43	353.6	33.38	0.891	0.812
	2	17.32	386.5	28.08		
1974	1	27.55	745.0	64.44	0.956	0.846
	2	25.97	677.7	53.34		
Test Period						
1975	1	24.00	812.1	52.30	0.962	0.848
	2	24.42	693.6	39.65		
1976	1	17.26	432.0	34.73	0.933	0.724
	2	17.28	412.9	34.78		
1977	1	18.22	378.5	40.35	0.857	0.854
	2	15.43	264.5	21.76		

* 1 Observed; 2 Predicted

** Partial year only (August - December)

Table 4.4 Statistical Comparison of Model Performance

Statistic			Optimization Period		Test Period	
			Monthly	Daily	Monthly	Daily
Mean*	Observed	$(\overline{\theta})$	636.4	20.89	603.5	19.82
	Predicted	(P)	647.9	21.26	579.8	19.04
Standard Deviation*	Observed	(σ_o)	686.2	52.40	565.1	43.15
	Predicted	(σ_p)	600.6	39.73	490.9	29.20
Coefficient of Variation	Observed	(C_{v_o})	1.078	2.508	0.936	2.177
	Predicted	(C_{v_p})	0.927	1.868	0.847	1.533
Standard Error of Estimates*		(SE)	169.4	18.4	132.2	12.92
Coefficient of Determination		(r^2)	0.920	0.785	0.927	0.805
Coefficient of Efficiency		(E)	0.913	0.769	0.917	0.755
Residual Mass Curve Coefficient		(R)	0.782	0.794	0.868	0.859
Coefficient of Variation of Residuals		(C_o)	0.314	1.206	0.266	1.076
Ratio of Relative Error to the Mean		(R_m)	0.018	0.018	-0.039	-0.039
Maximum Error of Model		(K)	0.260	0.734	0.228	0.700
Sign Test		(Z)	-	3.518	-	2.183

*All flow values are in cmsd x 10^{-3}

$$\overline{\theta} = \frac{\Sigma\, \theta_i}{n}$$

$$\sigma_o = \left[\frac{\Sigma(\theta_i - \overline{\theta})^2}{n-1}\right]^{1/2}$$

$$C_{v_o} = \sigma_o / \overline{\theta}$$

$$SE = \sigma_o\,(1 - r^2)^{1/2}$$

$$r^2 = \frac{[\Sigma(\theta_i - \overline{\theta})\,(P_i - \overline{P})\,]^2}{\Sigma(\theta_i - \overline{\theta})^2\;\Sigma(P_i - \overline{P})^2}$$

$$E = \frac{\Sigma(\theta_i - \overline{\theta})^2 - \Sigma(\theta_i - P_i)^2}{\Sigma(\theta_i - \overline{\theta})^2}$$

$$R = \frac{\Sigma(D_o - \overline{D}_o)^2 - \Sigma(D_o - D_p)^2}{\Sigma(D_o - \overline{D}_o)^2}$$

$$C_o = \left[\frac{\Sigma(P_i - \theta_i)^2}{n}\right]^{1/2} / \overline{\theta}$$

$$R_m = \frac{\Sigma(P_i - \theta_i)}{n\theta}$$

$$K = C_o \,/\, \left[\frac{(n-1)}{n} C_{v_o}^2 + 1\right]^{\frac{1}{2}}$$

θ_i = Observed flow

P_i = Predicted flow

D_o = Departure from mean for observed residual mass curve

D_p = Departure from mean for predicted residual mass curve

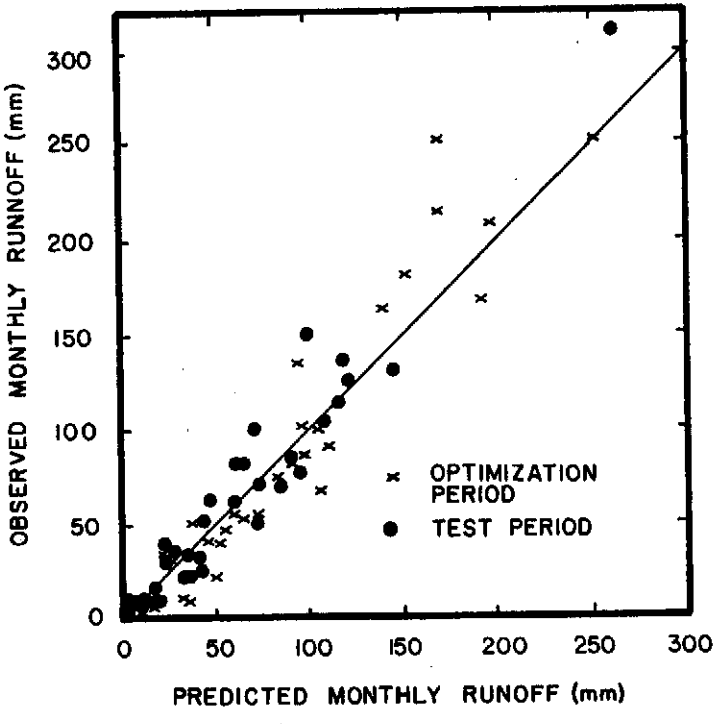

Figure 4.2 Observed and Predicted Monthly Runoff for the Optimization and Test Periods.

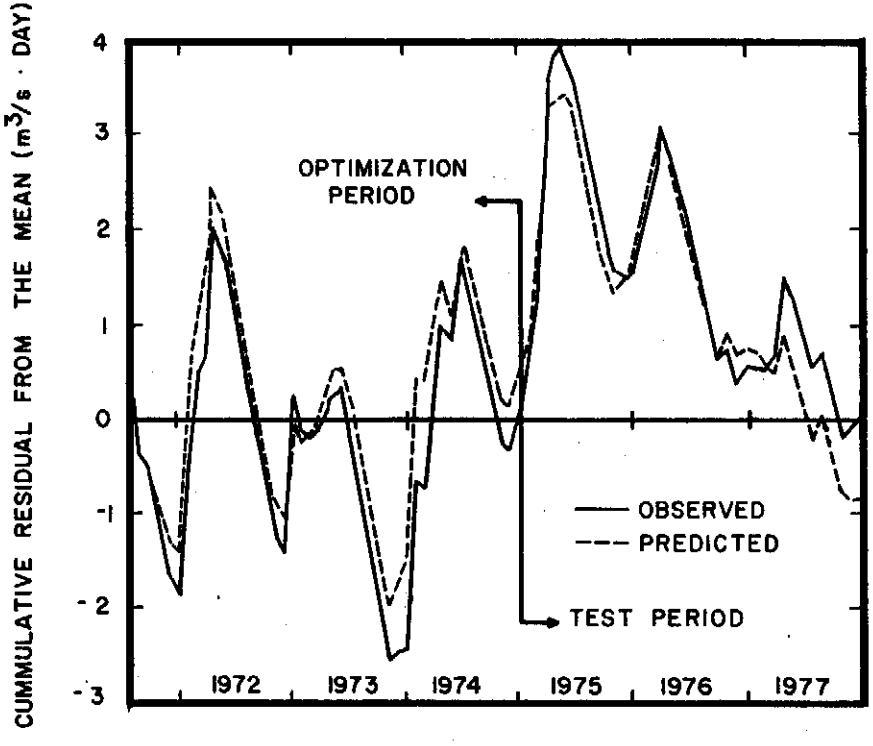

Figure 4.3 Observed and Predicted Residual Mass Curves for the Optimization and Test Periods.

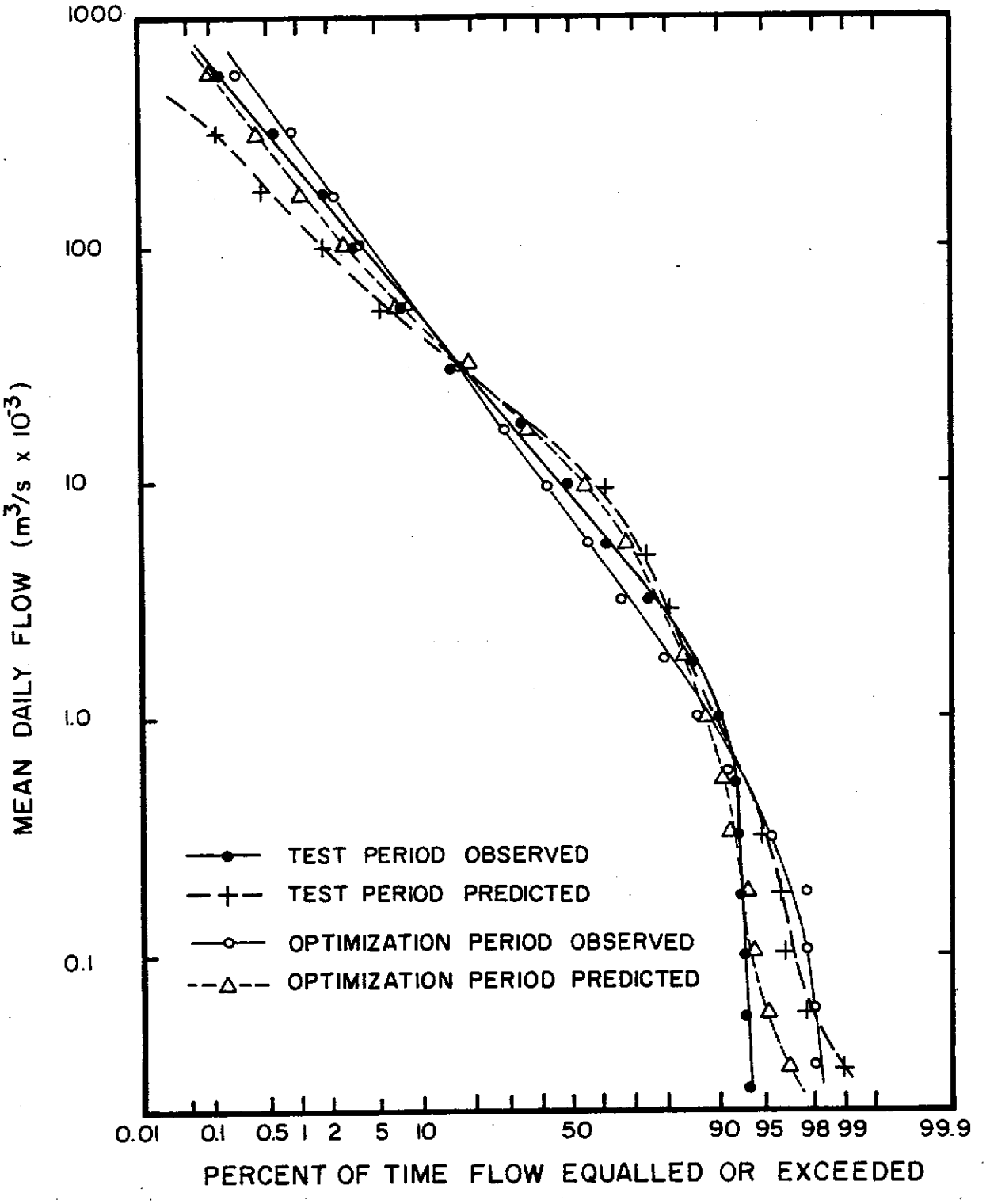

Figure 4.4 Observed and Predicted 1-Day Flow Duration Curves for the Optimization and Test Periods.

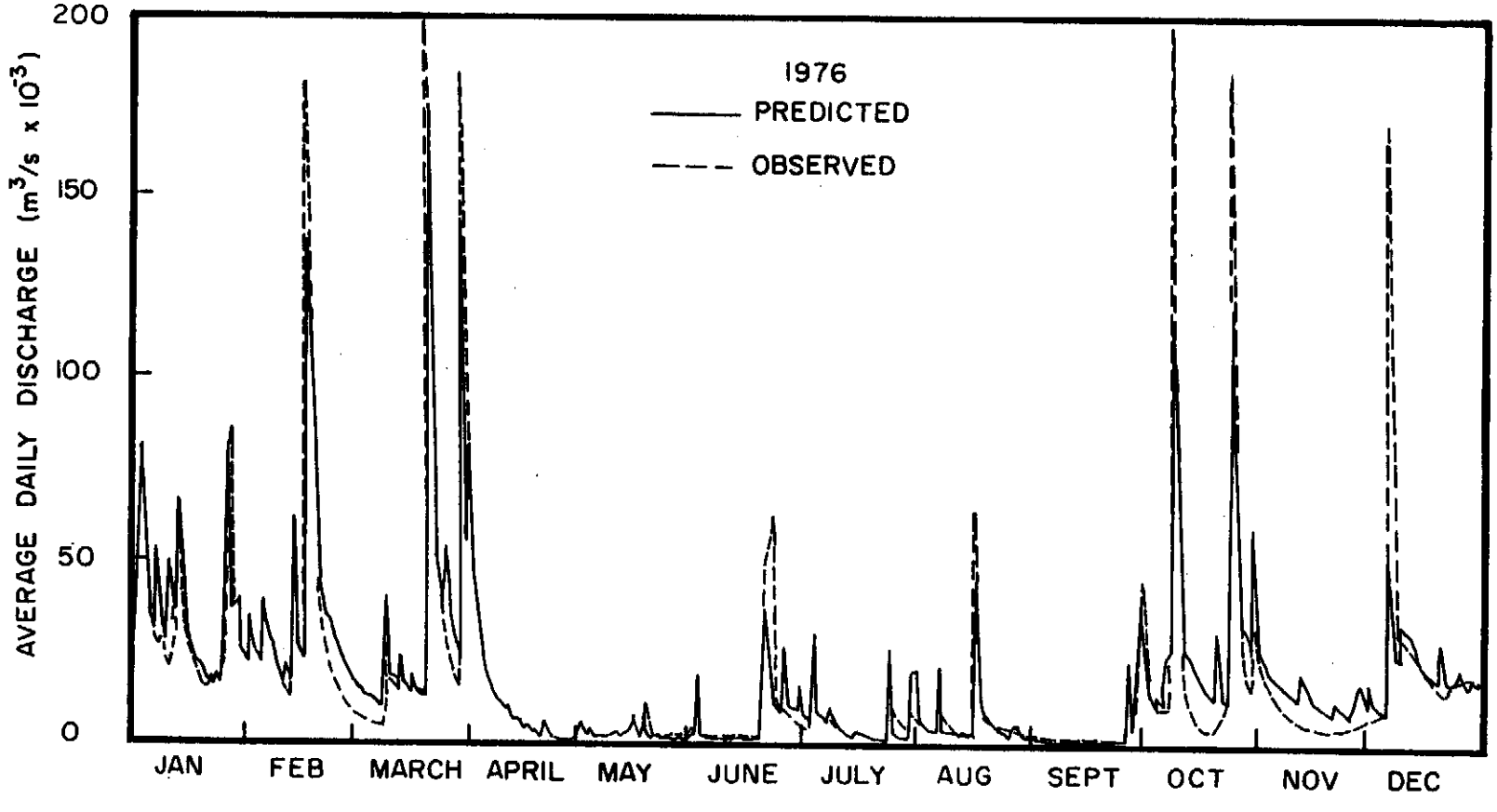

Figure 4.5 Annual Hydrographs of the Observed and Predicted Daily Flows on the Little Millseat Watershed for 1976.

However, the standard deviations of the daily flows predicted by the model are significantly lower than the observed (Tables 4.3 and 4.4). For example, the coefficient of variation (standard deviation/ mean) of the observed flows are 2.508 and 2.177 for the optimization and test periods, respectively, whereas those for the predicted flows are 1.868 and 1.533, respectively. Hence, the observed flows exhibit greater variability than the predicted flows.

The coefficients of determination (r^2) of the monthly and daily flows are uniformly high, averaging about 0.92 and 0.80, respectively. However, neither the mean, standard deviation, or coefficient of determination can indicate if there is bias, or systematic errors, in the predicted flows. Aitken (1973) indicated that the coefficient of efficiency (E) could be used to detect bias. If the coefficient of efficiency is less that the coefficient of determination then bias is indicated. Table 4.4 shows that in all cases the coefficient of efficiency is slightly less than the coefficient of determination, indicating a small bias in the model. The sign test (Weeks and Hebbert, 1980; Aitken, 1973) can also be used to detect systematic errors. The technique is based on the number of runs of residuals of the same sign that the data set exhibits. The expected number of runs is normally distributed, and a Chi-square test indicates systematic errors. If the magnitude of the normalized variate (Z in Table 4.4) is greater than 1.96, then the number of runs is significantly different from that expected for random errors at the 0.05 level of statistical significance. Table 4.4 shows that $|Z| > 1.96$ for the daily flows during both the optimization and test periods, thus indicating a small amount of bias in the model. This finding is consistent with the comparison of the coefficients of determination and efficiency.

Weeks and Hebbert (1980) described the maximum error of the model statistic (K in Table 4.4) and showed that it can be interpreted as being equivalent to a constant error in the results. Table 4.4 shows that the maximum error of the model ranges from 23 to 26% for the monthly flows and 70 to 73% for the daily flows. As expected, the

daily flows exhibit a relatively high error. The monthly predicted and observed runoff (Figure 4.2), the residual mass curve (Figure 4.3), and the daily flow duration curves (Figure 4.4) all show very good agreement between the predicted and observed flows. The residual mass curve coefficient (R) measures the relationship between individual flow events (Aitken, 1973). The residual mass curve coefficients are reasonable high, averaging about 0.79 and 0.86 for the optimization and test periods, respectively.

During the period of record, 1971 to 1977, the maximum observed peak daily flow was 0.837 m^3/s, and the corresponding peak predicted flow was 0.834 m^3/s. Generally, however, the extreme peaks were underestimated by the model, as is evident from an examination of the flow duration curves for probabilities of occurrence of less than about 1%. Figure 4.5 shows that the hydrograph recessions and the timing of the peak flows are modeled very well. These results, plus the steepness of the flow duration curves, indicate that the model represents the "flashy" behavior of the watershed very well. This "flashy" behavior is characteristic of the streams in Robinson Forest (Springer and Coltharp, 1978), and the Appalachian region in general.

4.4 CONCLUSIONS

A rainfall-runoff model was developed for predicting daily runoff from steep-sloped forested Appalachian watersheds. The model was validated on the Little Millseat watershed located in Eastern Kentucky, using a split-record technique. The initial estimates of the model parameters, determined from the physical characteristics of the watershed, were very close to the optimized values, indicating the physical significance of their values.

The results show very good agreement between the predicted and observed flows, and demonstrate the ability of the model to predict the "flashy" response of the watershed. The statistical and graphical comparison of the observed and predicted flows indicate a slight bias, or systematic error, in the predicted flows.

CHAPTER 5

SIMULATION OF DRAINAGE FROM A SLOPING SOIL BED

Hewlett (1961) and Hewlett and Hibbert (1963) constructed a series of concrete lined soil troughs filled with a reconstructed forest soil (C Horizon of a Halewood sand loam) to study the drainage characteristics (subsurface flow) of steep-slope segments of forested watersheds at the Coweeta Hydrological Laboratory in western North Carolina. These soil troughs were constructed at a slope of about 40%, which is similar to the natural slope of the Coweeta watershed. The Coweeta study is of practical interest because it provides data that can be used to evaluate the ability of subsurface flow models to simulate porous media flow in a shallow soil overlying a steeply sloping impermeable bed. This physical situation is similar to that found in many forested watersheds in the Appalachian region.

Because the soil was mixed and compacted in the bed of the soil troughs, the effects of macropores such as root holes, worm holes, and animal burrows cannot be evaluated by analyzing Hewlett's data. Hewlett's results are not directly applicable to the actual runoff process in the field, since it has been demonstrated that pipe flow through macropores is a significant mechanism in such cases. The comparison is only valid for hillslopes with no macropores, such as newly reclaimed lands, or in the analysis of the portion of subsurface flow that occurs within and through the soil matrix in steep forested watersheds.

Water movement in homogeneous soils with no macropores is the simplest physical subsurface flow system to represent mathematically. Therefore, use of Hewlett's experimental discharge data from the instrumented soil troughs at Coweeta (Hewlett, 1961; Hewlett and Hibbert, 1963) is a logical place to begin testing and/or developing and validating physically based models of subsurface flow, since Hewlett's system represents the simplest "ideal" condition.

This chapter examines four classes of subsurface flow models (2-D Richards, 1-D Richards, kinematic wave, and simple storage models) using the discharge data and soil properties measured by Hewlett (1961) and Hewlett and Hibbert (1963) at the Coweeta Hydrological Laboratory in western North Carolina. These models represent a range of mathematical sophistication in describing subsurface flow, with the 2-D Richards model being the most sophisticated, and the simple storage models being the least sophisticated. The 2-D Richards, 1-D Richards, and kinematic wave models were developed by other researchers and are briefly described in Chapter 2. Two types of storage models, involving different assumptions were developed by the authors for this study (kinematic storage model and Boussinesq storage model) and are described in this chapter.

5.1 THE COWEETA EXPERIMENT

A series of inclined soil troughs were built at the Coweeta Hydrological Laboratory, designed to approximate segments of natural watersheds in the southern Appalachians (Hewlett, 1961; Hewlett and Hibbert, 1963). Published data from the third soil trough were used to evaluate the four types of subsurface flow models. This soil trough consisted of a 0.92 x 0.92 x 13.72 m concrete trough constructed on a 40% slope (Figure 5.1) and was filled with natural soil excavated from nearby. Instrumentation included tensiometers, piezometers and access tubes for nuclear moisture readings. Outflow was measured using a water level recorder in a tank at the base of the trough. The soil was soaked using sprinklers, covered with plastic to prevent evaporation, and then allowed to drain.

The physical characteristics of the soil used in the trough are shown in Table 5.1. The soil water characteristic curve measured by Hewlett (1961) is presented in Figure 5.2. Three approximations of the measured soil water characteristic are also plotted in this figure, and these will be discussed later.

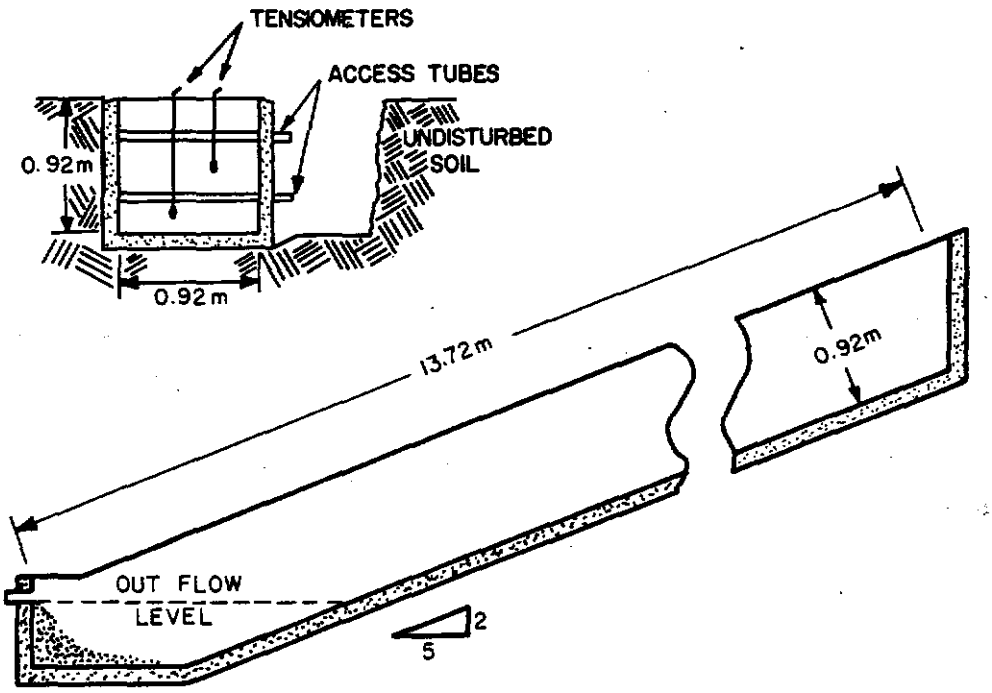

Figure 5.1 Physical Layout of Hewlett (1961) and Hewlett and Hibbert (1963) Soil Troughs, at the Coweeta Hydrological Laboratory, North Carolina

Table 5.1 Physical Characteristics of the Soil Used in Hewlett's Trough (from Hewlett, 1961)

Soil Characteristics	Mean	Std. Dev.
Bulk density in original position (g/cm^3)	1.33	0.06
Bulk density when packed in model (g/cm^3)	1.35	0.07
% water content by weight when packed	18.0	1.00
% water content by volume when packed	23.0	2.10
% water content by volume at saturation	49.0	1.50
% water content by volume under a -40 cm pressure head	36.0	1.30
% water content by volume under a -69 cm pressure head	32.0	1.60
% sand*	60	-
% silt*	18	-
% clay*	22	-

* Measured by the Bouyoueos method of hydrometer analysis.

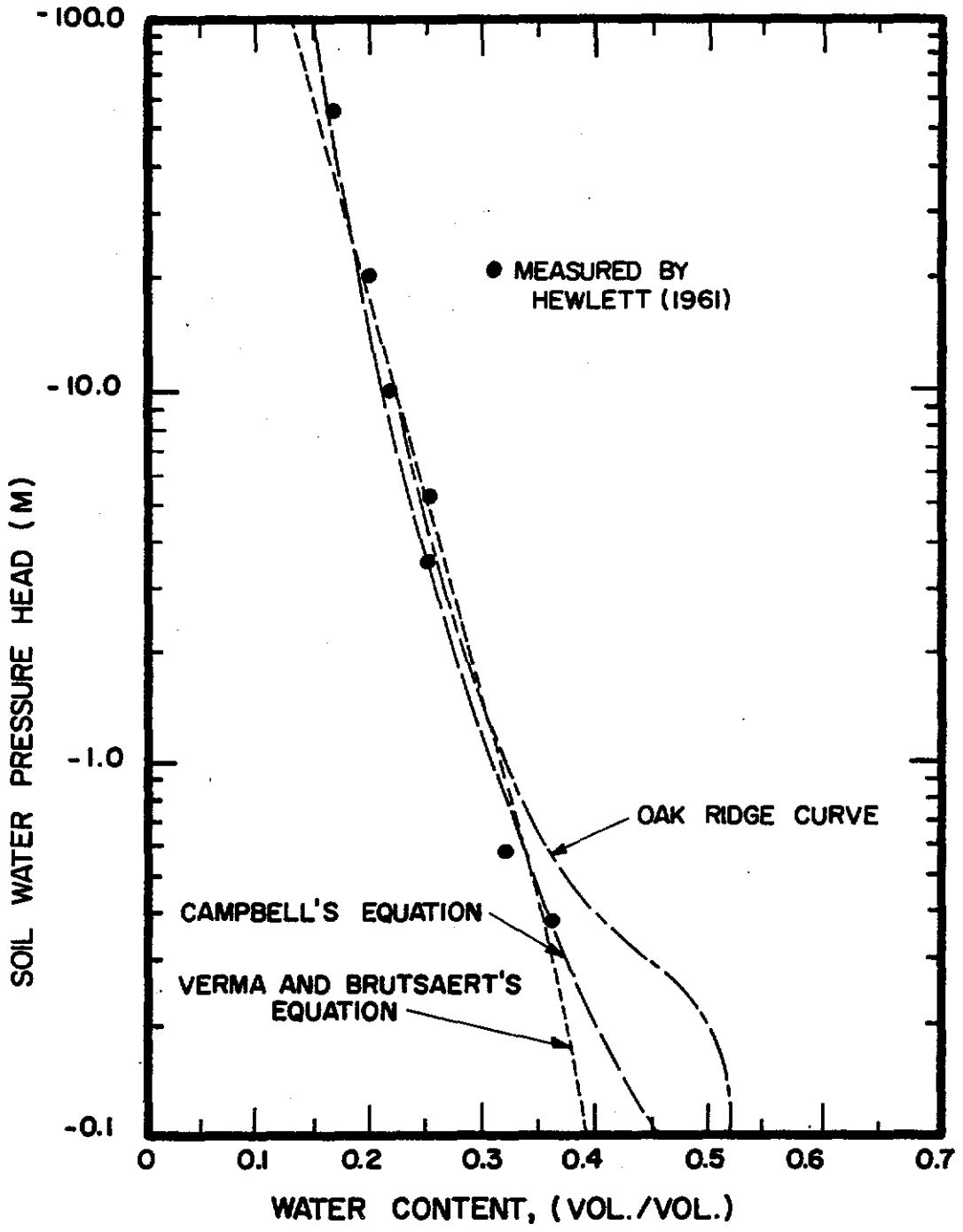

Figure 5.2 Soil Water Characteristic Curve for the C Horizon Halewood Sand Loam Used in the Soil Troughs.

The discharge hydrograph from the soil trough measured by Hewlett and Hibbert is presented in Figures 5.9 through 5.14 (compared to the simulation results). Seventy-six percent of the drainage occurred in the first 5 days, 19% in the next 45 days, and 5% occurred in the last 95 days (Hewlett and Hibbert, 1963). The discharge hydrograph suggests that saturated flow dominated during the first 1½ days to 5 days, and unsaturated flow dominated thereafter. Tensiometer data showed that the entire profile was unsaturated by the fifth day except for the saturated zone at the outlet.

In the following analysis it was assumed that steady state conditions existed prior to the beginning of drainage. The discharge hydrograph, as measured by Hewlett, therefore represents the recession limb of a hydrograph with time measured from the cessation of precipitation.

5.2 DESCRIPTION OF THE SUBSURFACE FLOW MODELS AND INITIAL CONDITIONS

5.2.1 Two-Dimensional Finite Element Models Based on Richards' Equation

A 2-D finite element saturated-unsaturated flow model developed by Nieber (1979) was obtained and applied to the Coweeta data described above. The Oak Ridge National Laboratory developed a finite element saturated-unsaturated flow model similar to Nieber's and used the Coweeta data in the process of validating their model (Reeves and Duguid, 1975). The published results of the Oak Ridge model simulation are included herein for comparison to Nieber's model.

5.2.1.1 Oak Ridge Model

The Oak Ridge 2-D model uses quadrilateral finite elements and the Galerkin method of residuals to solve Richards' equation (Equation 2.12) for transient saturated-unsaturated flow. Reeves and Duguid (1975) used a finite element mesh consisting of 612 elements and 690 nodes to describe the Coweeta soil trough (Figure 5.3). The sand, gravel and rock at the outlet was neglected and seepage was allowed from a height of 0.46 to 0.53 m on the vertical face AD.

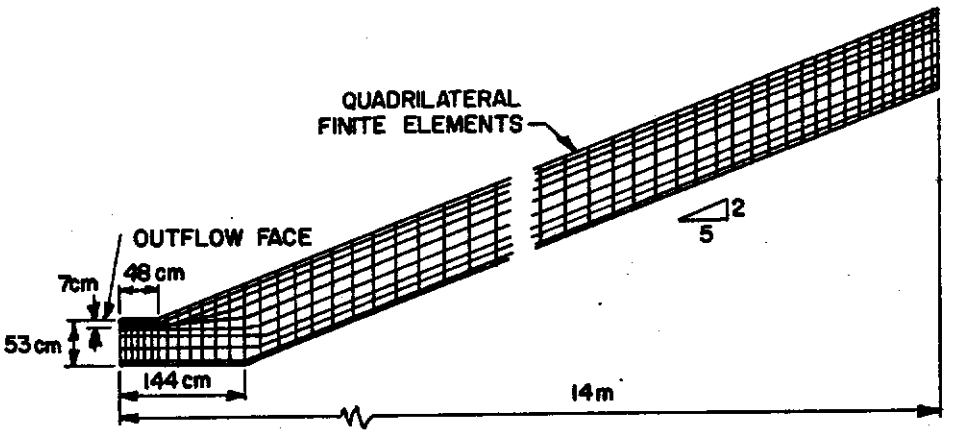

Figure 5.3 Finite Element Discretization of Hewlett's Soil Trough for the 2-D Oak Ridge Model (from Reeves and Duguid, 1975).

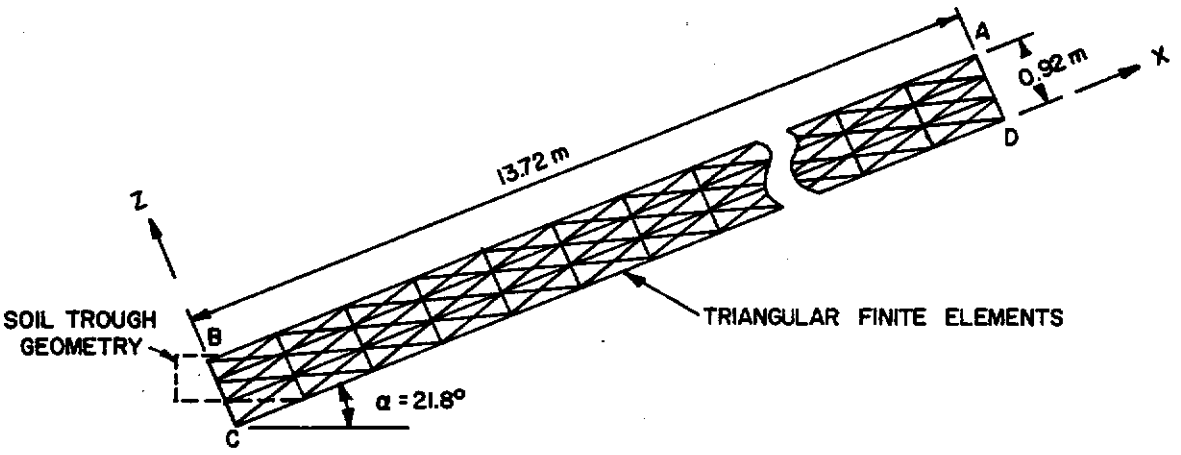

Figure 5.4 Finite Element Discretization of Hewlett's Soil Tough for Nieber's 2-D Model.

Seepage was also allowed to occur from the top surface when appropriate.

Hydraulic conductivity in the unsaturated region was calculated using the form proposed by Gardner (1958),

$$K = \frac{K_s}{(h/h_c)^d + 1} \qquad \ldots (5.1)$$

where h_c is the critical pressure, and d is the pore size distribution index. Both were treated as adjustable parameters. Reeves and Duguid (1975) determined the soil water characteristic from data generated from the fourth soil trough experiment (Scholl and Hibbert, 1973) and fitted a smooth curve to it as shown in Figure 5.2. A saturated hydraulic conductivity of 18.75 cm/hr and a saturated water content of 55% by volume were assumed.

To achieve the initial condition, Reeves and Duguid (1975) subjected the entire profile to heavy precipitation and wetted the entire profile to saturation. The profile was then allowed to drain until the total volumetric water content was 41%. Hewlett (1961) described this as the initial total volumetric water content of a soil trough in a previous experiment.

5.2.1.2 Nieber Model

The 2-D finite model developed by Nieber (1979) and discussed previously in Section 2.3.2.2 was also used to simulate the Coweeta study. The finite element mesh used in this simulation is shown in Figure 5.4 and consisted of 88 nodes and 144 triangular elements. Boundary AB in this figure is the infiltration and seepage boundary, while boundaries BC, CD, and AD are no flow boundaries. The representation of the outlet is not as detailed as that used by Reeves and Duguid (1975), but since the soil was graded to coarse sand and gravel in the horizontal section at the base of the soil trough this boundary condition may be more realistic than that used in the Oak Ridge simulation. It was assumed that the hydraulic conductivities

of the sand and gravel in the horizontal section were much greater than that of the forest soil, to that $\partial H/\partial x = 0$.

The Verma and Brutsaert (1971) equations were used for the soil water capacitance and unsaturated hydraulic conductivity functions (Equations 2.13 and 2.14). The constants A, B, and N in these equations (1.76, 0.36, and 14.6, respectively) were determined by fitting to the soil characteristic data measured by Hewlett (1961). The resulting approximation is shown in Figure 5.2. When validating his 2-D finite element model, Nieber found that hysteresis was important when considering drainage from a soil profile. However, hysteresis was not considered in this simulation because the soil trough was wetted to saturation before being allowed to drain. Therefore, the drying curve of the soil water characteristic could be used without error. If a wetting and drying simulation were made, hysteresis would need to be considered. A saturated hydraulic conductivity of 16.80 cm/hr, and residual and saturated water contents of 0% and 49% by volume, respectively, were used (Hewlett, 1961 and Hewlett, personal communication).

It was assumed that steady state discharge conditions (691.4 ℓ/d/m) were achieved before drainage of the soil profile began. This was achieved by allowing precipitation to occur at a rate of 0.21 cm/hr until steady state was reached. The profile was then allowed to drain.

5.2.2 One-Dimensional Finite Element Model Based on Richards' Equation

Nieber (1982) also developed a one-dimensional finite element model which was introduced in Section 2.3.2.3. The linear grid used with this model for the Coweeta simulation is shown in Figure 5.5 and has 20 nodes. The boundary conditions are the same as those used with Nieber's 2-D model. The nodes are located at the base of the profile and hydrostatic conditions are assumed in the direction normal to the finite element grid.

Since hydrostatic conditions are assumed, input to the saturated zone ceases when precipitation ceases. To overcome this problem

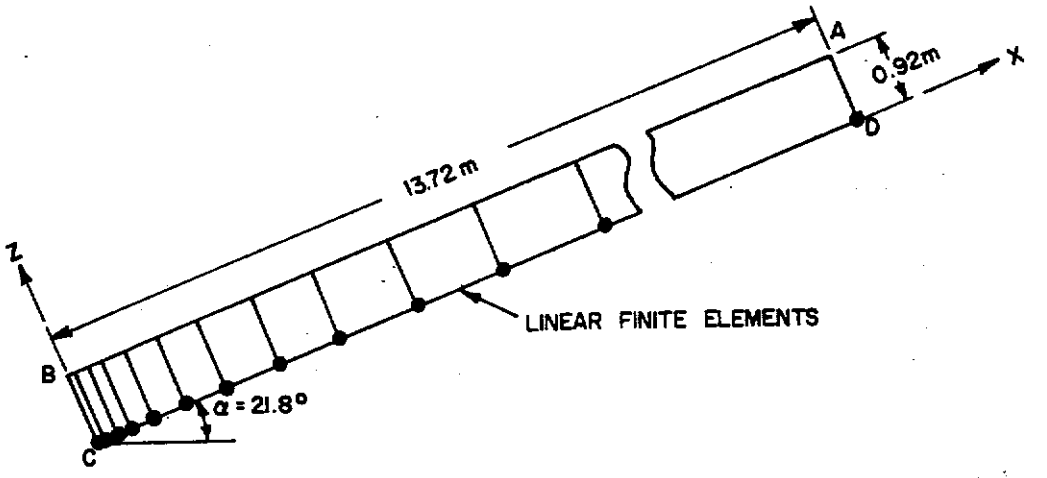

Figure 5.5 Finite Element Discretization of Hewlett's Soil Trough for Neiber's 1-D Model.

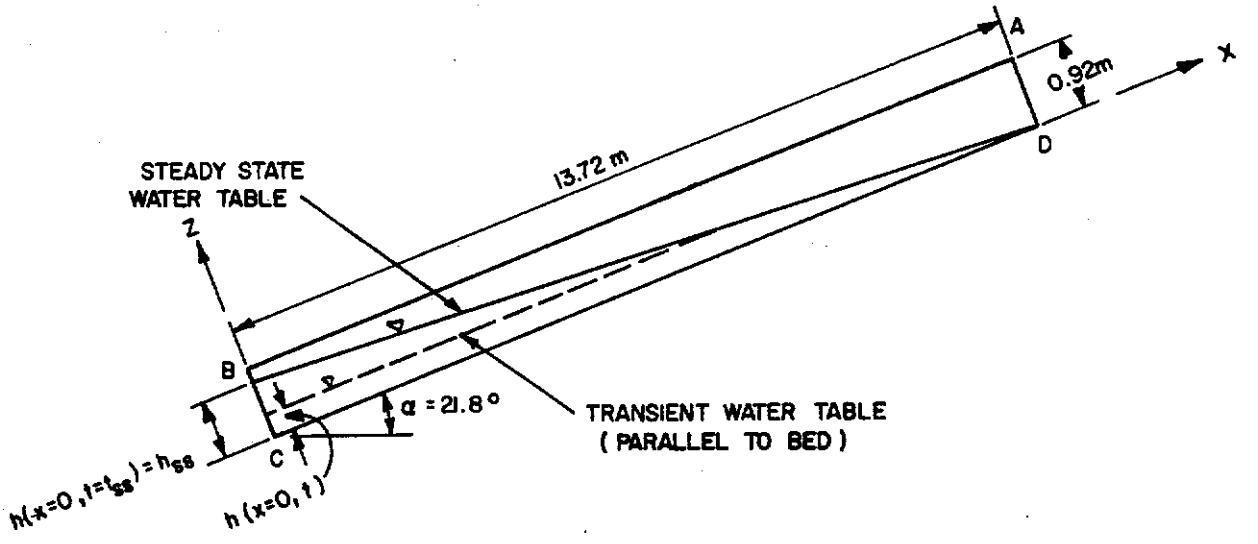

Figure 5.6 Conceptual Representation of Hewlett's Soil Trough for the Kinematic Wave Subsurface Flow Model.

a piston flow model of the wetting front and drying was presented in Section 2.3.2.3; however, it was not used here. Two different wetting/drying conditions were incorporated into two versions of the model; one that assumes an instantaneous input to the base of the soil profile (Model A), and another that assumes an input rate that is a function of the volume of water stored in the unsaturated zone (Model B), i.e.,

$$I = K(\theta_r) \qquad \ldots .(5.2)$$

where I is the vertical input rate to the base of the profile, and θ_r is the degree of saturation in the saturated zone. This latter condition is a correct assumption if gravity drainage dominates (i.e. $\partial H/\partial z = 1$). The unsaturated water content was simulated using a water balance approach,

$$\theta_{us} = \frac{\theta_{uso} V_{us} + L \Delta t_o (i - I_o)}{V_{us}} \qquad \ldots .(5.3)$$

where θ_{us} is the unsaturated water content, V_{us} is the volume of the unsaturated zone, i is the precipitation rate, L is the slope length, Δt is the time increment, and subscript "o" denotes the previous time step.

Soil parameters, soil water capacitance and hydraulic conductivity functions, and the initial condition used in the simulation are identical to those described in Section 5.2.1.2.

5.2.3 Kinematic Wave Subsurface Flow Model

The kinematic wave approximation of subsurface flow was introduced in Section 2.3.2.5 (Equations 2.23 and 2.24). Beven (1982) solved the equations for the case where saturated hydraulic conductivity and saturated water content decreased with depth. For the simulation of the Coweeta study Beven's solution was modified for a homogeneous profile (Figure 5.6).

Beven's (1982) piston flow model was used to simulate the movement of the wetting and drying fronts (Equations 2.17, 2.18,

and 2.19). Since a uniform initial water content, θ_o was assumed, the time for the wetting front to reach the base of the profile, t_{uz}, is,

$$t_{uz} = \frac{D}{i}(\theta_w - \theta_o) \quad \ldots .(5.4)$$

where θ_w is the water content at which $K(\theta_w) = i$, i is the precipitation rate, and D is the depth of the homogeneous soil.

Equation 2.23 can be solved by the method of characteristics in a manner similar to that used with kinematic overland flow (Beven, 1982). The set of characteristics can be described everywhere in the $(x, t > t_{uz})$ plane by,

$$\frac{dx}{dt} = \frac{K_s \sin \alpha}{(\theta_s - \theta_w)} \quad \ldots .(5.5)$$

where α is the angle of the impermeable bed to the horizontal, K_s is the saturated hydraulic conductivity, and θ_s is the saturated water content. Prior to steady state being reached at a position along the profile,

$$\frac{dh}{dt} = \frac{i}{(\theta_s - \theta_w)} . \quad \ldots .(5.6)$$

The depth of steady state flow for any point, x, can be found by dividing Equation 5.6 by Equation 5.5,

$$h = \frac{i(L - x)}{K_s \sin \alpha} . \quad \ldots .(5.7)$$

The time to achieve a particular h is,

$$t = \frac{(\theta_s - \theta_w)h}{i} + t_{uz} \quad \ldots .(5.8)$$

and the time at which steady state is reached, t_{ss}, for a particular x is found by substitution,

$$t_{ss}(x) = \frac{(\theta_s - \theta_w)(L - x)}{K_s \sin \alpha} + t_{uz} \quad \ldots .(5.9)$$

After precipitation ceases it was assumed that input to the water table continues at the rainfall rate, i, until the drying front reaches the water table and then input ceases.

$$t_d(x) = t_r + \frac{(\theta_s - \theta_d)}{i} (D - h(x)) \qquad \ldots .(5.10)$$

where $t_d(x)$ is the time that input ceases at x, t_r is the time that rainfall ceases, and θ_d is the water content that the profile dries to (field capacity). After $t = t_d(x)$, $dh/dt = 0$, since $i = 0$, and,

$$\frac{dx}{dt} = \frac{K_s \sin\alpha}{(\theta_s - \theta_d)} \qquad \ldots .(5.11)$$

The time at which a particular depth, h(x), reaches the outlet is then,

$$t = \frac{x(\theta_s - \theta_d)}{K_s \sin\alpha} + t_d(x) \qquad \ldots .(5.12)$$

5.2.4 Simple Storage Models

Finally, two simple storage type models were developed. In the first (Kinematic Storage Model) the hydraulic gradient was assumed to be equal to the bed slope, as in the kinematic wave approximation. In the second (Boussinesq Storage Model) the hydraulic gradient was assumed to be equal to the gradient of the water table. The continuity (water balance) equation is the basis of both models, and can be written as,

$$\frac{dS}{dt} = I - q \qquad \ldots .(5.13)$$

or in explicit finite difference form as,

$$\frac{S_2 - S_1}{t_2 - t_1} = I - \tfrac{1}{2}(q_1 + q_2) \qquad \ldots .(5.14)$$

where S is the drainable volume of water stored in the saturated zone per unit width, q is the discharge from the profile per unit width, [q = f(S)], I is the vertical input from the unsaturated zone per unit width, and subscripts 1 and 2 refer to the beginning and end of the time period, respectively.

5.2.4.1 Kinematic Storage Model

Equations 2.23 and 5.2 were used to describe q and I for the kinematic storage model. The soil water characteristic was described by Equation 2.14. Assuming that the water table is linear between the outlet face and the upper boundary (Figure 5.7),

$$S = Lh(\theta_s - \theta_d)/2 \qquad \ldots .(5.15)$$

where h is the depth of the water table at the outlet, and L is the slope length. The boundary conditions assumed in this case are the same as those assumed with the kinematic wave model. By substitution, the head at the outlet at the end of time increment Δt, can be found explicitly by,

$$h_2 = \frac{h_1[L(\theta_s - \theta_d)/\Delta t - V]/2 + LI_1}{[L(\theta_s - \theta_d)/\Delta t + V]/2} \qquad \ldots .(5.16)$$

where V is the discharge per unit cross sectional area, and subscripts 1 and 2 refer to the beginning and end of the time interval, respectively,

$$V = K_s \sin\alpha \qquad \ldots .(5.17)$$

$$q = hV \qquad \ldots .(5.18)$$

5.2.4.2 Boussinesq Storage Model

In order to develop a storage type model that possessed

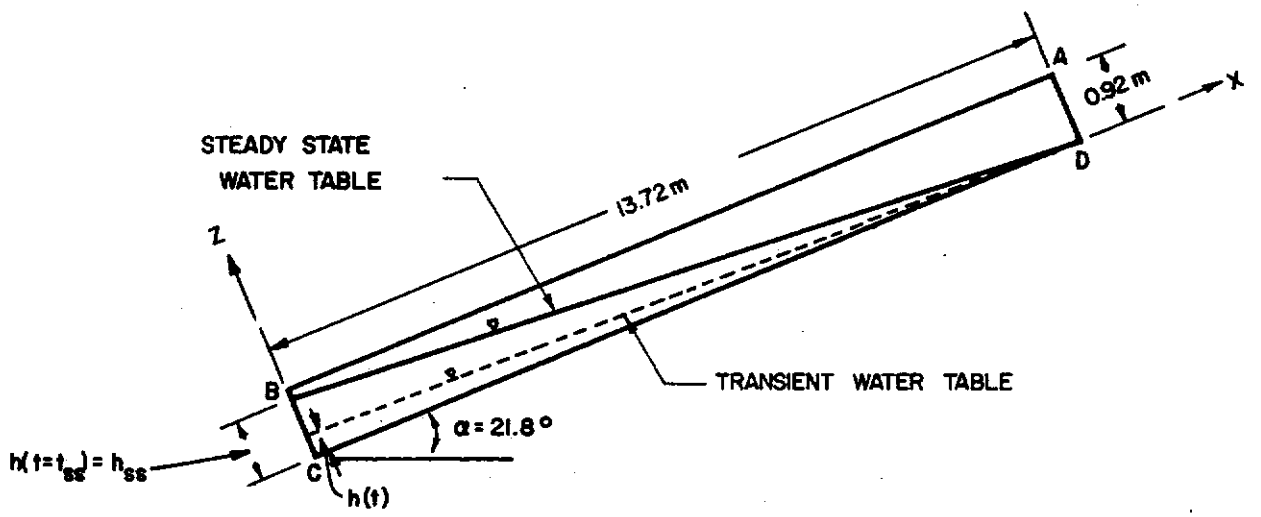

Figure 5.7 Conceptual Representation of Hewlett's Soil Trough for the Kinematic Storage Model.

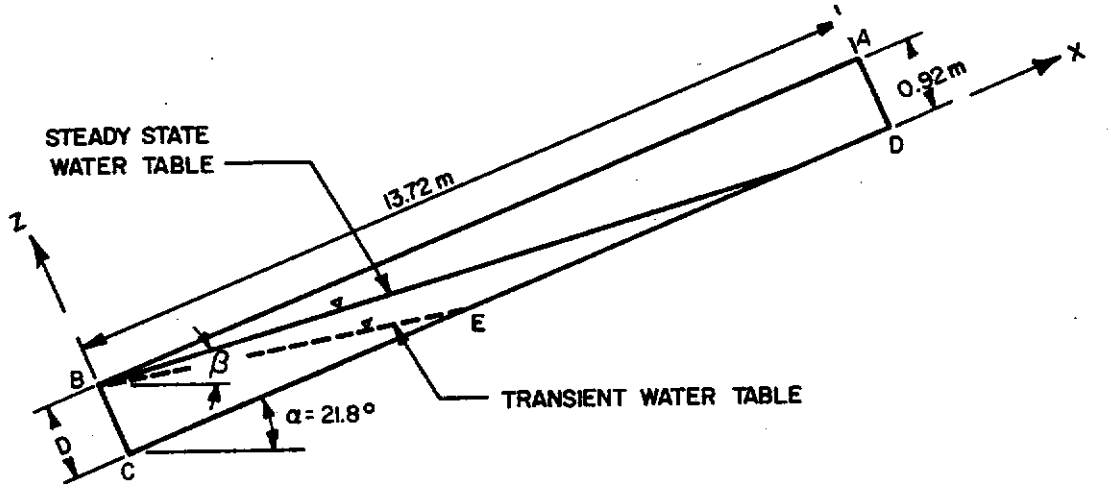

Figure 5.8 Conceptual Representation of Hewlett's Soil Trough for the Boussinesq Storage Model.

boundary conditions similar to those of the finite element models, the water table was assumed to be fixed at the outlet (point B) at a height D above the impermeable bed, and inclined at the angle necessary to produce the required storage (Figure 5.8). The Boussinesq assumption therefore gives discharge as,

$$q = D\ K_s \sin\beta \qquad \ldots (5.19)$$

where β is the angle of the water table to the horizontal. The volume of water stored in the saturated zone is therefore a function of β and when $\beta < \alpha - \arctan(D/L)$,

$$S = (\theta_s - \theta_d)\ \frac{D^2}{2} / \tan(\alpha - \beta) \qquad \ldots (5.20)$$

where S is the drainable volume of water stored in the saturated zone per unit width, and α is the angle of the impermeable bed to the horizontal.

5.3 RESULTS

The results obtained by Reeves and Duguid (1975) from the application of the Oak Ridge 2-D model to the soil trough described in Section 5.1 (see Figure 5.1) are presented in Figure 5.9. The results of three simulations are shown in this figure corresponding to three different assumed critical pressure heads (h_c in Equation 5.1). A critical pressure head of -30 cm of water gave the best results, and this simulation is used subsequently for the comparison to the other models. Reeves and Duguid (1975) reported that the Oak Ridge model required 500K bytes of core storage and took 16.5 minutes of CPU time to simulate 13.5 days of drainage on an IBM 360/91 computer.

The discharge hydrograph predicted by Nieber's 2-D model is presented in Figure 5.10 and is compared to the results from the Oak Ridge 2-D model and the measured discharge hydrograph. The initial conditions for the two models, described in Section 5.2.1, were

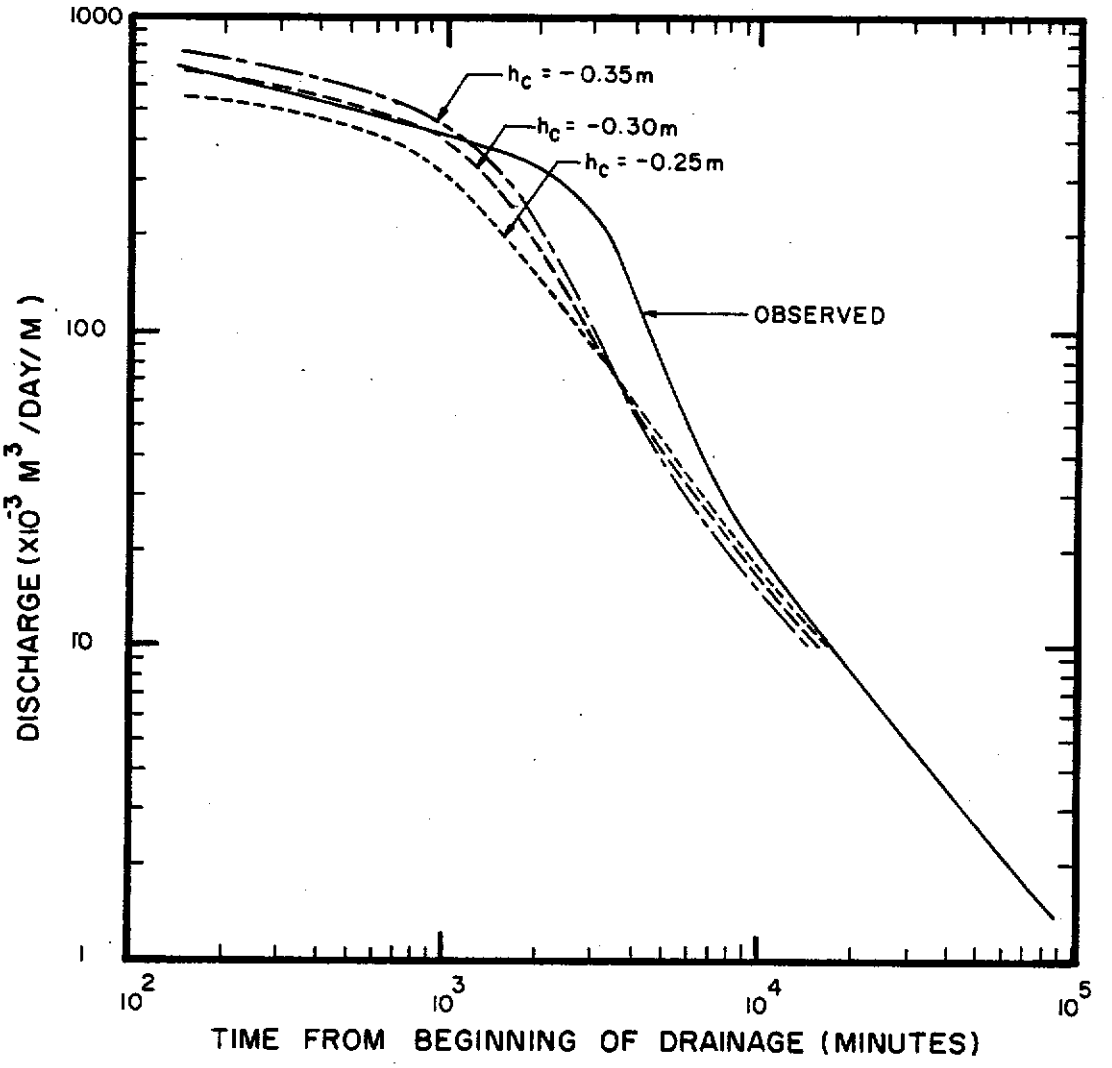

Figure 5.9 Comparison of Observed and Predicted Drainage Hydrographs for the Oak Ridge 2-D Model at Three Critical Pressure Heads (from Reeves and Duguid, 1975).

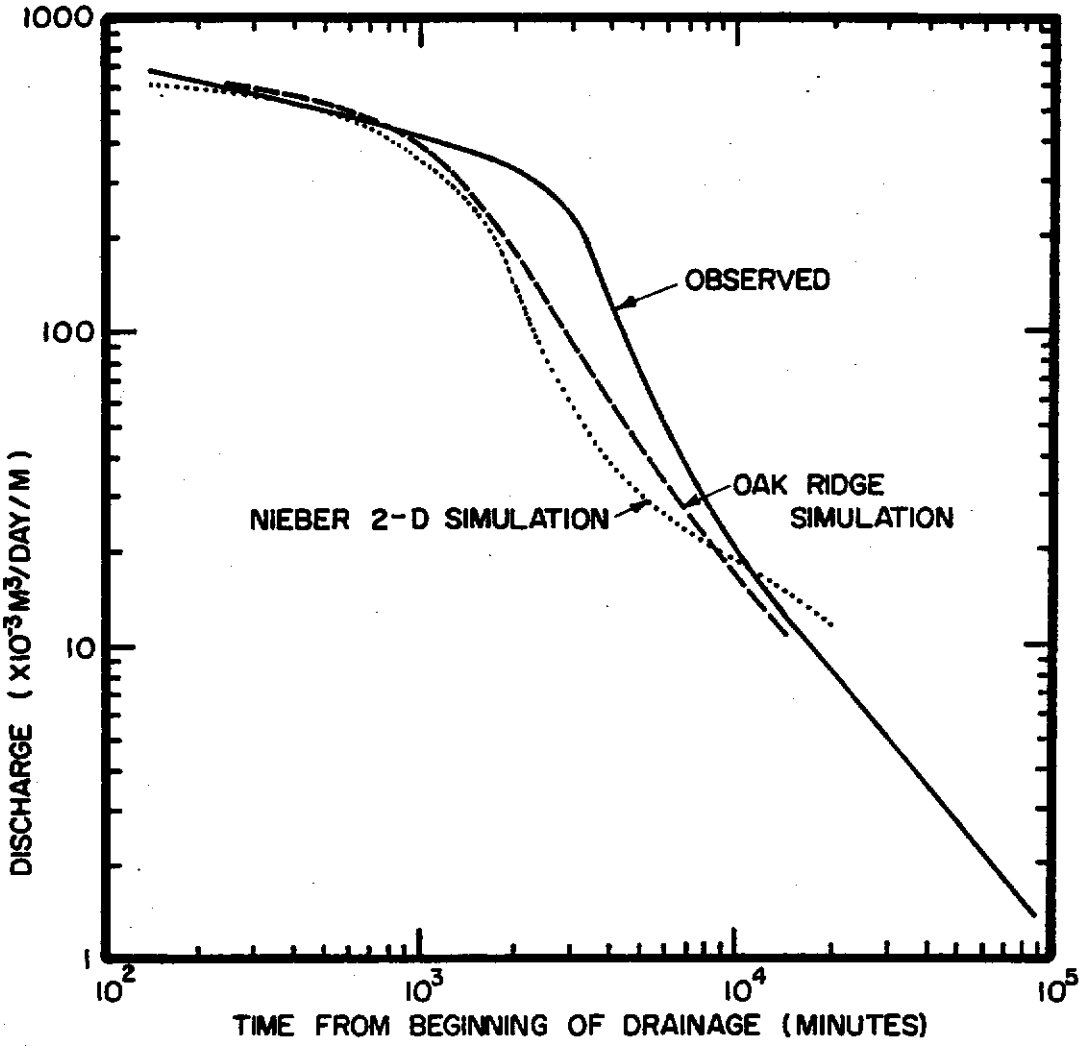

Figure 5.10 Comparison of Observed and Predicted Drainage Hydrographs for Nieber's 2-D Model (K_s=16.8 cm/hr) and the Oak Ridge 2-D Model (K_s=18.75 cm/hr).

obtained in different ways and the assumed saturated hydraulic conductivities were also different (18.75 cm/hr and 16.8 cm/hr, for the Oak Ridge and Nieber 2-D models, respectively). The drainage predicted by Nieber's 2-D model drops off more rapidly than the Oak Ridge hydrograph because water content as a function of pressure head (and similarly unsaturated hydraulic conductivity) decreases more rapidly using the Verma-Brutsaert equation than that predicted by the Oak Ridge approximation, as is shown in Figure 5.2. Nieber's 2-D model required approximately 360K bytes of core storage and 13.8 minutes of CPU time to simulate 13.5 days of drainage on an IBM 370/165 computer (WATFIV compiler).

Two versions of Nieber's 1-D model (Model A and Model B) were applied to the Coweeta data, and the results are presented in Figure 5.11. The sensitivity of Model B to variations in the assumed saturated hydraulic conductivity, K_s, of 16.8 cm/hr was examined by carrying out additional simulations with K_s values equal to ± 20% of 16.8 cm/hr. These results are also presented in Figure 5.11. Nieber's 1-D model required 11K bytes of core storage and 24.1 minutes of CPU time to simulate 37.5 days of drainage on an HP-3000 computer.

The kinematic wave subsurface flow model results are presented in Figure 5.12. The sensitivity of the simulation to variations in K_s and field capacity, θ_d, was examined by carrying out simulations at two field capacities and three saturated hydraulic conductivities (θ_d = 0.32 and 0.26 by volume, and K_s = ±20% of 16.8 cm/hr). The field capacities of 0.32 and 0.26 correspond to pressure heads of -0.059 and -0.34 bars, respectively (-60 and -347 cm of water, respectively). The initial steady state water table position for the kinematic wave model is shown in Figure 5.6. This was attained by applying precipitation at a rate of 0.21 cm/hr, and yielded a steady state runoff of 691.5 ℓ/day/m. The kinematic wave subsurface flow model required 3.5K bytes of core storage and 5 seconds of CPU time

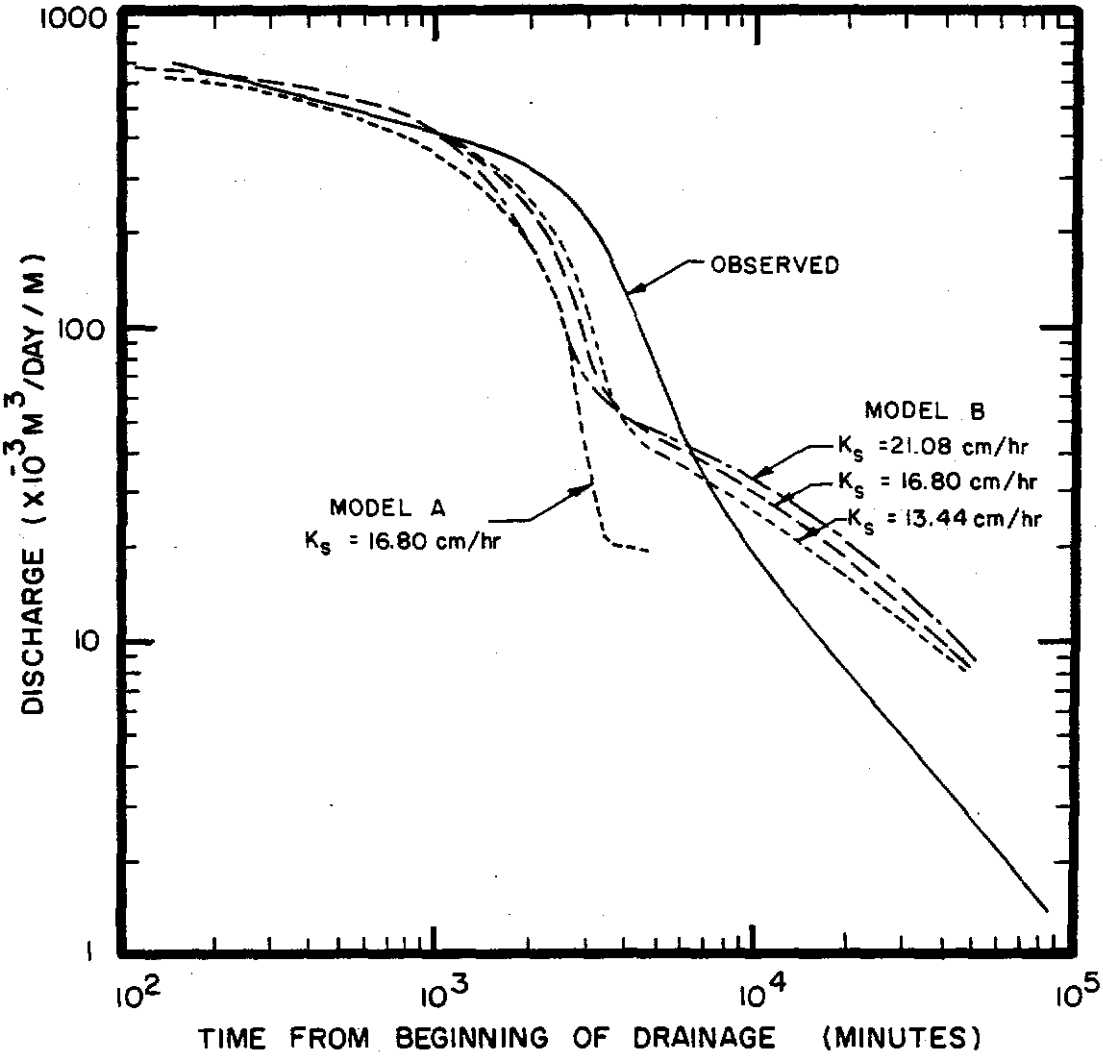

Figure 5.11 Comparison of Observed and Predicted Drainage Hydrographs for Two Versions of Nieber's 1-D Model Corresponding to Two Different Wetting/Drying Mechanisms (Model A and Model B).

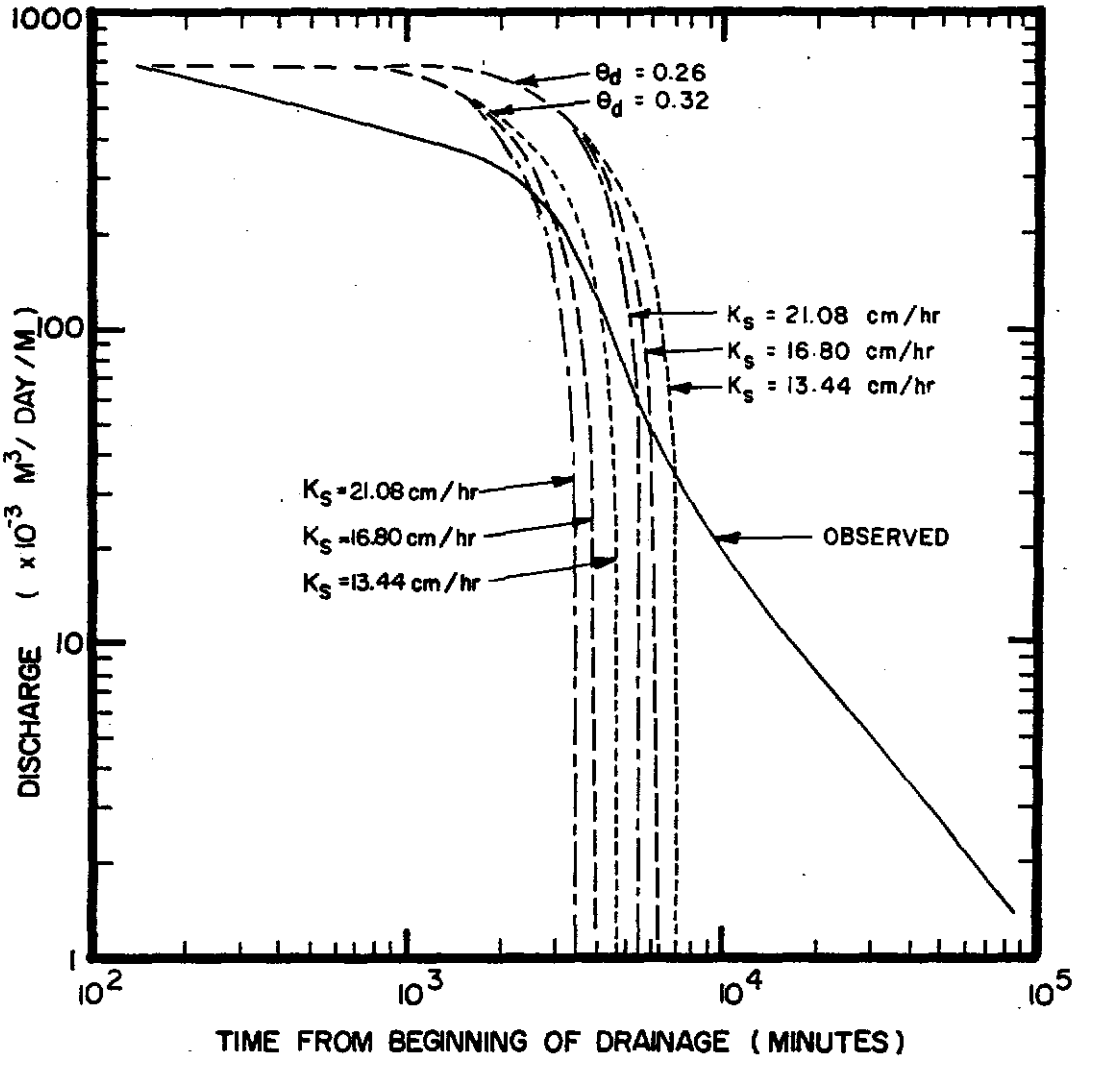

Figure 5.12 Comparison of Observed and Predicted Drainage Hydrographs for the Kinematic Wave Subsurface Flow Model at Two Field Capacities (θ_d) and Three Saturated Hydraulic Conductivities (K_s).

to simulate 3 days of drainage on an HP-3000 computer.

The discharge hydrographs predicted by the kinematic storage model and the Boussinesq storage model are presented in Figures 5.13 and 5.14, respectively. The sensitivity of both models to variations in K_s was evaluated by carrying out simulations with K_s equal to ±20% of 16.8 cm/hr. These results are also presented in Figures 5.13 and 5.14. The kinematic storage model required 2.7K bytes of core storage and 5 seconds of CPU time to simulate 41 days of drainage on an HP-3000 computer, while the Boussinesq storage model required 3K bytes and 14 seconds to simulate 35 days of drainage.

5.3.1 Comparison of Subsurface Flow Models

The accuracy of the various models in predicting the observed drainage from the soil trough used in the Coweeta study was assessed by visual inspection of the drainage hydrographs and the cumulative runoff curves, and comparison of the coefficient of determinations and timing errors. The discharge hydrographs predicted by each model, for a saturated hydraulic conductivity of 16.8 cm/hr (Oak Ridge study used K_s = 18.75 cm/hr), are shown in Figure 5.15. Similarly, the cumulative runoff curves are shown in Figure 5.16. Table 5.2 is a summary of the coefficients of determination (r^2), timing errors, simulation costs, and core storage requirements for each of the models.

The simplest model, the kinematic storage model, had one of the highest coefficients of determination, while the most sophisticated model, the 2-D finite element model, did not do as well. Simulation cost for the simple models was negligible, while the sophisticated 2-D model cost $120 (on WATFIV) to simulate 19375 minutes of drainage (would cost $30 - $40 if program were run on FORTRAN G). The more sophisticated models, the 1-D and 2-D models both based on Richards' equation, were the most accurate at the small times (0 to 1000 minutes), while the simple storage models were better at large times (5000 to 50000 minutes).

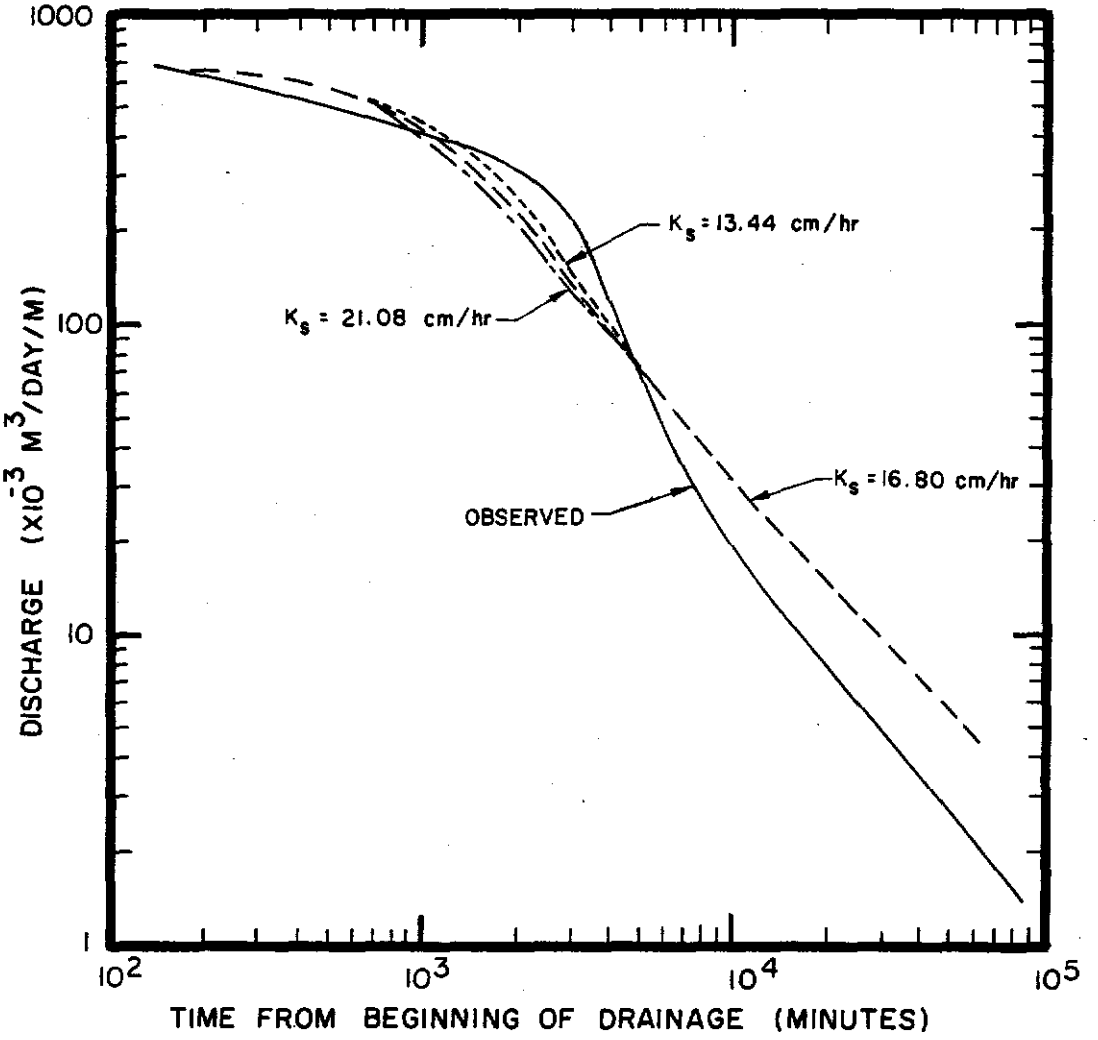

Figure 5.13 Comparison of Observed and Predicted Drainage Hydrographs for the Kinematic Storage Model at Three Saturated Hydraulic Conductivities (K_s).

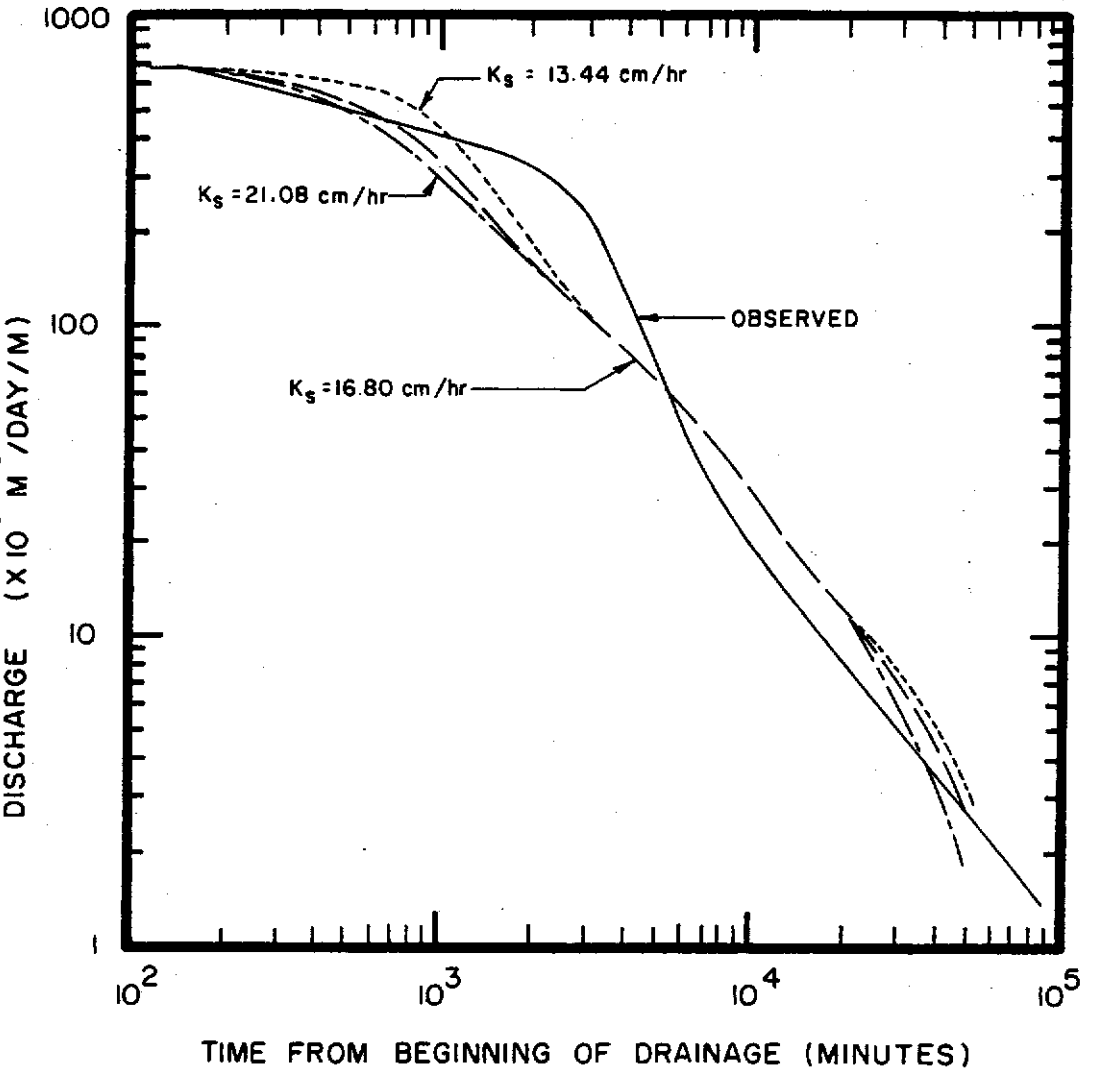

Figure 5.14 Comparison of Observed and Predicted Drainage Hydrographs for the Boussinesq Storage Model at Three Saturated Hydraulic Conductivities (K_s).

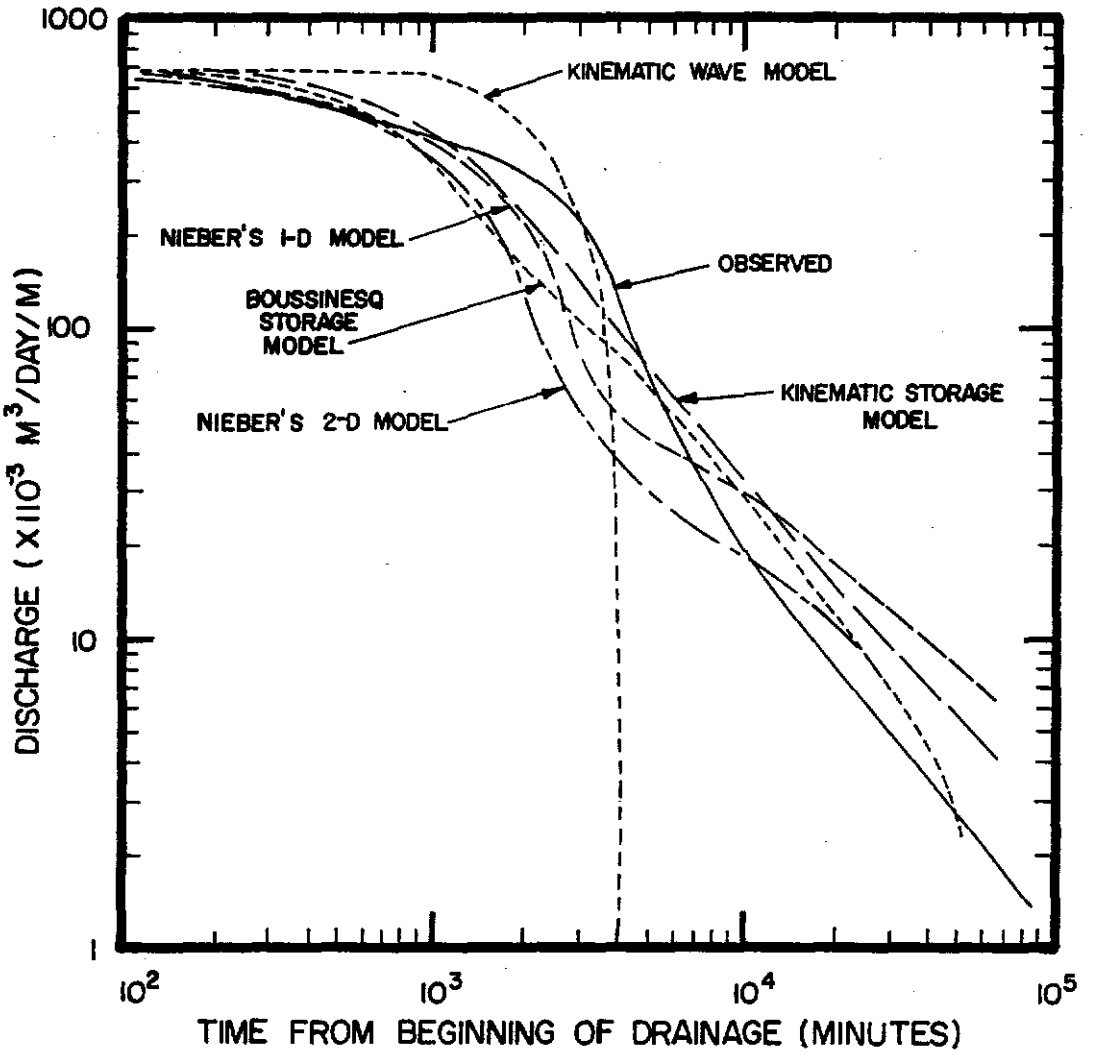

Figure 5.15 Comparison of Observed and Predicted Drainage Hydrographs for Nieber's 1-D and 2-D Models, the Kinematic Wave Subsurface Model, and the Kinematic and Boussinesq Storage Models for K_s = 16.8 cm/hr.

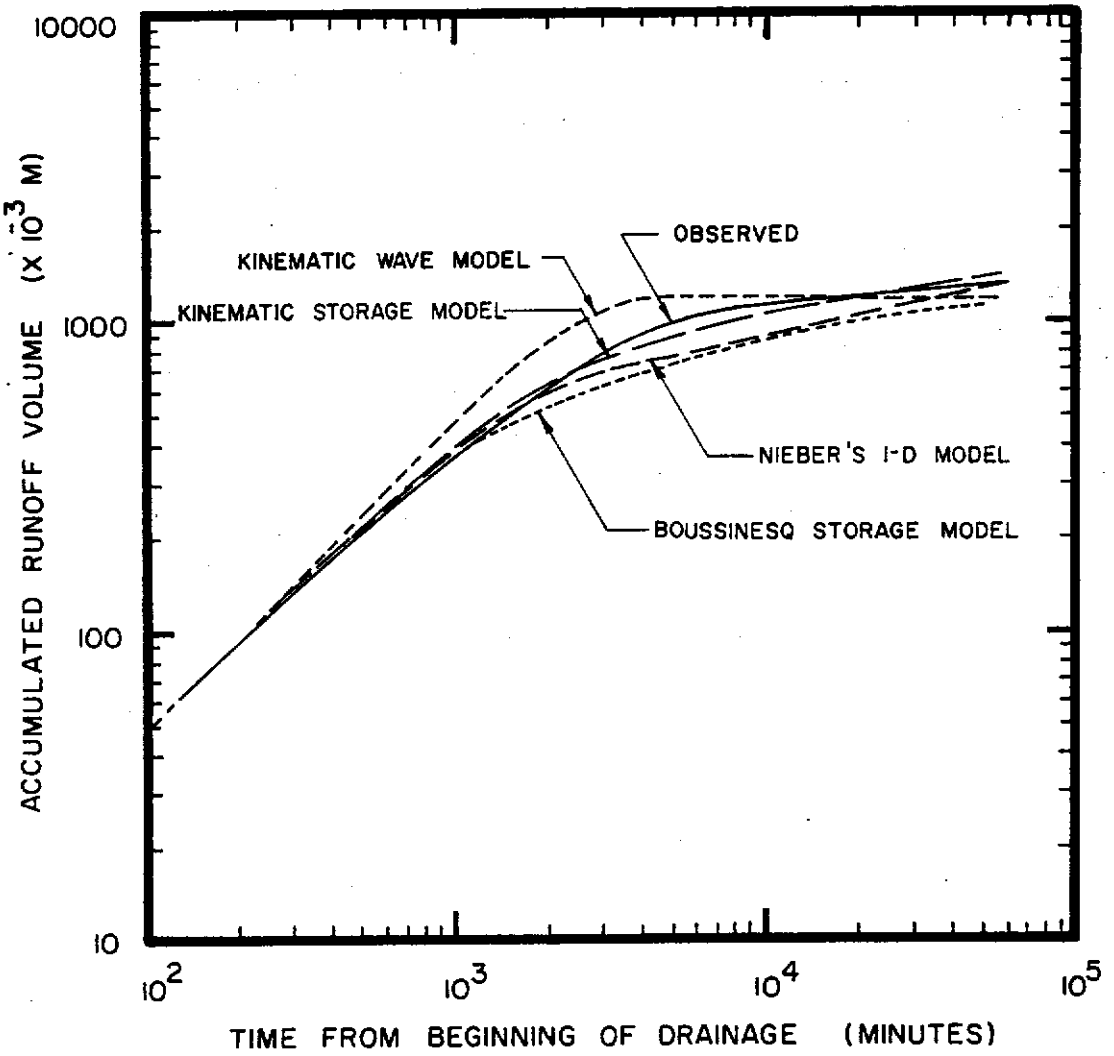

Figure 5.16 Comparison of Observed and Predicted Cumulative Runoff Curves for Nieber's 1-D and 2-D Models, the Kinematic Wave Subsurface Model, and the Kinematic and Boussinesq Storage Models for K_s= 16.8 cm/hr.

Table 5.2 Model Comparisons

Model	r^2 *	Timing Error (%) $0.75Q_p$	Timing Error (%) $0.25Q_p$	CPU Time (sec)	Core (K bytes)
Nieber's 2-D	0.958	0	-47	828	133**
Model A 1-D	0.975	0	-46	-	11
Model B 1-D	0.973	+ 43	-32	1440	11***
Kinematic Wave (32%)	0.942	+286	- 3	5	3.5
Kinematic Wave (26%)	0.880	+579	+53	5	3.5
Kinematic Storage	0.969	+ 61	-26	5	2.7
Boussinesq Storage	0.950	+ 31	-47	14	3

* Coefficient of Determination between t=0 and t=7000 minutes.

** Additional storage required for the compiler must be added before compiling and executing. The model was run using the WATFIV compiler, and a region of 360K was required. Additional storage requirements would be less for a production compiler.

*** 22K bytes of storage was required on the IBM 370/165 because the IBM machine has 4 bytes/word, whereas the HP has 2 bytes/word. Speed of execution was 400% faster using the IBM 370/165.

Field capacity water content (% by volume).

The cumulative runoff curves (Figure 5.16) show that both the kinematic wave model and the kinematic storage model overestimated the volume of water drained, and the other models underestimated the amount of runoff for times greater than 1500 minutes. All of the models did well for times less than 800 minutes. The kinematic wave model had the largest error, because the infiltration model assumes that all water above field capacity is released as the drying front progresses. The kinematic storage model, as well as the kinematic wave model, overestimated the volume of water drained because of their different boundary condition.

5.4 DISCUSSION OF RESULTS

5.4.1 Effect of Boundary Condition

The boundary condition used at the outlet of the sloping bed varied according to the model used. The Oak Ridge 2-D model used the most detailed and accurate boundary condition, but it may have been counter-productive because the soil characteristics were not varied to account for the freely draining sand, gravel and rock in the horizontal section at the outlet. For Nieber's 1-D and 2-D models and the Boussinesq model a simplified version of the Coweeta boundary condition was used that assumed a constant head equal to the soil depth at the outlet. The kinematic wave model and the kinematic storage model assumed a constant head at the outlet equal to atmospheric pressure. For steep slopes this boundary condition is acceptable because in a short distance from the outlet the flowlines are parallel to the impermeable bed (Figures 5.17 to 5.19). The similarity of hydrographs for the different models shows that results are not significantly sensitive to the outlet boundary conditions.

5.4.2 Transient Water Table Positions

Transient water table positions predicted by the various models are plotted for t=0, 1000, and 3000 minutes in Figures 5.17, 5.18, and 5.19, respectively. The steady state water tables (t=0) for the two models using Richards' equation and the two models using the kinematic wave assumption show very close agreement for distances greater than 2 m upslope. The Boussinesq storage model predicted a water table that is at about the same slope as the Richards' equation models at the outlet. However, 2 m upslope from the outlet it deviates significantly from the predictions of the Richards' equation models. At t=1000 minutes the water tables generated by the complex models and the kinematic storage model show good agreement for $x>3$ m. The kinematic wave model overestimated the saturated zone depth compared to these. This is due to the piston flow infiltration assumed rather than the kinematic assumption being in error. The

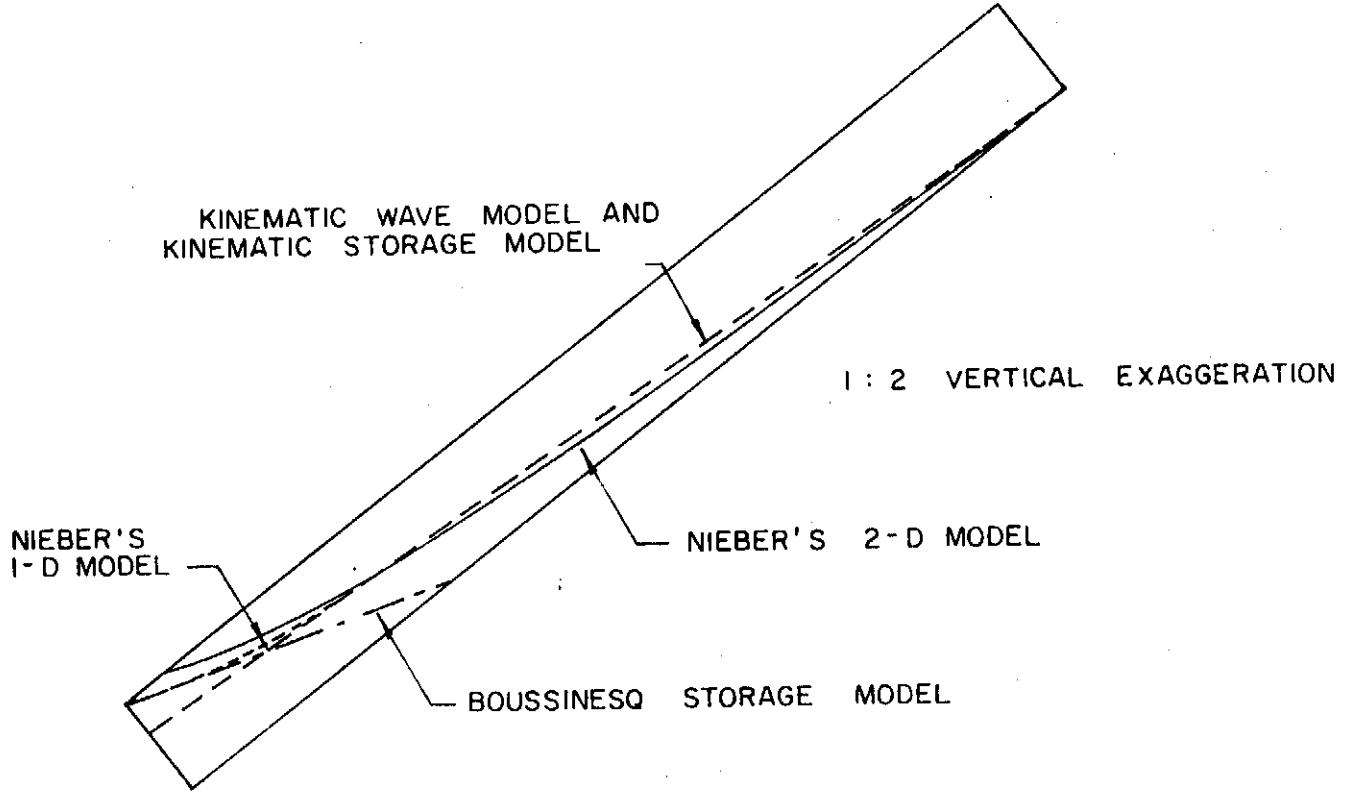

Figure 5.17 Comparison of Predicted Water Table Positions for Nieber's 1-D and 2-D Models, the Kinematic Wave Subsurface Model, and the Kinematic and Boussinesq Storage Models at t=0 minutes.

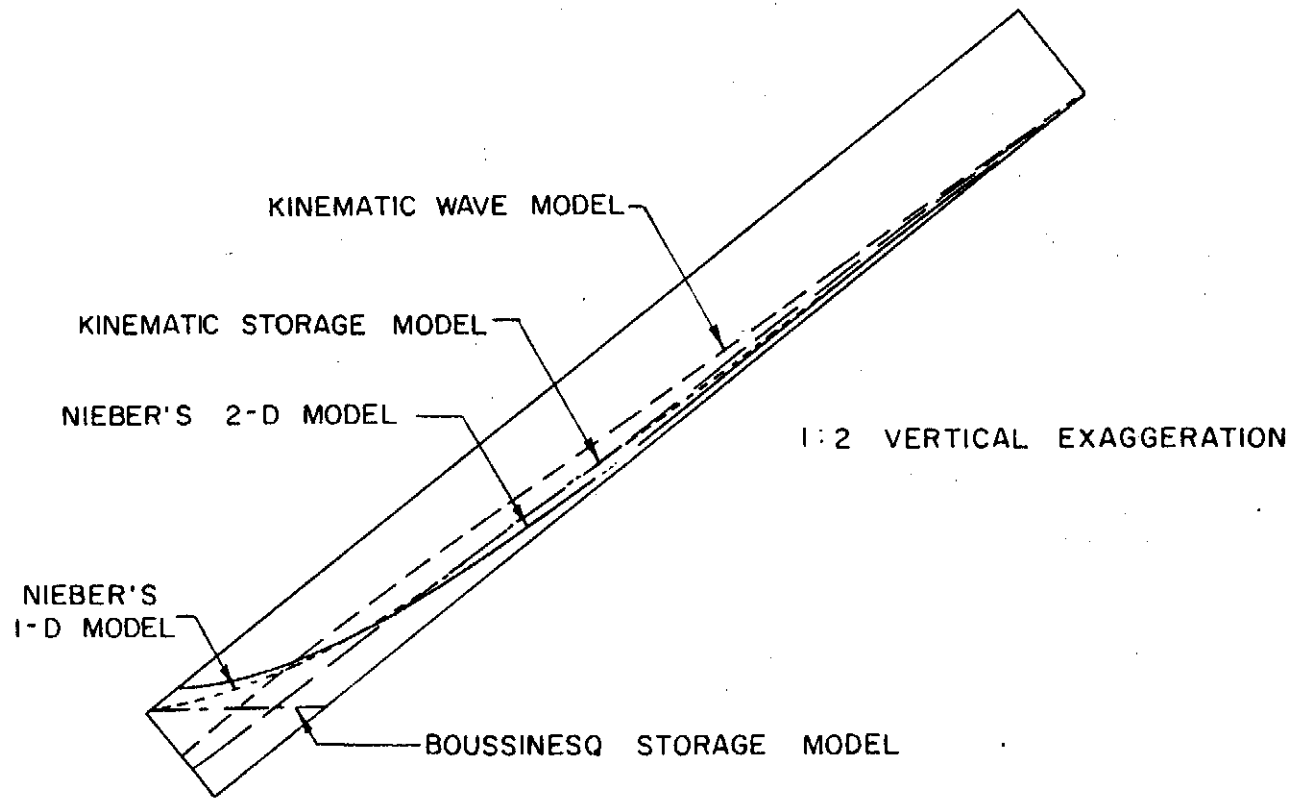

Figure 5.18 Comparison of Predicted Water Table Positions for Nieber's 1-D and 2-D Models, the Kinematic Wave Subsurface Model, and the Kinematic and Boussinesq Storage Models at t=1,000 minutes.

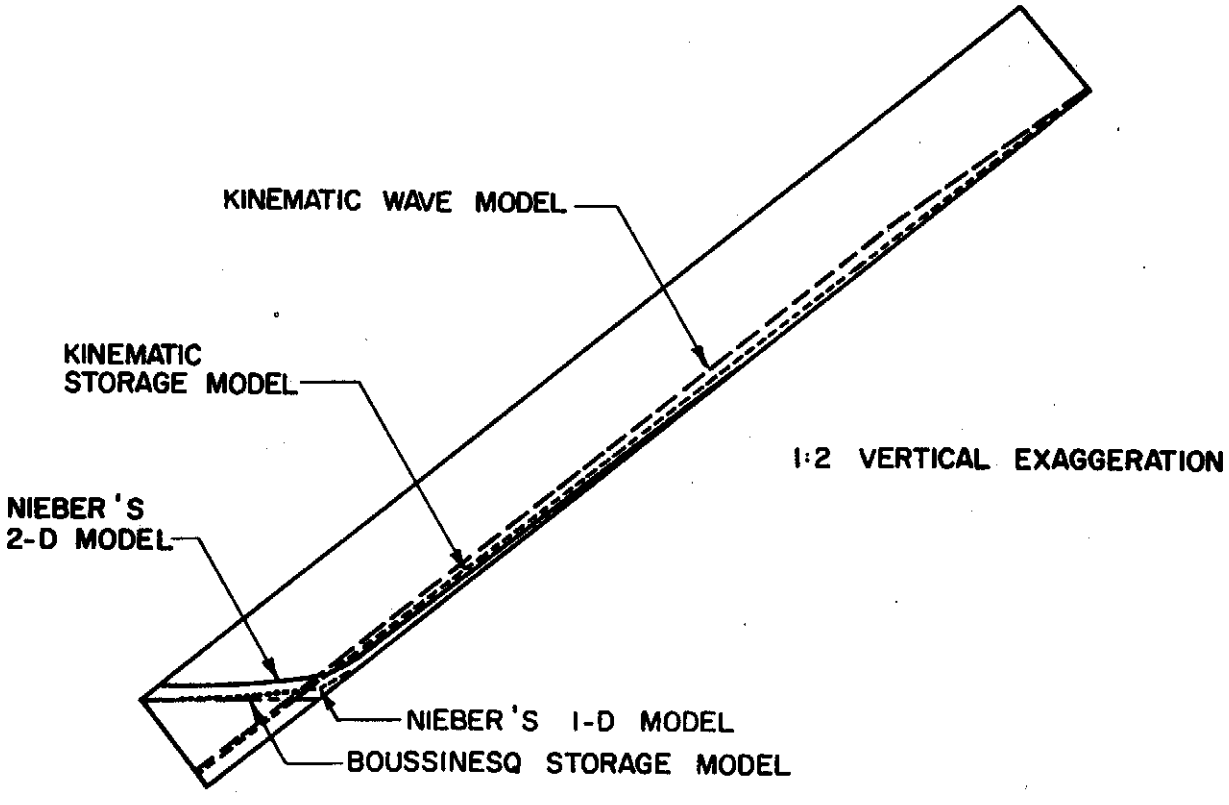

Figure 5.19 Comparison of Predicted Water Table Positions for Nieber's 1-D and 2-D Models, the Kinematic Wave Subsurface Model, and the Kinematic and Boussinesq Storage Models at t=3,000 minutes.

water table predicted by the Boussinesq storage model is just about horizontal by this time and does not extend upslope. Similar results are shown for t=3000 minutes.

For steep slopes, as with the Coweeta soil trough which is at 40%, the Boussinesq assumption is not valid. The kinematic wave approximation, $dH/dx = \sin\alpha$, however, is accurate upslope from the outlet ($x > 2$ to 3 m).

5.4.3 Effect of Infiltration Model

Infiltration for the 1-D models and the storage models must be estimated using a coupled model. The piston drying front model used in the kinematic wave model is not as accurate as the unsaturated storage algorithm used for the other models. The simple kinematice storage model, on the other hand, is a good example of the effectiveness of the storage algorithm, because at large times the predicted discharge is very close to the observed. Both coupled infiltration models tend to overestimate vertical input early in the simulation, but the storage model does much better than the piston model. A simulation was made with vertical input varying over the slope for Nieber's 1-D finite element model, and the resulting discharge hydrograph was virtually the same as that predicted by Model B (using average vertical input).

5.5 CONCLUSIONS

Five physically based computer models were evaluated in this chapter and results from the Oak Ridge model were included for comparison. The model parameters are all physically measureable as opposed to the parameters in the watershed models described in Section 2.3.1 and to some extent the watershed model described in Chapter 4. Model parameters were estimated from the Coweeta data (Hewlett, 1961; Hewlett and Hibbert, 1963), and no optimization of parameters was carried out.

Simple subsurface flow models which make assumptions compatible with the actual process can be as effective as the sophisticated 1-D

and 2-D models with much less investment of money and time. The kinematic wave model and the kinematic storage model did just about as well as the models using Richards' equation in predicting the extent of the saturated zone. When the kinematic wave assumption is coupled with the simple infiltration model assuming gravity drainage the simulation results are very satisfactory for the Coweeta study. Although the assumptions in the Boussinesq storage model are not valid for steep slopes, as shown by the predicted transient water table positions, the model nevertheless did a reasonable job of predicting the discharge hydrograph in comparison to the more sophisticated 1-D and 2-D models.

CHAPTER 6

TEST PLOT RUNOFF ESTIMATION AND EVALUATION OF THREE SUBSURFACE FLOW MODELS ON SELECTED EVENTS

The most reliable and complete measurements from the test plot were obtained during the period extending from October 27, 1982 to December 1, 1982. Four readily definable rainfall-runoff events occurred during this time.

The precipitation and soil water storage data are used to estimate the hillslope runoff for these events. Three subsurface flow models; Nieber's 1-D finite element model (based on Richards' equation), the kinematic wave model, and the kinematic storage model, are evaluated in this chapter by applying them to the observed and calculated rainfall-runoff relationships for the four events on the test plot. These results provide the basis for determining the major runoff processes occurring on the test plot hillslope.

The three models selected for evaluation using the test plot data were chosen on the basis of the results from the previous chapter (Chapter 5), in which five process models were applied to the Coweeta experiment results. The 1-D finite element model was chosen as a representative of the more complex subsurface flow models based on Richards' equation. It performed as well as the 2-D finite element model but was much less expensive to use in terms of computer time. Both models were written by Nieber (1979, 1982) and the 1-D algorithm is a simplified version of the 2-D computer program. The kinematic storage model was selected because its assumptions appear to be conceptually correct for steep hillslope subsurface flow. It performed as well as the complex models in predicting drainage and water table position, but at a fraction of the cost. The kinematic wave model, based on a solution by the method of characteristics, was the third category of models tested in Chapter 5. It was included for completeness, since others (for example: Beven, 1981, 1982) have recommended it as an appropriate model for subsurface stormflow.

6.1 TEST PLOT PRECIPITATION AND SOIL WATER CONTENT MEASUREMENTS

6.1.1 Precipitation

Test plot precipitation was measured on a 30 minute time interval using the four tipping-bucket rain gauges described in Chapter 4. These gauges performed very well. The records were checked against precipitation measurements obtained from a continuously recording weighing-bucket rain gauge located just upstream from the test plot.

Figure 6.1 presents the average of the daily precipitation measured by the four tipping-bucket gauges and the daily precipitation record obtained from the weighing-bucket rain gauge located at the confluence of the Little Millseat and Field Branch watersheds (Figure 3.2). The data logger was inoperative on the two occasions shown, so no rainfall data were collected at those times. The two records agree farily well even though two of the test plot rain gauges were under the forest canopy. It appears that at this time of the year, November, the canopy does not intercept rainfall to any great degree. On November 23, the test plot gauges showed some rainfall, whereas the weighing-bucket gauge did not. This difference is probably due to timing errors in the weighing-bucket gauge record. The data logger, with an internal clock and recording on a 30 minute interval, was more accurate in recording the timing of rainfall than the weighing-bucket rain gauge with the drum record.

6.1.2 Weekly Water Contents: Nuclear Moisture Probe Measurements

The weekly soil water contents obtained using the nuclear moisture probe measure the long-term response of the hillslope. Rapid movements of water, such as the movement of wetting fronts, lateral pulses of water moving downslope during runoff events, and rapid drainage of the soil profile cannot be seen using a weekly measurement interval. Water content profiles for three consecutive weeks: November 17, November 24, and December 1, are presented in Figures 6.2a, 6.2b, and 6.2c, respectively. Inspection of the precipitation record,

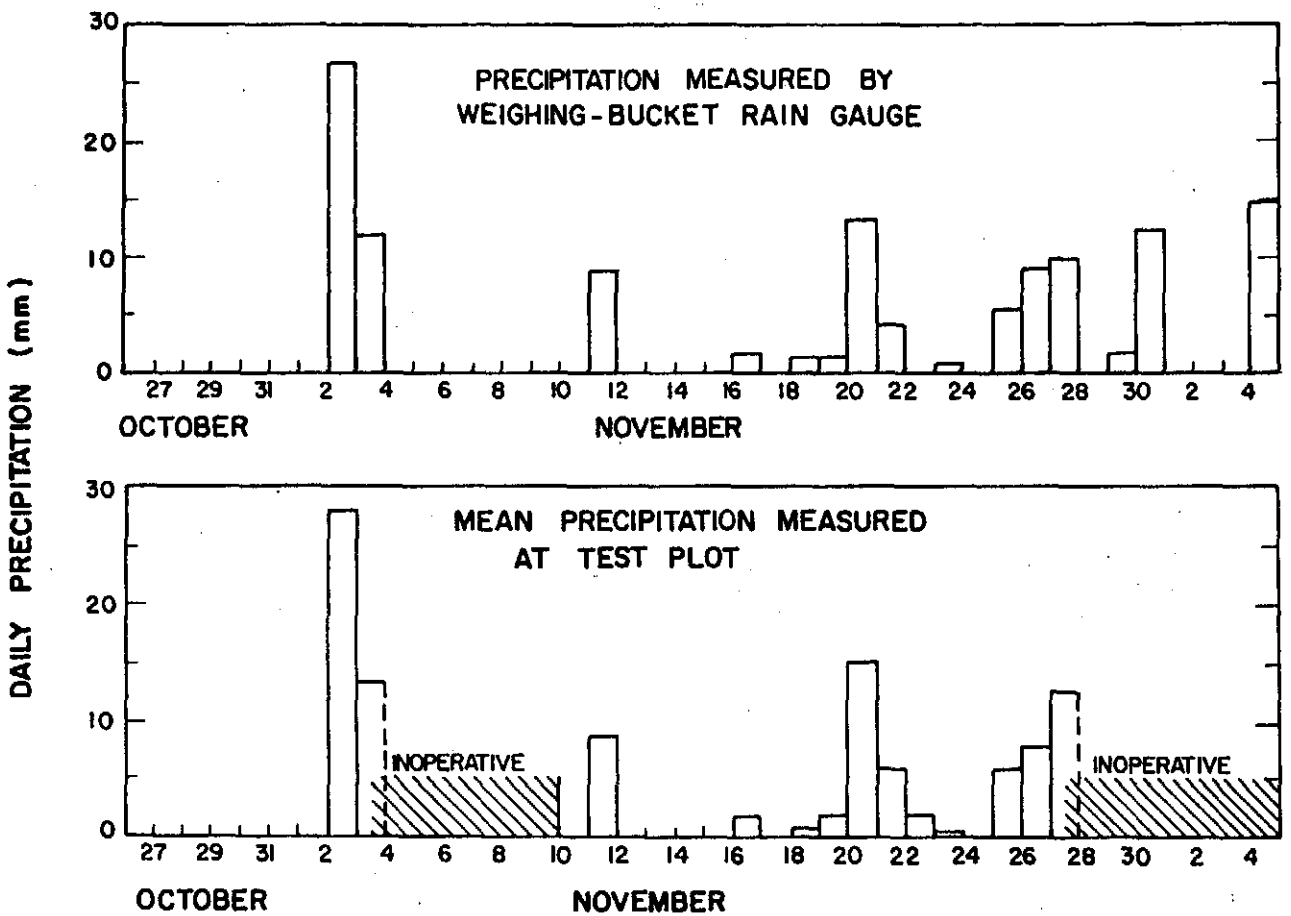

Figure 6.1 Comparison of Daily Precipitation Recorded by the Weighing-Bucket Gauge and the Mean Precipitation Recorded by the Four Tipping-Bucket Gauges on the Test Plot.

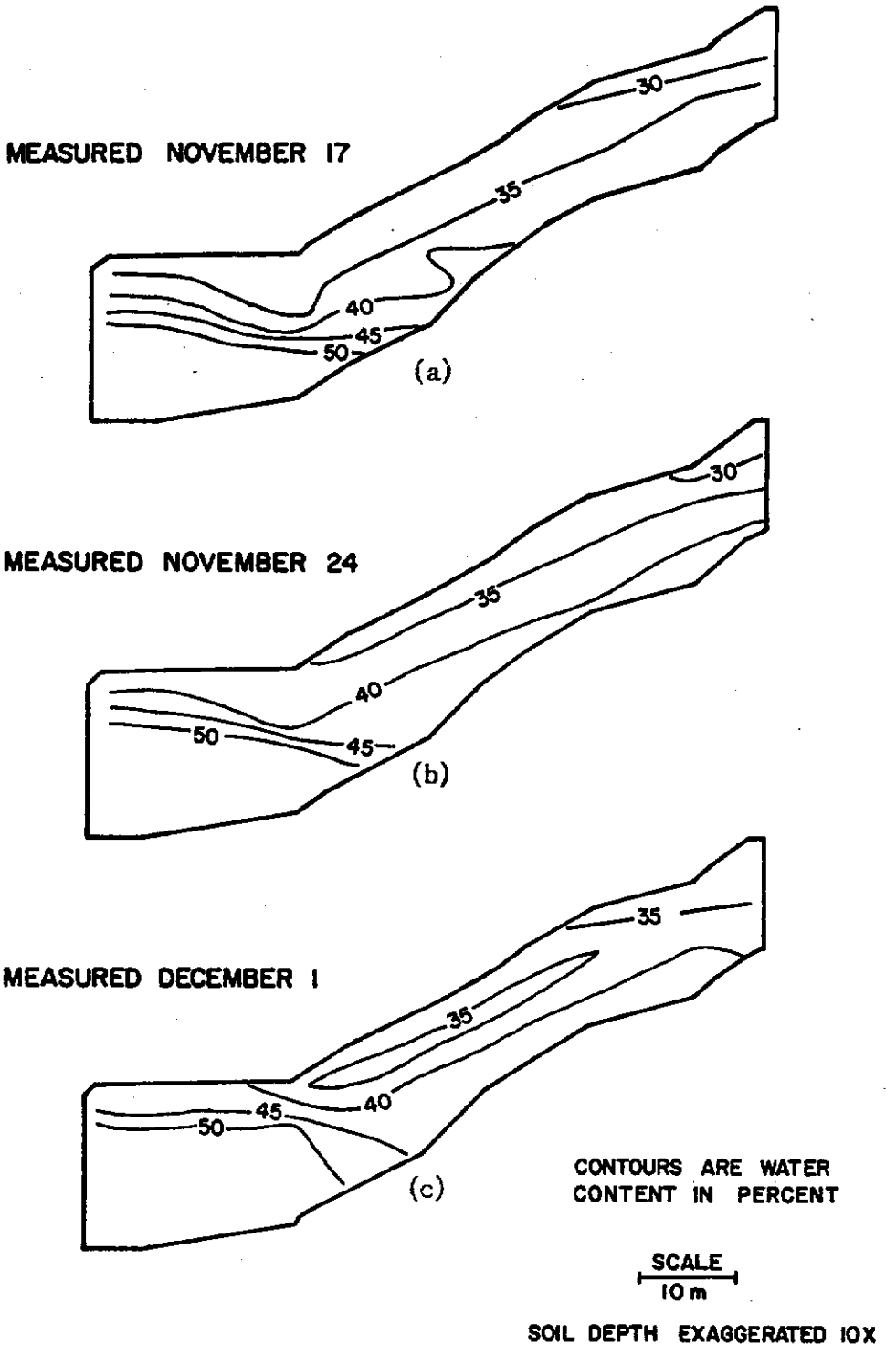

Figure 6.2 Water Content Profiles on the Test Plot Measured on: (a) November 17; (b) November 24; and (c) December 1, 1982.

Figure 6.1, shows that November 17 was during a fairly dry period. The two following weeks had substantial amounts of rainfall during the week preceding the water content measurement. The water content contours were generated using data from access tubes A, B, E, J, H, and I (see Figure 3.5 for locations on the test plot).

The water content profiles show a slow wetting up of the entire hillslope in response to precipitation. However, significant water content gradients exist in the hillslope profile at all times, even following major precipitation events. In Figure 6.2a it appears that the soil upslope has undergone drainage. This upslope drainage supplies the near stream saturated zone, much like that seen in the Coweeta soil troughs and that proposed in Figure 2.1. The response of the hillslope to rainfall is shown in Figures 6.2b and 6.2c. Water stored in the hillslope increases most significantly during the first week as the water content increases uniformly throughout the profile.

6.1.3 Weekly Water Table Measurements

The water table position was also measured weekly at the four piezometer locations (see Figure 3.5). The depths of the water table during the period of record at the four locations are presented in Figure 6.3. This figure shows the response of the saturated zone to rainfall, which could not be seen explicitly in the weekly water content profiles.

Piezometer 2, near the base of the hillslope, was the best indicator of the extent of the saturated zone, while the water table depth at Piezometer 1, near the stream, was fairly uniform. From Figure 3.5 it can be seen that the ground is fairly flat around Piezometer 1. In addition, the surface elevation of the stream does not fluctuate greatly in comparison to upslope changes in water table elevation, and hence, tends to fix the water table position at Piezometer 1 at an almost constant level. On November 19 the saturated zone still extended upslope as far as Piezometer 3, 7 days after a 35 mm precipitation event. Measurements on November 24 and December 1 show the buildup of the saturated zone in response to two precipitation events on November 21-22 and November 26-27.

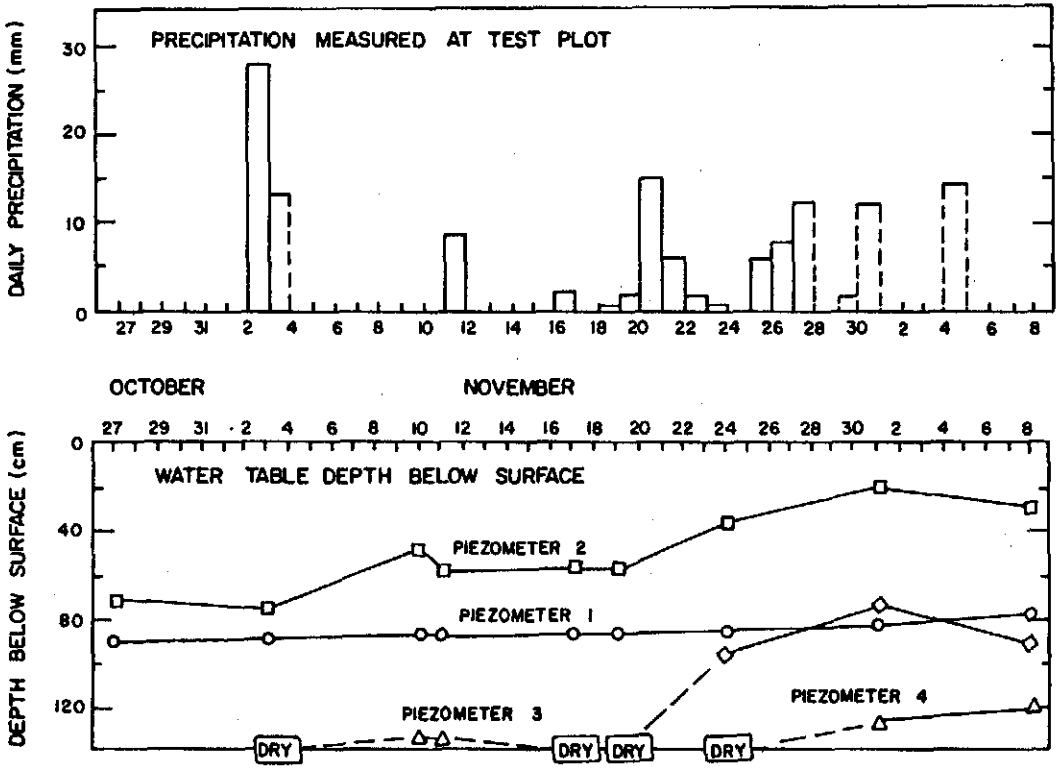

Figure 6.3 Water Table Positions at the Four Piezometer Locations and the Daily Precipitation Record on the Test Plot.

6.1.4 Tensiometer Measurements

As was discussed in Chapter 3, the tensiometer results were not as accurate as originally hoped. The tensiometers were designed to provide information concerning the rapid response of the hillslope to rainfall during rainfall-runoff events. The tensiometer system was tied into the data logger, together with the tipping-bucket precipitation recording system, and so the tensiometer and precipitation records are in phase with each other. Like the precipitation record, tensiometer measurements were made at a 30 minute time interval.

The soil water pressure heads measured by the tensiometers, together with the the soil-water characteristic curves measured and described in Chapter 3, provide an estimate of the water stored in the hillslope. Hysteresis effects were taken into account in determining the soil water content using Mualem's method (Mualem, 1971, 1977). Hence, the 30 minute precipitation and soil water content measurements (made via the tensiometer pressure measurements) provide the basic data for performing the rainfall-runoff analysis on the test plot for selected events. This analysis is described below in Section 6.2.

6.2 RAINFALL-RUNOFF ANALYSIS

6.2.1 Analysis Procedures

Since subsurface stormflow is the primary focus of this study, the procedure developed for the rainfall-runoff analysis considered only the time during which precipitation was falling and immediately thereafter. This minimizes the impact of failing tensiometers on the storage calculations because the analysis is over a shorter time period.

Runoff from the test plot can be estimated using the water balance equation,

$$R = P - \Delta S \qquad \ldots (6.1)$$

where R and P are the runoff and precipitation volumes during the time interval, and ΔS is the change in storage over the time period. For this analysis the time interval was 30 minutes. As noted earlier,

ΔS is estimated from the tensiometer measurements of soil water pressure head. Evapotranspiration was neglected in the calculations because of the short time periods involved.

As a first trial, this procedure was used by dividing the hillslope into three layers and letting the water content of each layer be a function of the tensiometer reading in that layer. The properties of the layers are presented in Chapter 3. The result for the period from October 31 through November 4 is presented in Figure 6.4. For the dry period, October 31 to November 3, the tensiometers show a gradual decrease in storage (i.e. an increase in measured soil-water pressure head) as unsaturated drainage occurs, similar to that observed by Hewlett (1961). However, this procedure does not work well during a precipitation event, since not all of the tensiometers were working, and as the wetting front passed a tensiometer the predicted soil-water storage in the layer increased abruptly. This creates a discontinuity or step function response of soil water and negative runoff, which is contrary to the actual physical process. Therefore, the runoff calculations must include some estimation of the wetting front movement in order to obtain meaningful runoff estimations.

The wetting front movement was taken into account by developing a wetting front velocity-depth relationship with velocity as a function of depth. This was accomplished for each event by observing when the wetting front passed each tensiometer depth. The velocity calculated using the time lag and change in depth was assumed to be the velocity at the midpoint of that depth increment. The velocity function was also assumed to be linear between the depth increment midpoints. Using the velocity function and a central difference procedure, the depth of the wetting front was calculated at each time step (30 minute increments).

The water content of the wetting front was calculated using the tensiometer data and the estimated soil water characteristic for that layer.

Having the change in storage estimated in this manner, runoff was then calculated using Equation 6.1. The tensiometers only measure

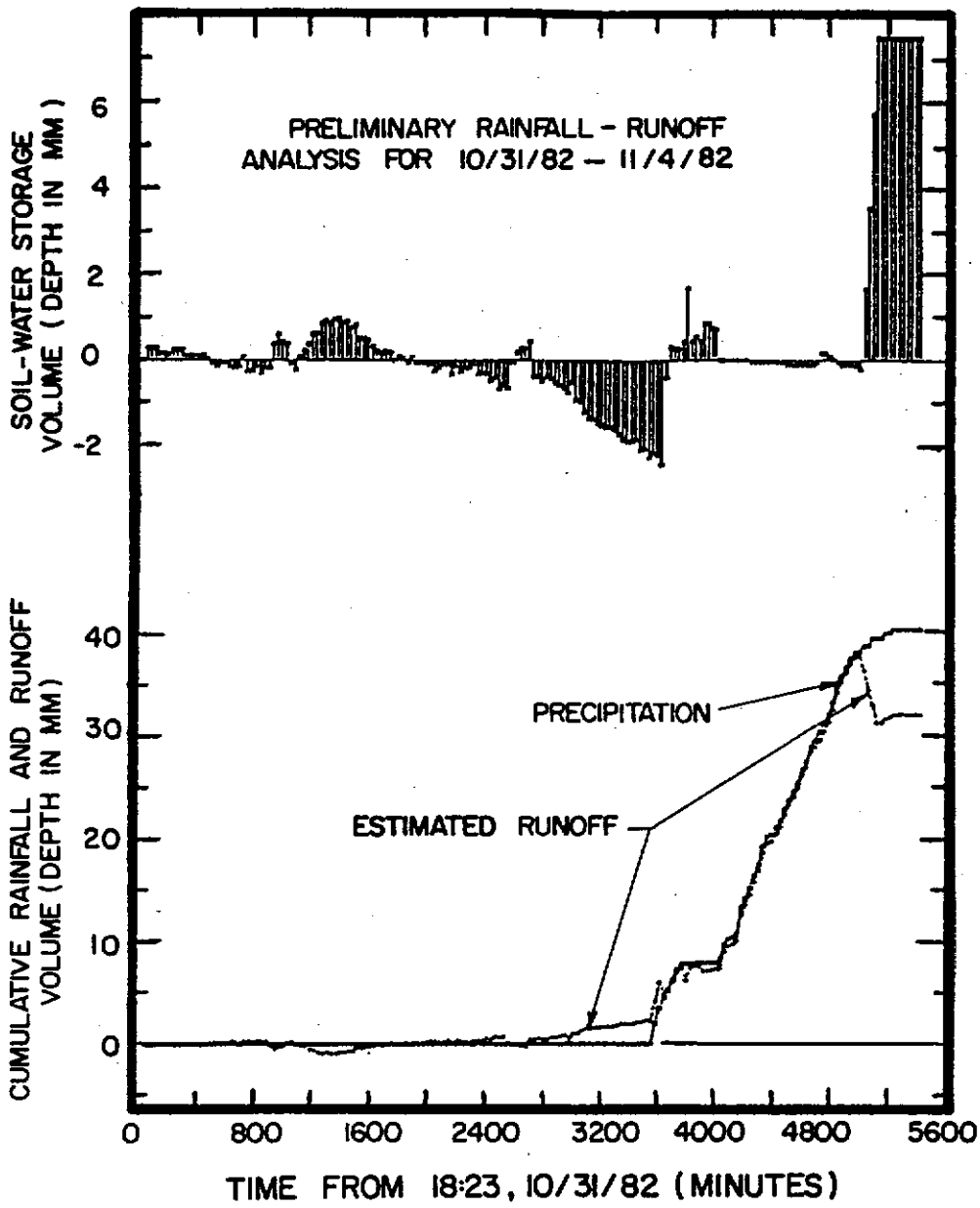

Figure 6.4 First Trial Rainfall-Runoff Analysis for the Period From October 31 to November 4, 1982. Does not include an allowance for continuous wetting front movement and so creates a step function response of soil water resulting in negative estimated runoff at times (indicated by a decrease in the cumulative runoff volume).

water within the soil matrix and so the analysis assumes that if water is not stored in the soil matrix then it is runoff. In other words, all water in the macropores is routed immediately to the stream. This is not entireely correct, but it is the best estimate possible with the instrumentation used.

6.2.2 Rainfall-Runoff Results

The rainfall-runoff analysis was conducted on four events in 1982: November 3-4, November 12, November 21-22, and November 26-27. The results are shown in Figures 6.5 through 6.8. On inspection of these figures, it can be seen that the hillslope responds very quickly to precipitation in each case. This is to be expected if macropore flow dominates, and the change in storage in the soil matrix, indicated by the tensiometers, does not change rapidly.

The November 3-4 event (Figure 6.5) was preceeded by a dry spell of 8 days, so the first 8-9 mm of precipitation went towards satisfying the hillslope deficits. The soil water tension was great enough that it could rapidly absorb that much water. After that, however, the macropores (root holes, burrows, etc.) became locally saturated and runoff began, responding rapidly to precipitation.

Precipitation for the November 12 event (Figure 6.6) was short in duration, but intense. Again, most of the rainfall was converted to runoff. The antecedent water content for the November 21-22 event (Figure 6.7) was fairly high and the hillslope was primed for runoff, since it had rained the two previous days. The analysis shows that the soil matrix did not respond to precipitation, so all storage and runoff for this event must have taken place in the macropores. The November 26-27 event (Figure 6.8) is a small event, like the November 12 event, and similar results are observed. In these figures, the runoff response that follows the precipitation initially but then drops below the precipitation is probably due to a lagging or erroneous tensiometer response.

6.3 EVALUATION OF THREE SUBSURFACE STORMFLOW MODELS

The precipitation records for the four rainfall events identified above were applied to three subsurface flow models. The runoff predicted by each of the models for each of the events was then compared to that calculated from the plot data in the rainfall-runoff

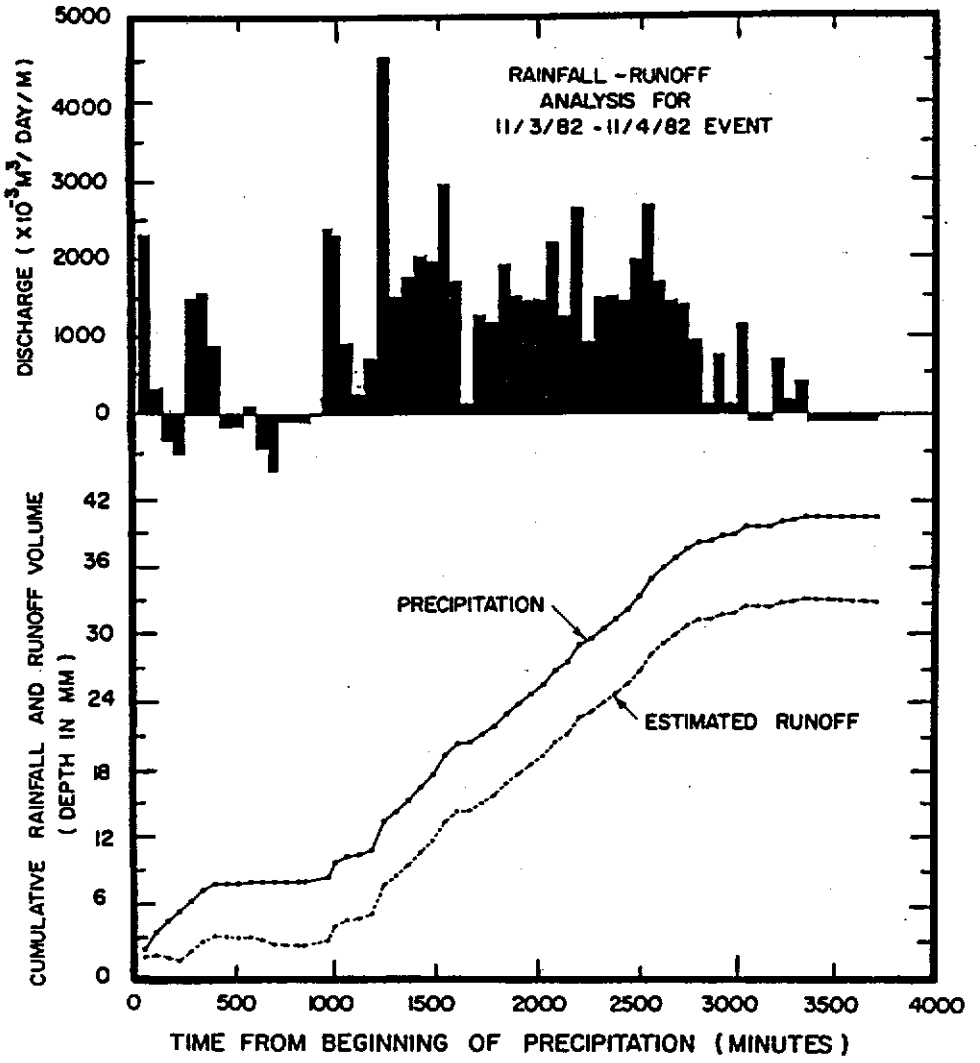

Figure 6.5 Rainfall-Runoff Analysis Results for the November 3-4, 1982 Event.

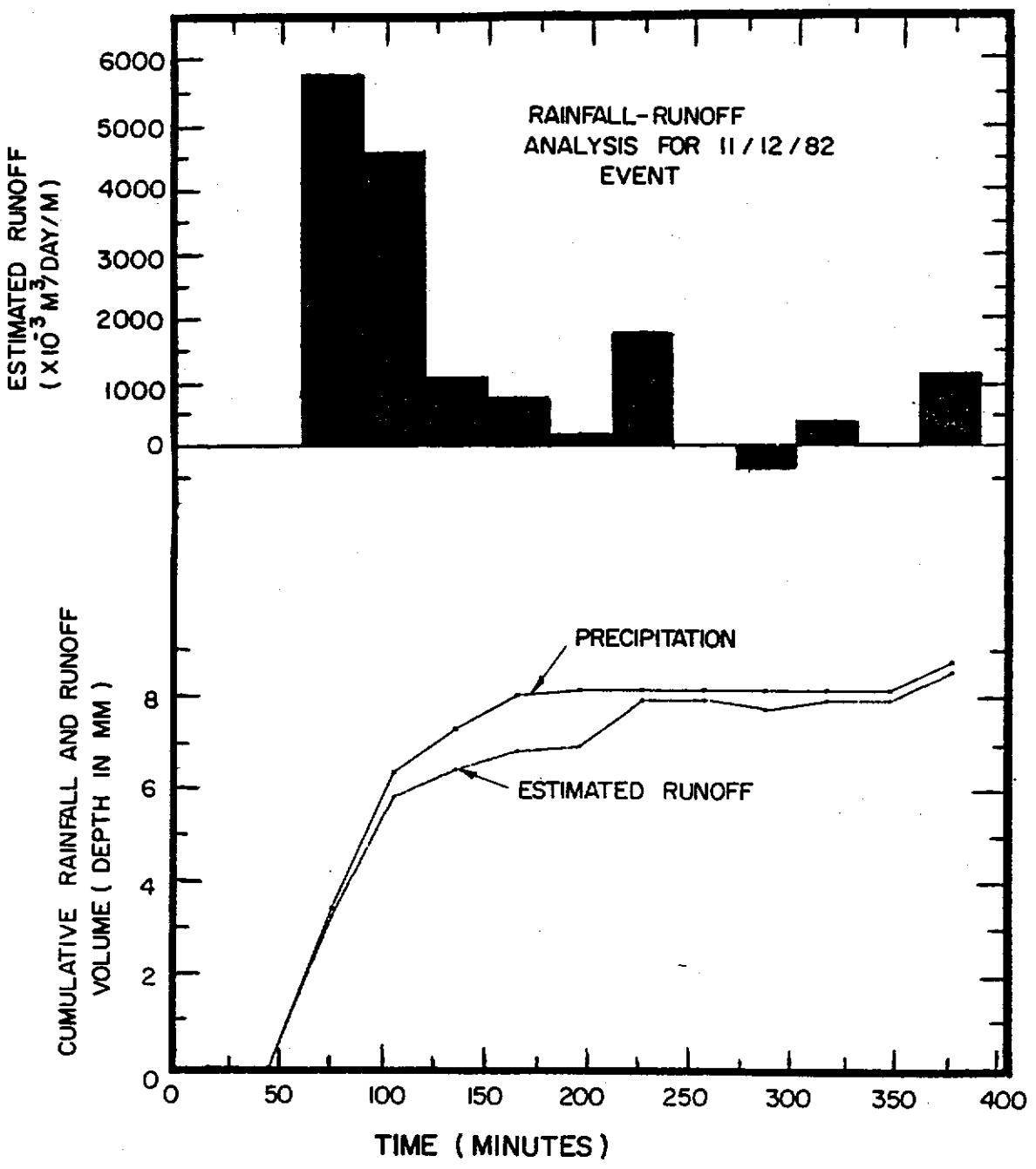

Figure 6.6 Rainfall-Runoff Analysis Results for the November 12, 1982 Event. The magnitude of the negative runoff (which can not occur in practice) indicates the potential error in the calculations.

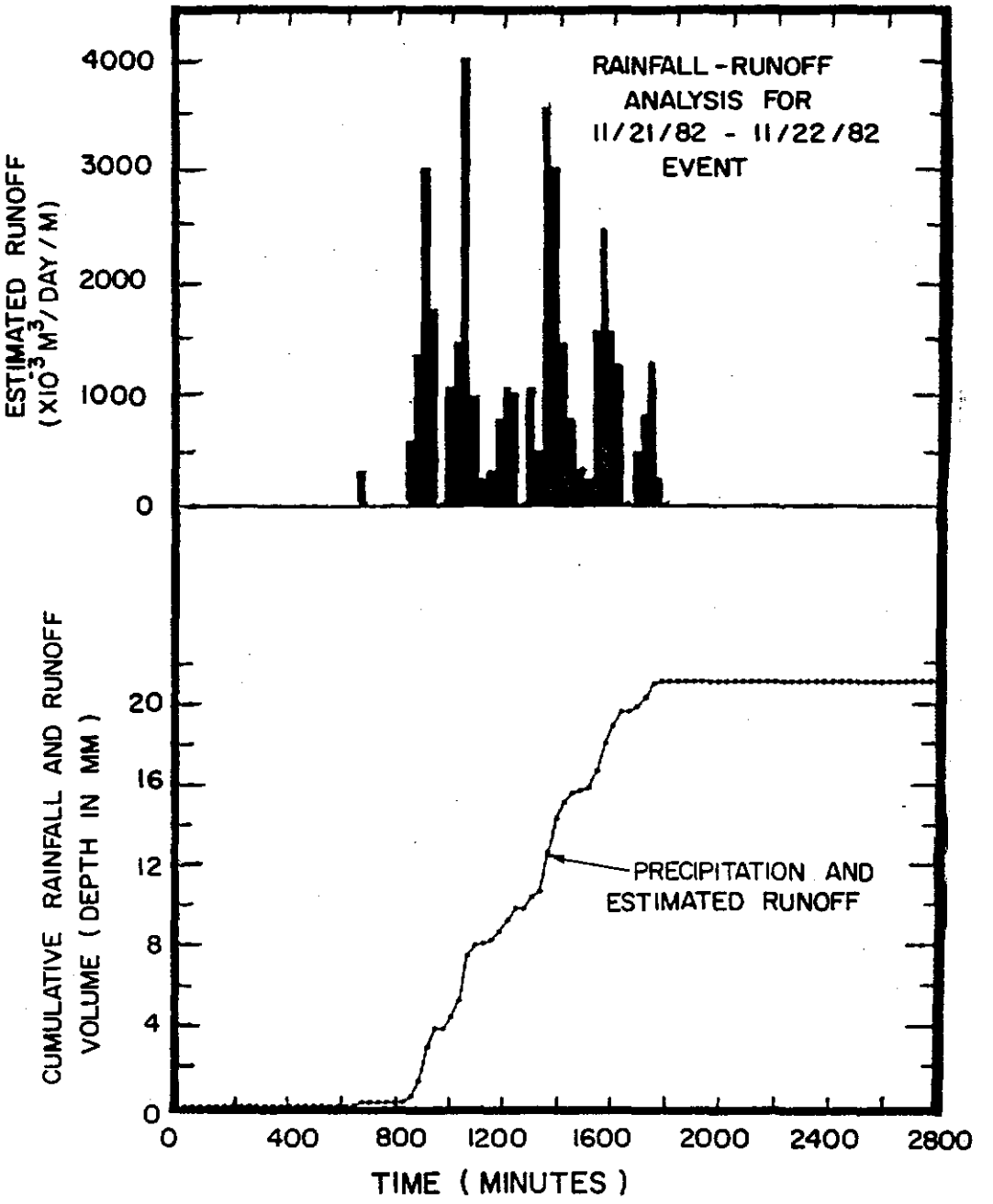

Figure 6.7 Rainfall-Runoff Analysis Results for the November 21-22, 1982 Event.

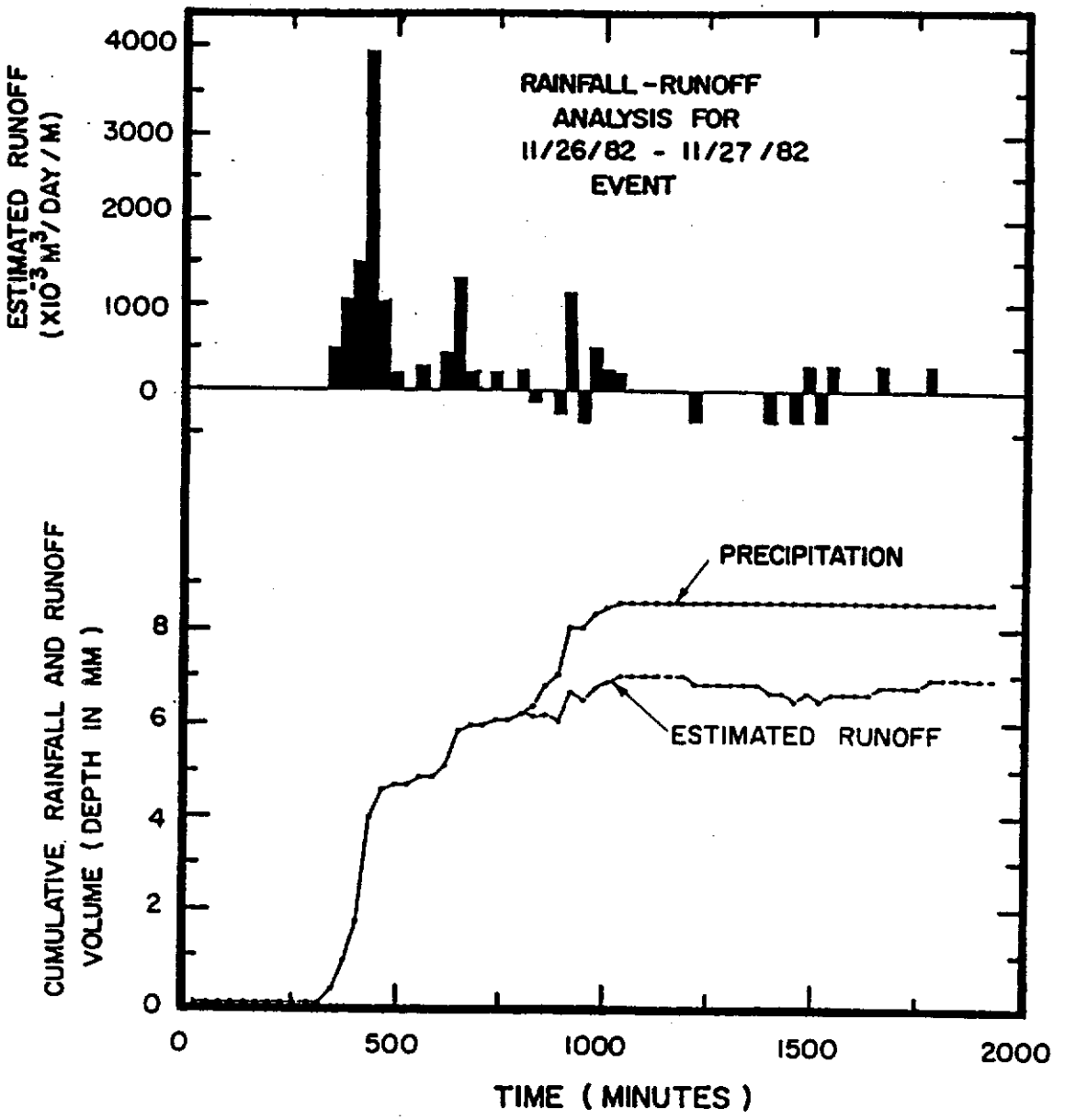

Figure 6.8 Rainfall-Runoff Analysis Results for the November 26-27, 1982 Event. The magnitude of the negative runoff (which can not occur in practice) indicates the potential error in the calculations. This error is reflected in the cumulative runoff volume curve at t=900 minutes.

analysis. The three models are Nieber's 1-D finite element model, based on Richards' equation, the kinematic storage model, and the kinematic wave model. Precipitation input for the 1-D model and the kinematic storage model had a 30 minute time increment, while the kinematic wave model used a constant rainfall rate for the storm duration, since it is not set up for varying precipitation.

Three levels of hydraulic conductivity (K_s) were used in order to demonstrate the effect of using an effective hydraulic conductivity for the hillslope. The baseline hydraulic conductivity is 12 cm/hr and is an average for the hillslope profile based on the 7.6 cm core permeameter measurements presented in Chapter 3. As stated in Chapter 3 this would be the lower limit for the effective hydraulic conductivity. The second level is 120 cm/hr, one order of magnitude above the baseline, and the third level is 600 cm/hr, one and a half orders of magnitude above the baseline. The high hydraulic conductivities represent quick subsurface stormflow through macropores. For comparison, Mosley (1979) calculated an effective hydraulic conductivity of 4920 cm/hr on a New Zealand watershed using tracer velocities, an effective porosity, and a hydraulic gradient equal to the bed slope.

None of the models used in these simulations took into account hysteresis. The version of the 1-D mdoel used in Chapter 5 did consider hysteresis when calculating water content and hydraulic conductivity, but the version used for the following analysis does not include a coupled infiltration model or hysteresis. It was assumed that the error introduced by hysteresis was less than the error in approximating the soil water characteristic (Equations 2.6 and 2.7, and Table 3.2).

6.3.1 Kinematic Storage Model

6.3.1.1 Modifications to the Model

The kinematic storage model presented in Chapter 5 does not allow for surface runoff where the saturated zone reaches the

surface, as can be the case when there are high precipitation rates. Modifications to account for this were made before beginning the test plot simulation studies. However, for the four events examined, the hydraulic conductivities were high enough and precipitation rates small enough so that surface runoff did not occur anywhere on the hillslope.

Surface runoff is easily accounted for in this model by using the same geometry as proposed in Chapter 5 (Figure 5.7). The water table still remains hinged at point D (Figure 5.7). When the water table intersects the soil surface, Equations 5.15 and 5.18 become

$$S = [DL_s + (L - L_s)D/2] [\theta_s - \theta_d] \quad \ldots .(6.2)$$

$$q = i L_s + DV \quad \ldots .(6.3)$$

where L_s is the saturated slope length and the other symbols are as previously defined.

6.3.1.2 Kinematic Storage Model Results

The kinematic storage model was initially run with the unsaturated storage input algorithm (described in Chapter 5) which was used for the Coweeta soil trough simulation. With the model in this form the initial water content was determined by letting the hillslope drain from saturation for a period equal to the time since the last precipitation event. This estimate of the antecedent water content was consistent with the unsaturated storage input algorithm, and did not give excessive inputs as would be the case if the tensiometer and nuclear probe data were used. However, the resulting initial water contents were unrealistically low compared to the measured water contents. For example, for the November 3-4 event the average initial water content given by the tensiometer data was 0.335, from the nuclear probe data, 0.30, and the simulated water content was 0.190 for K_s = 12 cm/hr (less for the higher hydraulic conductivities).

Figure 6.9 presents the results of the simulations for the three hydraulic conductivities. For all three simulated hydrographs the time lag is excessive and the unsaturated storage input zone dampens out the predicted rainfall-runoff relationship. The Coweeta simulation showed that the model performed very well for a homogeneous reconstructed soil, where all flow was through the soil matrix. For actual forest conditions, however, the assumptions are not as valid. The forest soil profile is interlaced with many macropores allowing quick vertical flow to the impermeable bed or lateral soil pipes. Therefore, in the subsequent discussion it was assumed that there is no time delay between precipitation and input to the base of the hillslope profile (saturated zone).

Figures 6.10 through 6.13 present the results of the kinematic storage model simulations where no time delay was used. These results are much better that those in Figure 6.9 where the unsaturated storage zone was included. In all cases the simulation improves as the hydraulic conductivity is increased. The discharge hydrographs show that the timing of runoff is good for the higher conductivities and lags only slightly behind the field data. The hydrograph in Figure 6.10 is an example of this. In all four events the baseline hydraulic conductivity is not a good estimate of the effective hydraulic conductivity. Increasing the hydraulic conductivity by one order of magnitude is a substantial improvement as shown by the hydrographs and the cumulative runoff curves. Increasing the hydraulic conductivity further does not improve the cumulative runoff curves very much, but the hydrographs show that the runoff peaks are estimated better.

6.3.2 Kinematic Wave Model Results

Results for the kinematic wave model are shown in Figures 6.14 through 6.17. These results are somewhat limited because of the assumption of a constant precipitation rate during the event. The kinematic wave model uses the piston flow equations (Equations 2.17 - 2.19) to estimate input to the saturated zone. The initial

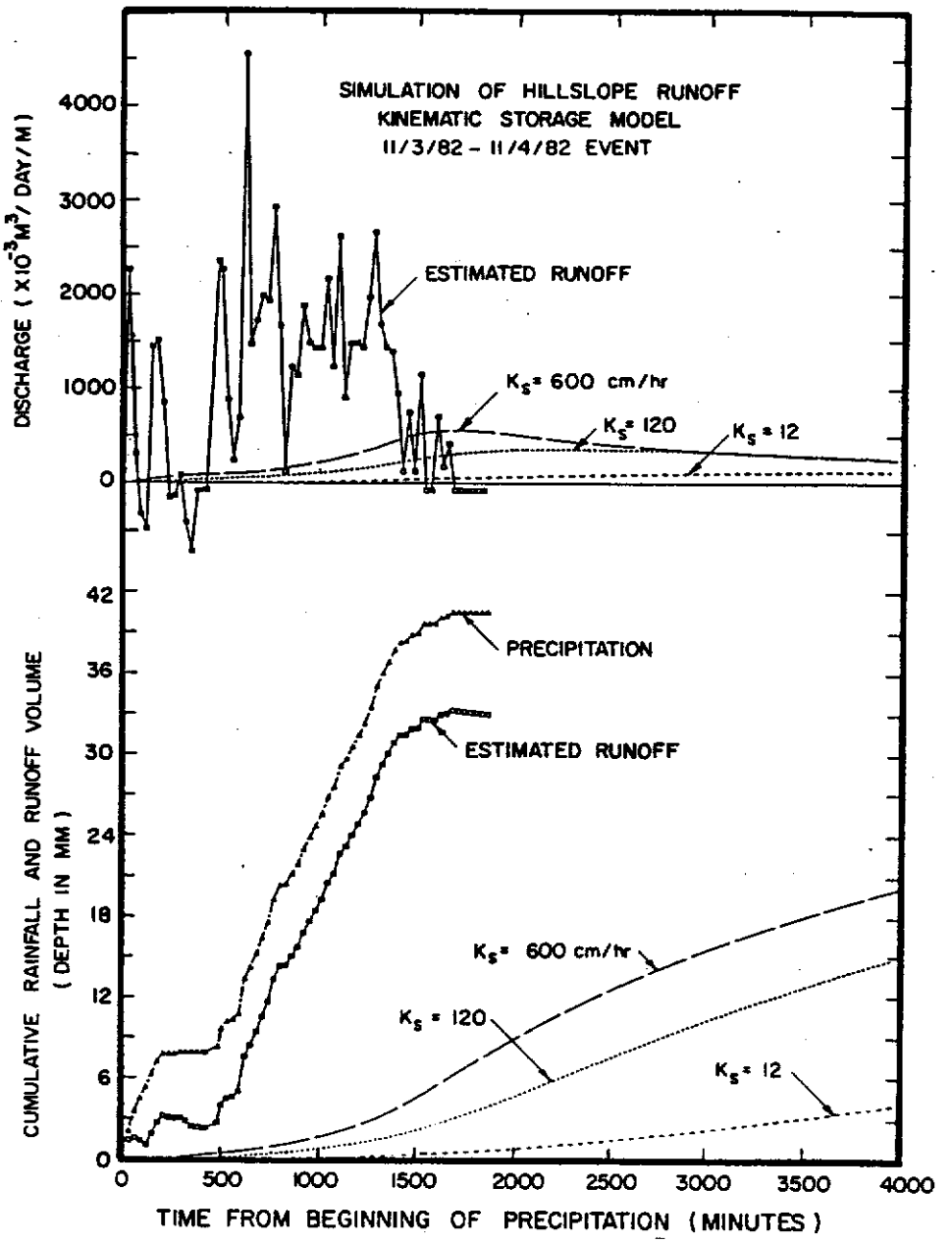

Figure 6.9 Comparison of Estimated and Predicted Runoff Hydrographs and Cumulative Runoff Volumes for the Kinematic Storage Model at Three Saturated Hydraulic Conductivities (K_s = 12, 120, and 600 cm/hr) for the November 3-4 Event. The magnitude of the negative runoff (which can not occur in practice) indicates the potential error in the calculations.

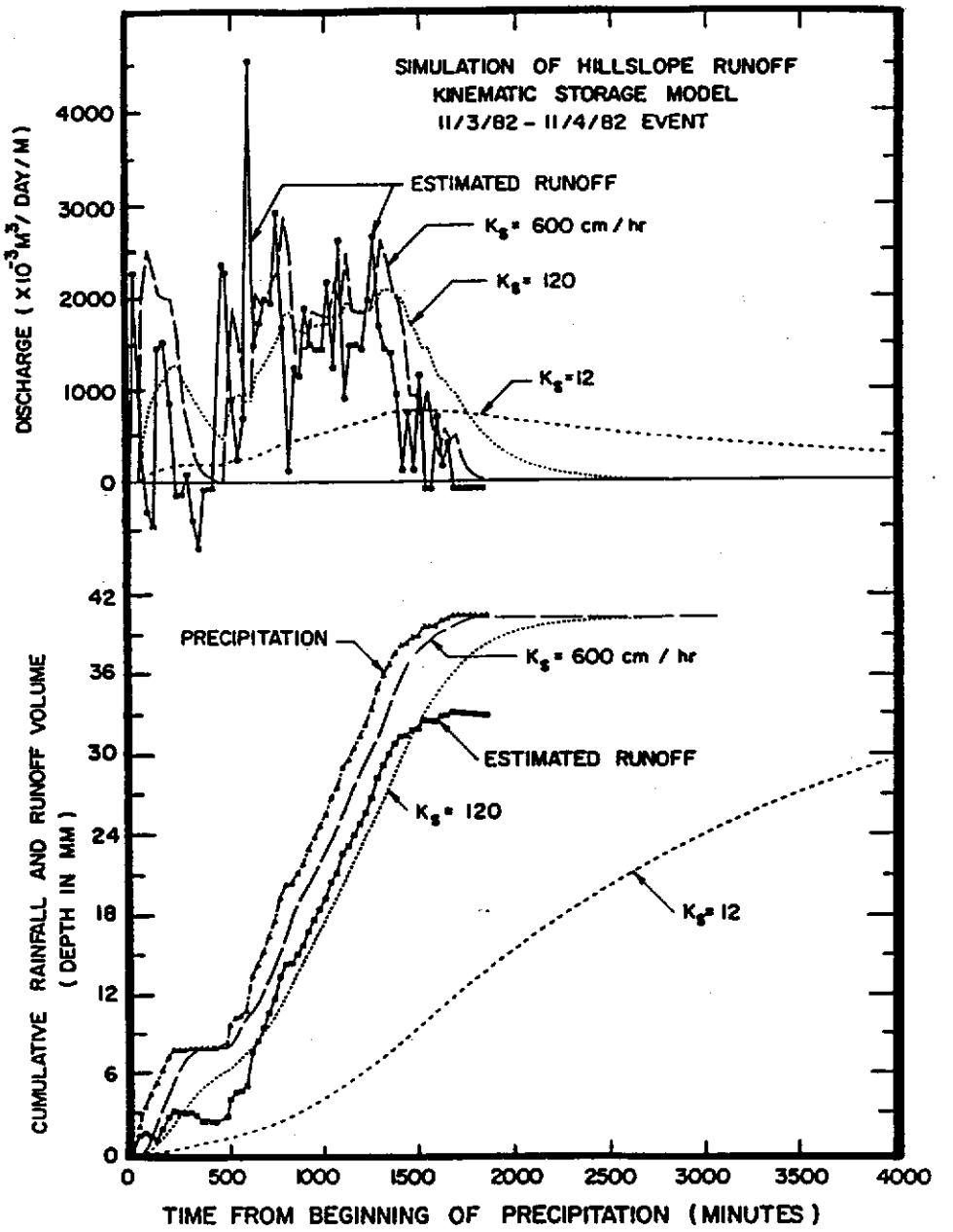

Figure 6.10 Comparison of Estimated and Predicted Runoff Hydrographs and Cumulative Runoff Volumes for the Kinematic Storage Model with no Time Delay, at Three saturated Hydraulic Conductivities (K_s= 12, 120, and 600 cm/hr) for the November 3-4 Event. The magnitude of the negative estimated runoff (which can not occur in practice) indicates the potential error in the calculations.

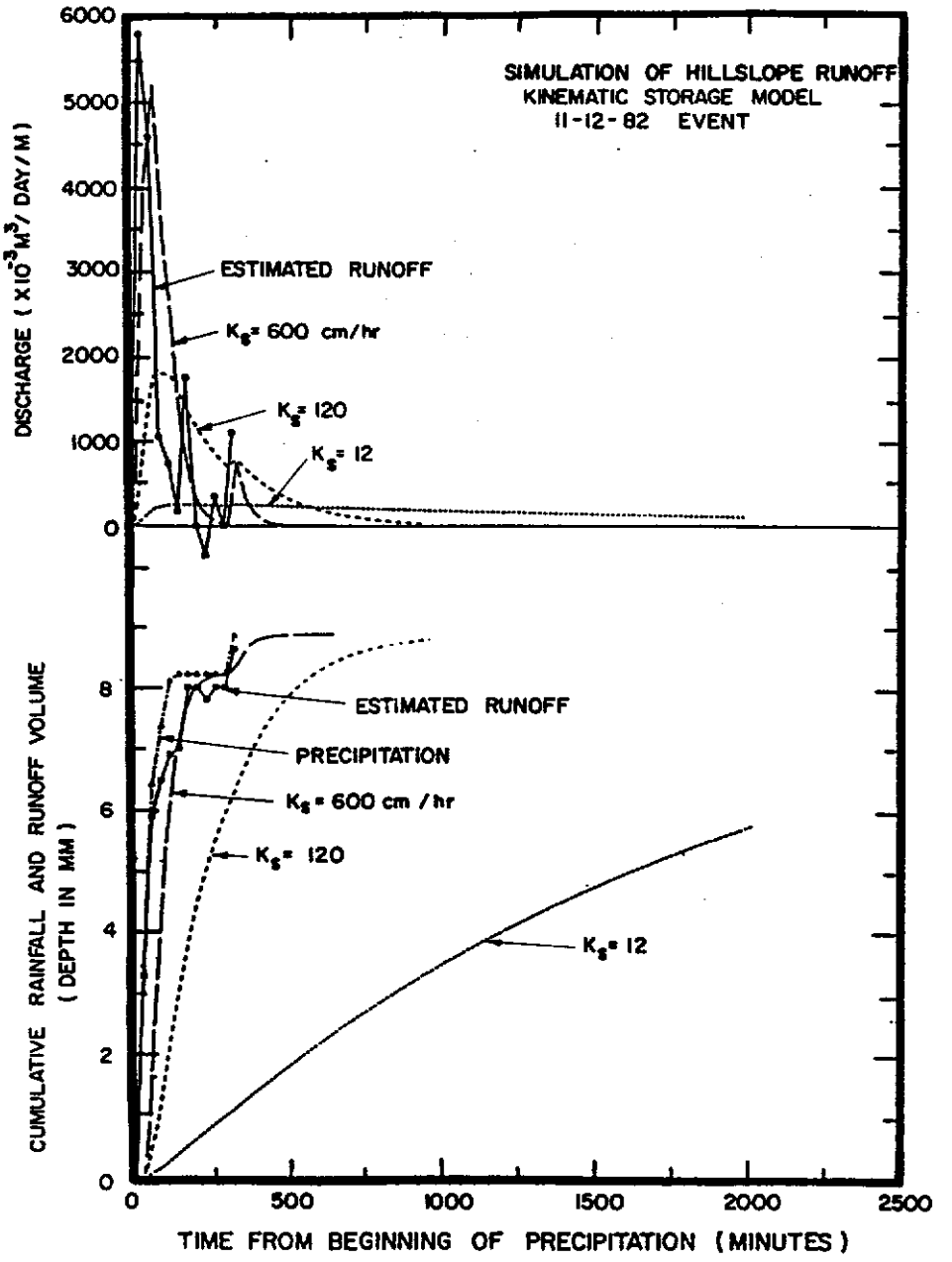

Figure 6.11 Comparison of Estimated and Predicted Runoff Hydrographs and Cumulative Runoff Volumes for the Kinematic Storage Model with no Time Delay, at Three Saturated Hydraulic Conductivities (K_s = 12, 120, and 600 cm/hr) for the November 12 Event. The magnitude of the negative estimated runoff (which can not occur in practice) indicates the potential error in the calculations.

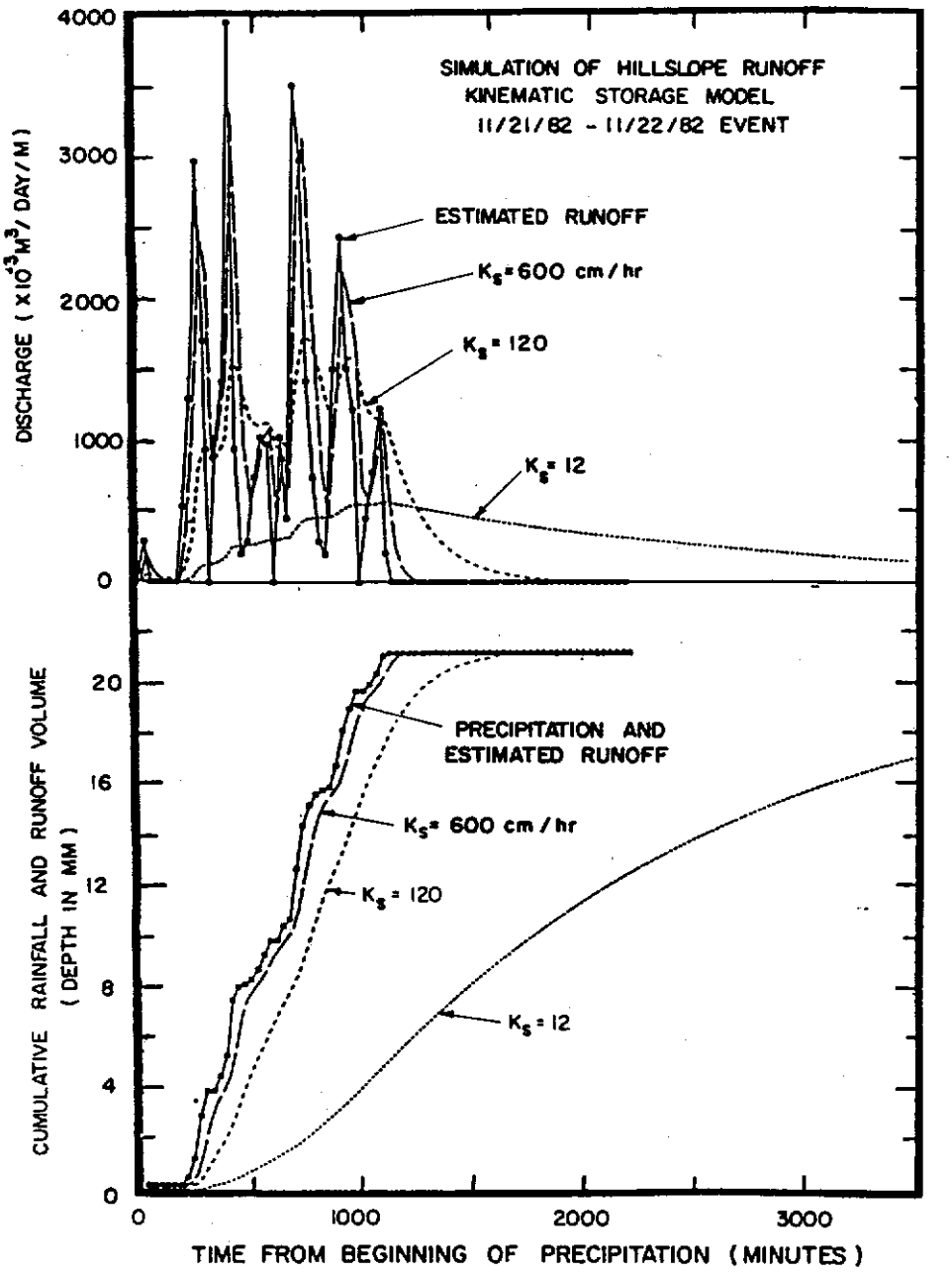

Figure 6.12 Comparison of Estimated and Predicted Runoff Hydrographs and Cumulative Runoff Volumes for the Kinematic Storage Model with no Time Delay, at Three Saturated Hydraulic Conductivities (K_s= 12, 120, and 600 cm/hr) for the November 21-22 Event. The magnitude of the negative estimated runoff (which can not occur in practice) indicates the potential error in the calculations.

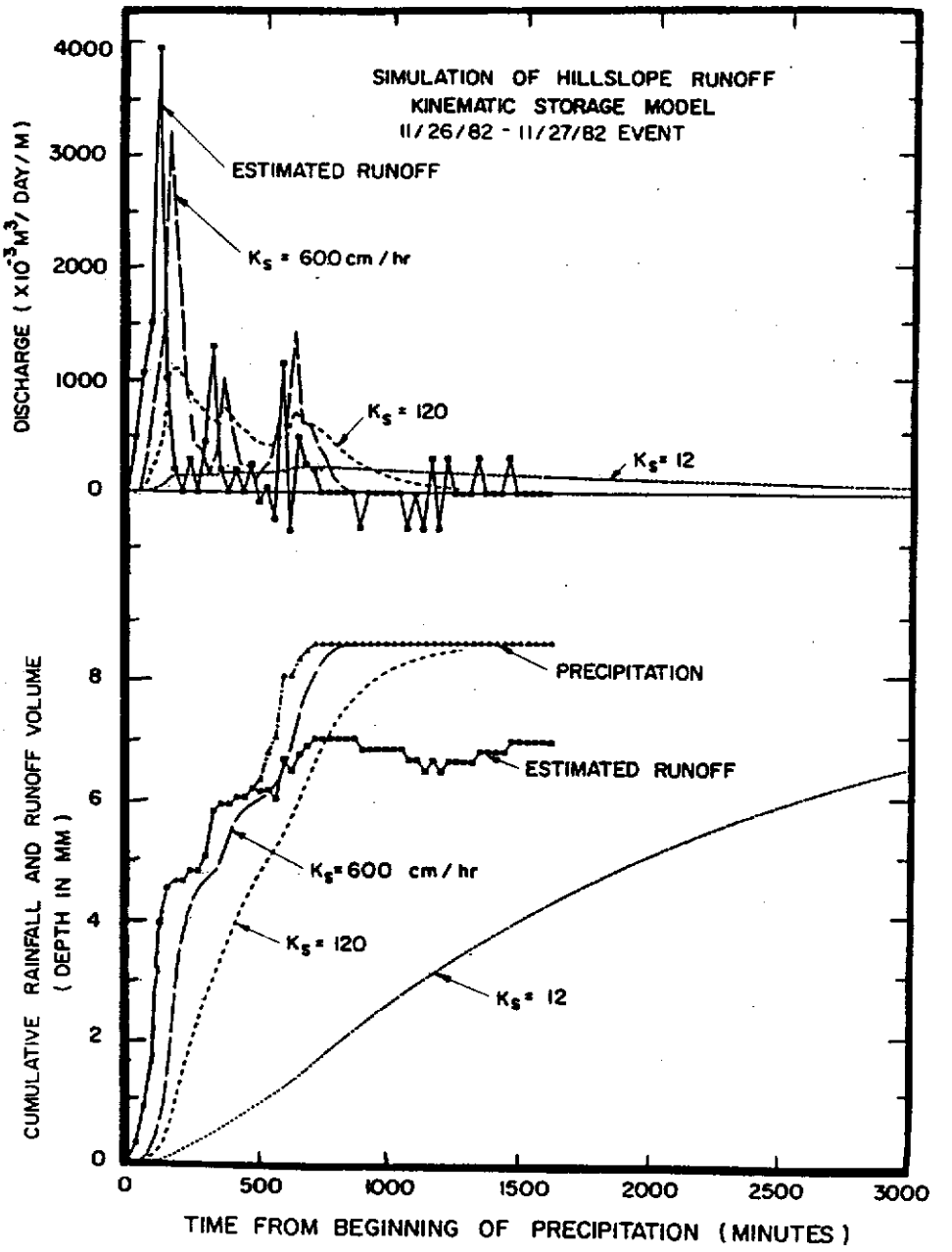

Figure 6.13 Comparison of Estimated and Predicted Runoff Hydrographs and Cumulative Runoff Volumes for the Kinematic Storage Model with no Time Delay, at Three Saturated Hydraulic Conductivities (K_s = 12, 120, and 600 cm/hr) for the November 26-27 Event. The magnitude of the negative estimated runoff (which can not occur in practice) indicates the potential error in the calculations.

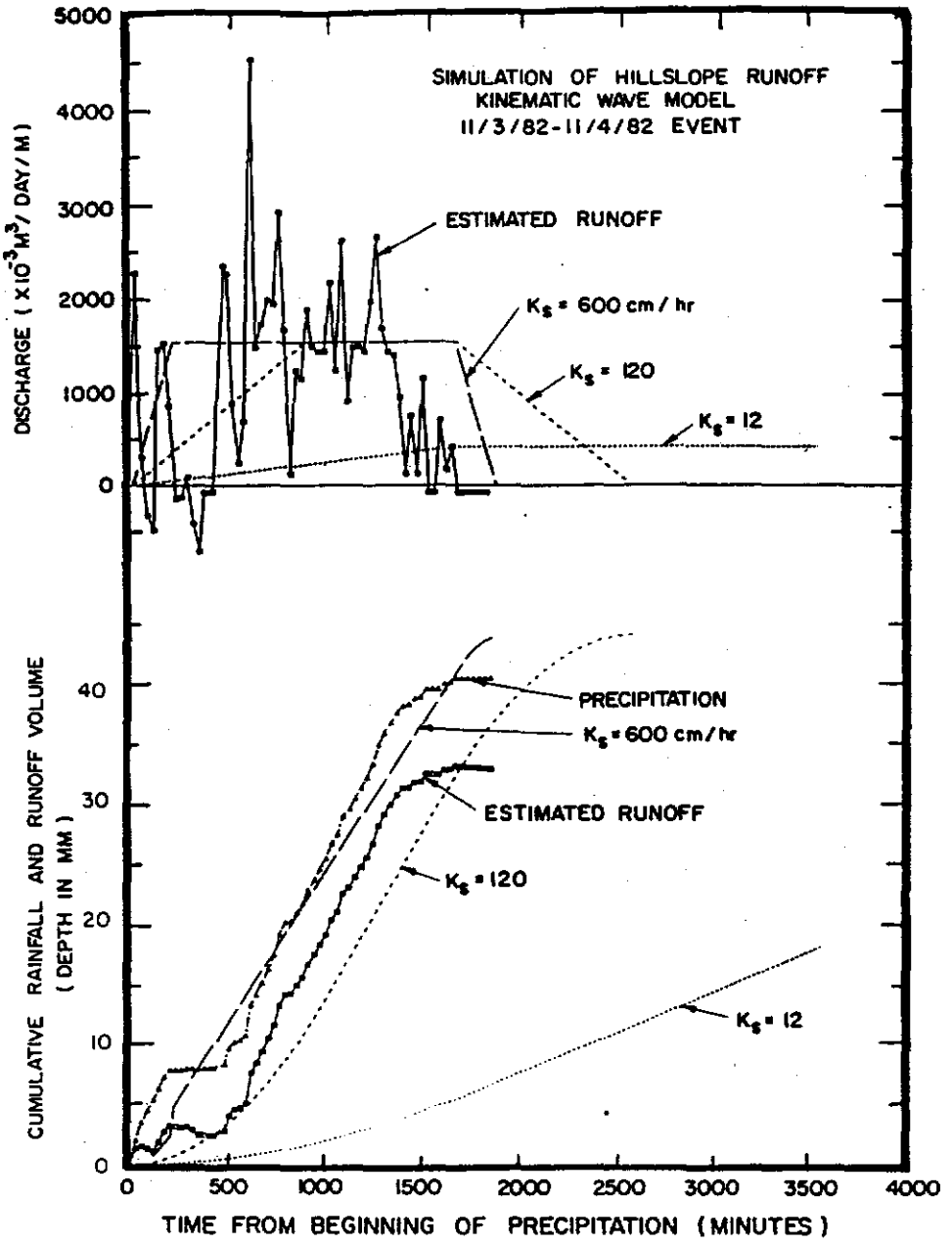

Figure 6.14 Comparison of Estimated and Predicted Runoff Hydrographs and Cumulative Runoff Volumes for the Kinematic Wave Model (constant precipitation rate used) at Three Saturated Hydraulic Conductivities (K_s = 12, 120, and 600 cm/hr) for the November 3-4 Event. The magnitude of the negative estimated runoff (which can not occur in practice) indicates the potential error in the calculations.

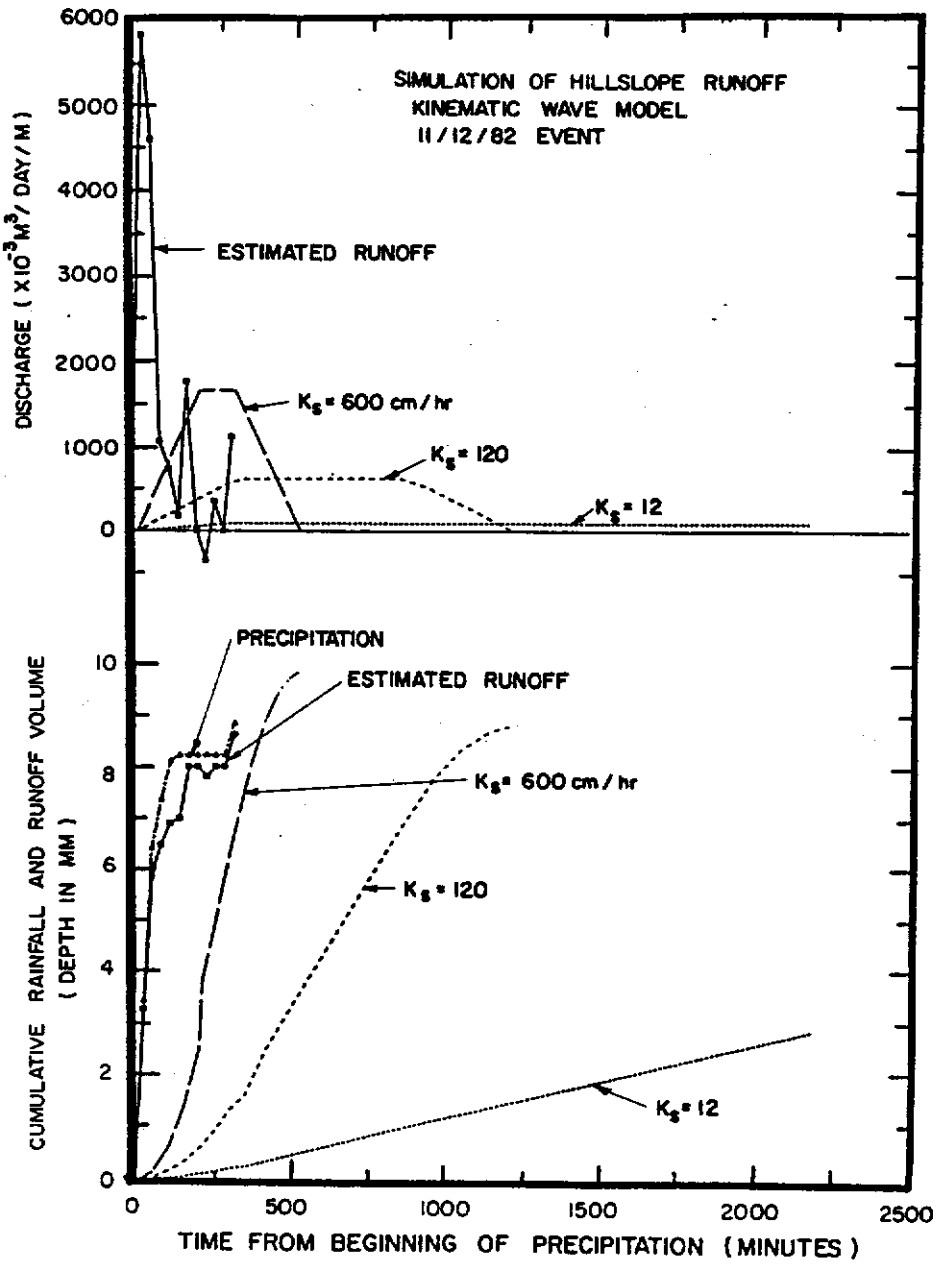

Figure 6.15 Comparison of Estimated and Predicted Runoff Hydrographs and Cumulative Runoff Volumes for the Kinematic Wave Model (constant precipitation rate used) at Three saturated Hydraulic Conductivities (K_s = 12, 120, and 600 cm/hr) for the November 12 Event. The magnitude of the negative estimated runoff (which can not occur in practice) indicates the potential error in the calculations.

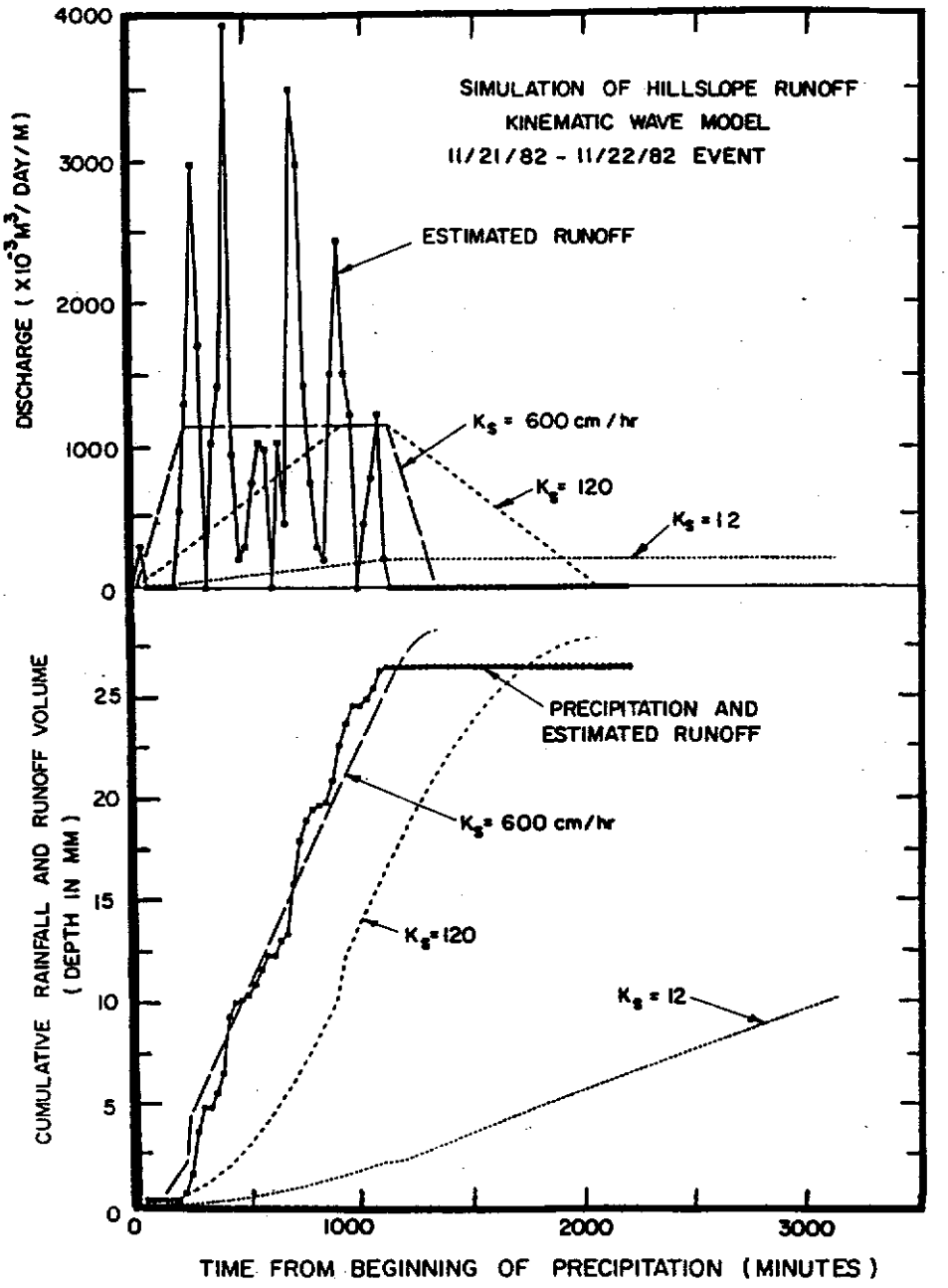

Figure 6.16 Comparison of Estimated and Predicted Runoff Hydrographs and Cumulative Runoff Volumes for the Kinematic Wave Model (constant precipitation rate used) at Three Saturated Hydraulic Conductivities (K_s = 12, 120, and 600 cm/hr) for the November 21-22 Event.

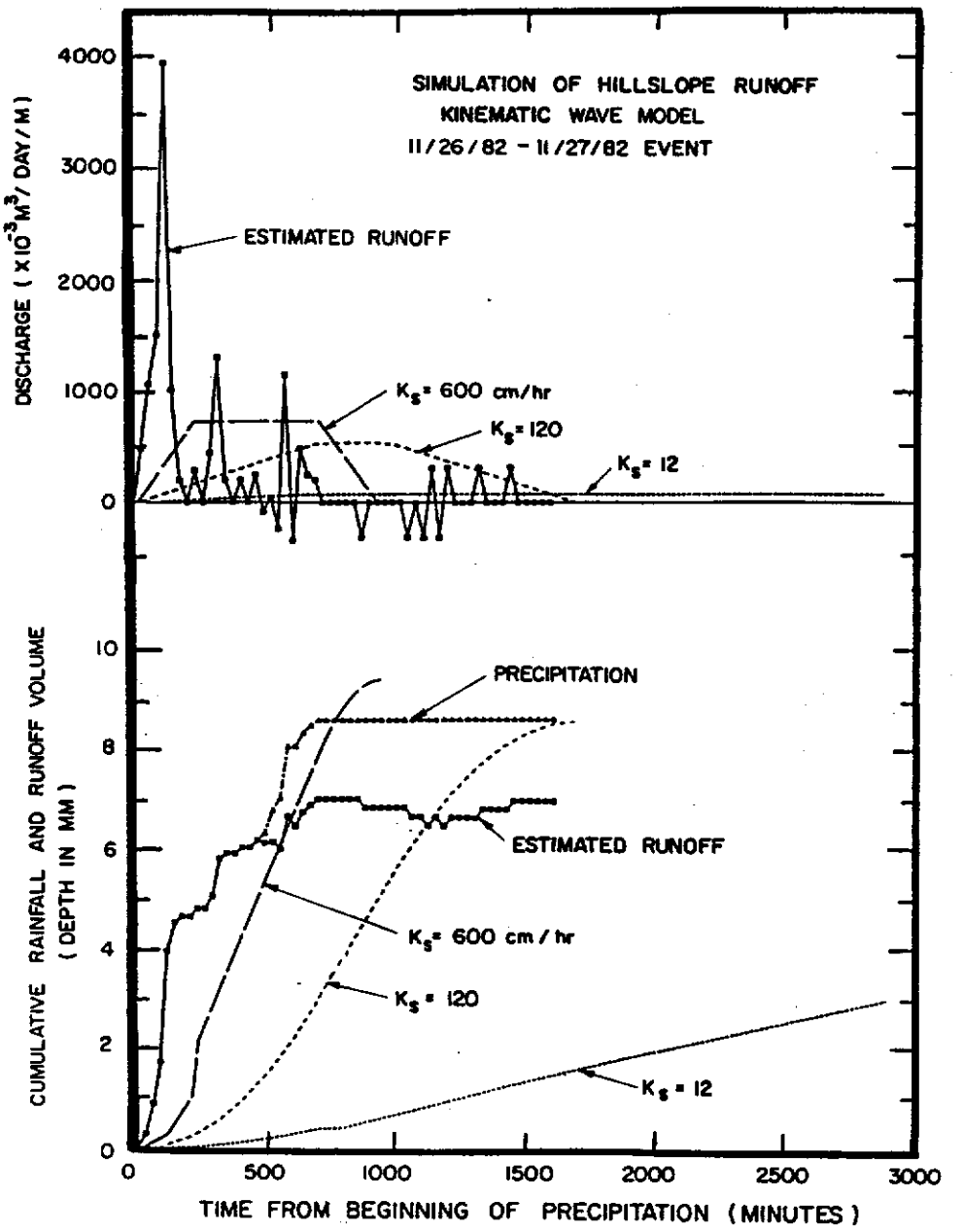

Figure 6.17 Comparison of Estimated and Predicted Runoff Hydrographs and Cumulative Runoff Volumes for the Kinematic Wave Model (constant precipitation rate used) at Three Saturated Hydraulic Conductivities (K_s = 12, 120, and 600 cm/hr) for the November 26-27 Event. The magnitude of the negative estimated runoff (which can not occur in practice) indicates the potential error in the calculations.

water contents for all the events were such that the unsaturated hydraulic conductivities (at the respective initial water contents) were greater than the rainfall rate. Therefore, there is no time lag for input to the base of the hillslope profile (saturated zone). This is consistent with the rainfall-runoff analysis which showed a high responsiveness of runoff to precipitation.

The cumulative runoff curves show that the greater the hydraulic conductivity the better the simulation of runoff. This occurs because the time lag for routing to the outlet is less at the higher conductivity levels. Inspection of the discharge hydrographs shows that the model cannot predict the runoff variations during an event because of the assumed constant precipitation rate.

6.3.3 One-Dimensional Finite Element Model Results

Nieber's 1-D finite element model was tested without the coupled infiltration model, because analysis with the kinematic storage model indicated that the infiltration model assumption was not appropriate for the conditions encountered on the test plot. Precipitation, therefore, was applied directly to the base (saturated zone) with no time delay.

Simulations were made for two events, November 21-22 and November 26-27, at the three hydraulic conductivities and with two different initial soil-water conditions. The first initial condition assumed gravity drainage, that is, no movement of water prior to the event. The results of these simulations are shown in Figures 6.18 and 6.19. The second initial condition used the average antecedent water content measured by the nuclear probe. The capillary pressure along the entire hillslope was assumed to be equal to the soil water pressure head calculated from the water content using the soil water characteristic curve. For the 1-D model boundary condition a horizontal water table was assumed initially, so the soil water pressure head at any point was not allowed to be less than the profile depth. To achieve the proper initial condition the profile was then allowed to drain until sustained baseflow was achieved. Figures 6.20 and 6.21 present the results for this initial condition.

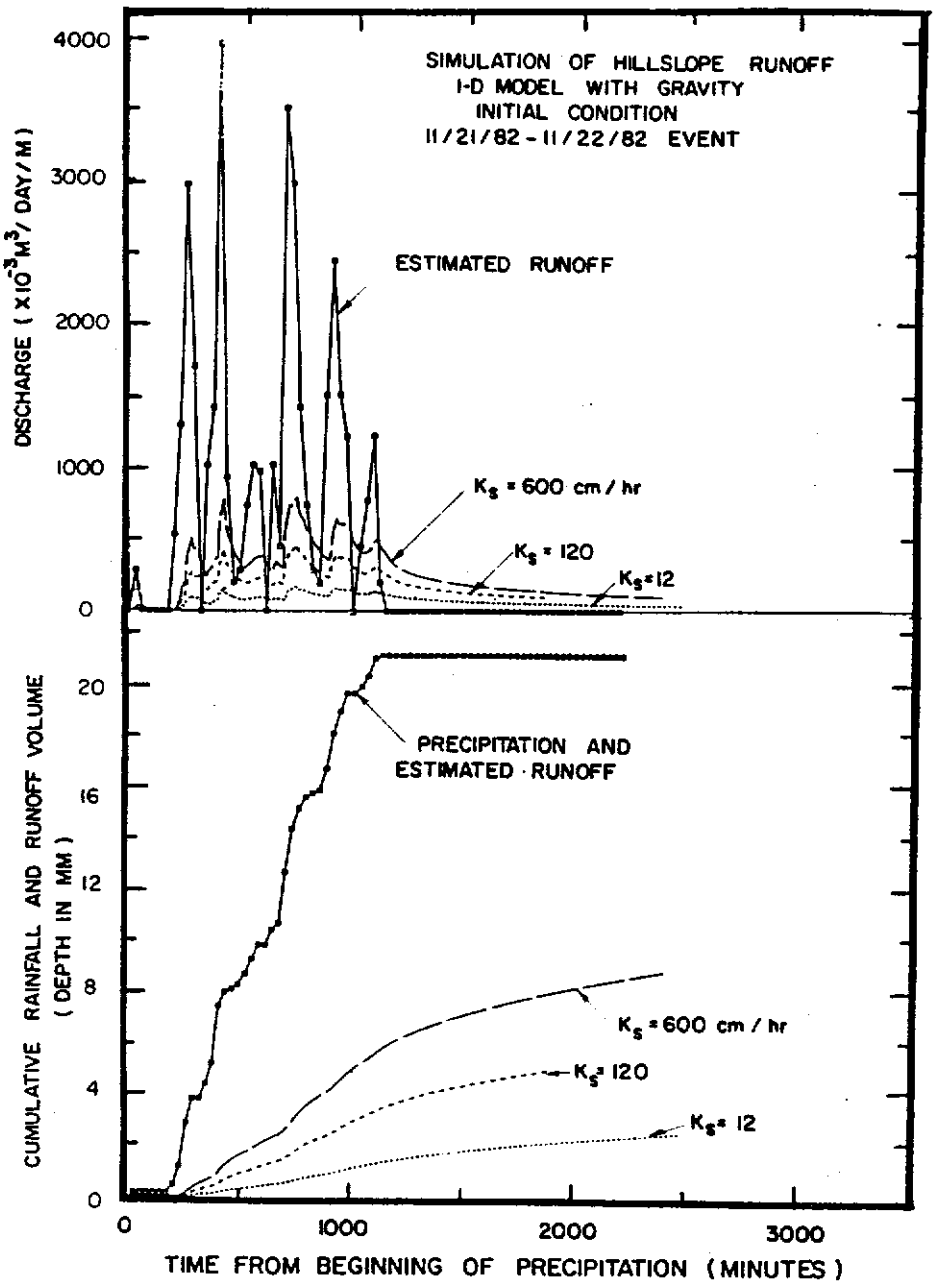

Figure 6.18 Comparison of Estimated and Predicted Runoff Hydrographs and Cumulative Runoff Volumes for Nieber's 1-D Model with the Gravity Drainage Initial Condition, at Three Saturated Hydraulic Conductivities (K_s = 12, 120, and 600 cm/hr) for the November 21-22 Event.

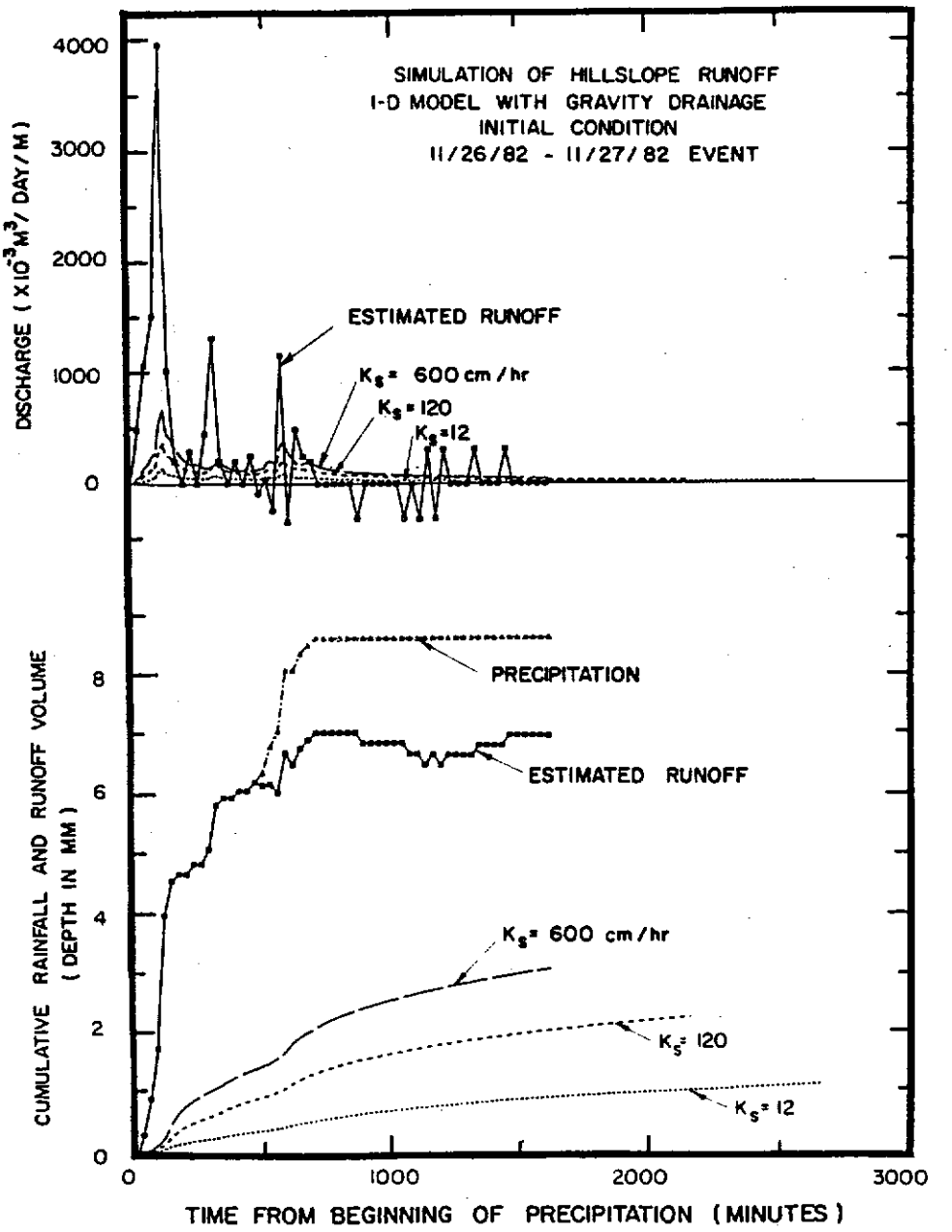

Figure 6.19 Comparison of Estimated and Predicted Runoff Hydrographs and Cumulative Runoff Volumes for Nieber's 1-D Model with the Gravity Drainage Initial Condition, at Three Saturated Hydraulic Conductivities (K_s = 12, 120, and 600 cm/hr) for the November 26-27 Event. The magnitude of the negative estimated runoff (which can not occur in practice) indicates the potential error in the calculations. This error is reflected in the cumulative runoff volume curve at t=900 minutes.

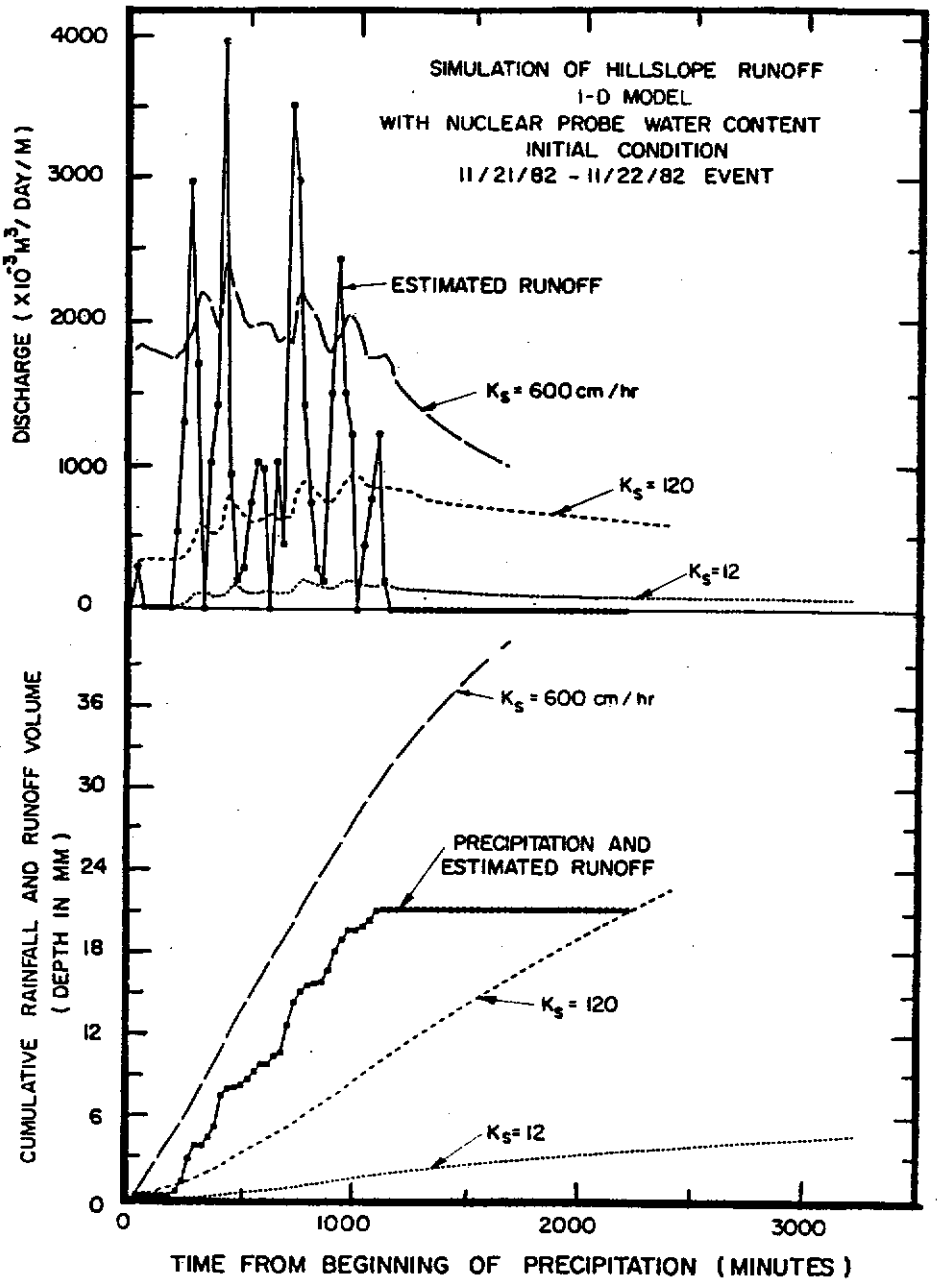

Figure 6.20 Comparison of Estimated and Predicted Runoff Hydrographs and Cumulative Runoff Volumes for Nieber's 1-D Model with the Nuclear Probe Water Content Initial Condition, at Three Saturated Hydraulic Conductivities (K_s = 12, 120, and 600 cm/hr) for the November 21-22 Event.

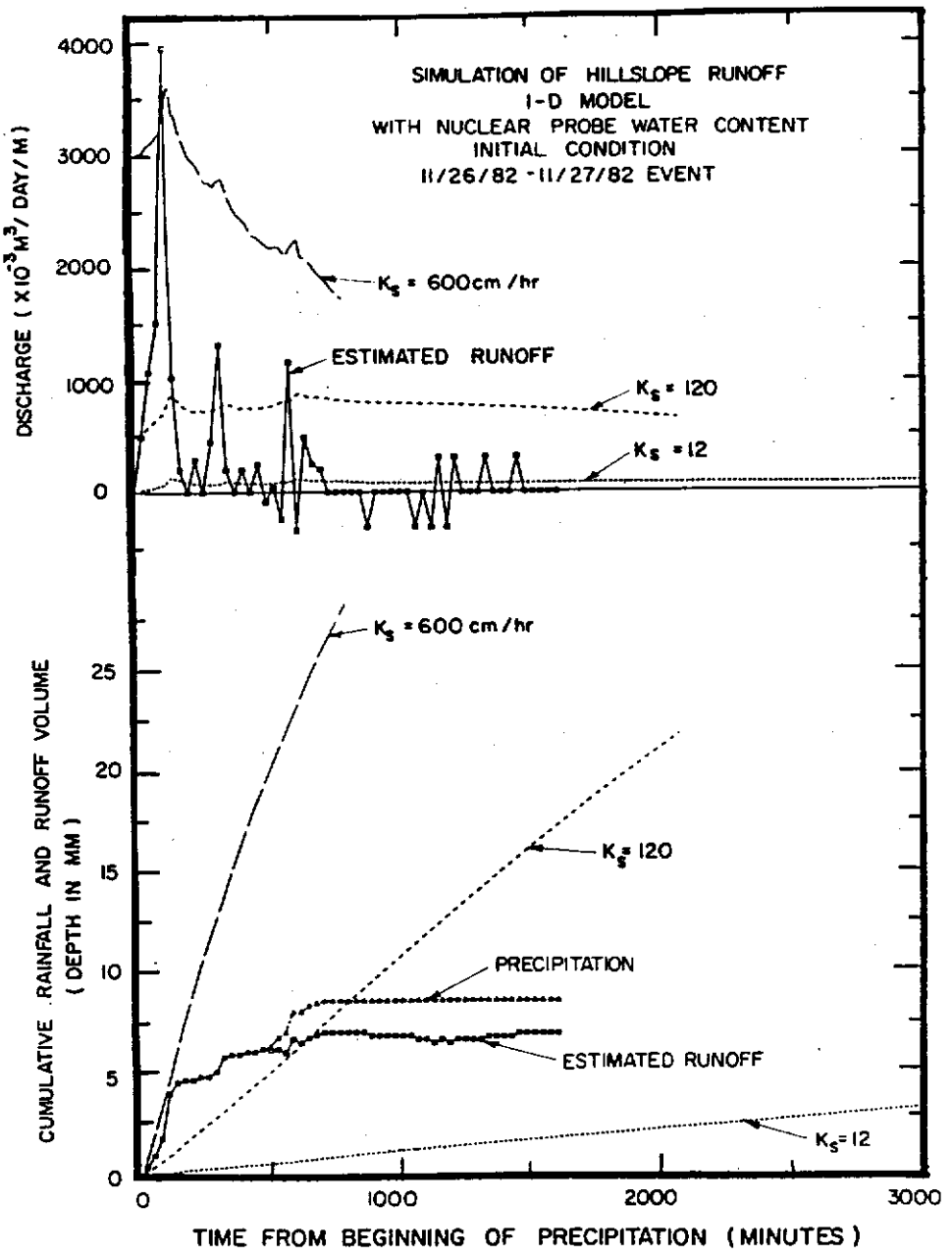

Figure 6.21 Comparison of Estimated and Predicted Runoff Hydrographs and Cumulative Runoff Volumes for Nieber's 1-D Model with the Nuclear Probe Water Content Initial Condition, at Three Saturated Hydraulic Conductivities (K_s = 12, 120, and 600 cm/hr) for the November 26-27 Event. The magnitude of the negative estimated runoff (which can not occur in practice) indicates the potential error in the calculations. This error is reflected in the cumulative runoff volume curve at t=900 minutes.

The simulation using the second initial condition for the November 26-27 event and K_s = 12 cm/hr shows a sustained baseflow which is about 72 ℓ/day/m. As the hydraulic conductivity is increased, however, this initial condition loses its importance to the overall simulation. The baseline hydraulic conductivity is appropriate for the soil matrix, which carries baseflow, while the higher effective hydraulic conductivities are applicable only to quick flow through macropores. So, as expected, the baseline hydraulic conductivity does well for long-term drainage, while the higher hydraulic conductivities do better during the storm. However, while giving better storm predictions, these high conductivities yield erroneous long-term baseflow results.

6.4 DISCUSSION OF RESULTS

The extensive review of literature dealing with the hydrology of steeply sloping forested watersheds in humid regions suggested that overland flow is a rare occurrence in these areas. Field observations and measurements made at Robinson Forest in eastern Kentucky support this conclusion. For the period of data collection, March through December, 1982, evidence of Hortonian overland flow was never observed. However, exfiltration of subsurface stormflow and precipitation on saturated areas did appear to occur along ephemeral channels and rock outcroppings.

The measured surface hydraulic conductivities were high enough that one would not expect saturation from above to occur except in isolated areas and on rare occasions of very intense rainfall. A network of soil pipes consisting of roots, decayed root holes, and animal and insect burrows were observed in the field which increased the overall effective hydraulic conductivity. Runoff simulations verified this because the greater hydraulic conductivities did better at simulating runoff, particularly the stormflow peaks. For these reasons it can be concluded that subsurface stormflow is the primary process involved in runoff generation as a component in the variable source area concept.

The kinematic storage model was the most effective in simulating runoff from the test plot. The kinematic wave model has the potential for doing well also, if it were modified to accept a varying precipitation record. The 1-D model showed trends similar to the other models, but did not do as well.

The understanding of subsurface stormflow can be visualized by comparing the kinematic storage model and the 1-D model results. The kinematic storage model assumes that the hydraulic gradient is equal to the bed slope, much like uniform flow in open channel hydraulics. The 1-D model, on the other hand, uses Richards' equation, which is based on Darcian flow.

The 1-D model used with the gravity drainage initial condition gave better results with increasing hydraulic conductivities, like the other models. However, it did not do as well as the kinematic storage model. This is because the kinematic subsurface flow assumption for stormflow through macropores and soil pipes is valid, while Darcian flow, simulated by the 1-D model, is not. The boundary condition used for the 1-D simulations probably also contributes to the problem, and the saturated outlet face may not be appropriate for hillslopes with quick stormflow.

The simulations made using the 1-D model and the nuclear probe antecedent water contents yielded results similar to the other initial condition, except that baseflow was superimposed on the storm hydrograph. Therefore, it would appear that models based on Richards' equation are applicable to homogeneous soils and hillslopes with no macropores or soil pipes, or can be used to estimate baseflow.

Subsurface stormflow, i.e. flow through macropores and soil pipes, is best described by the kinematic subsurface flow equations and the use of effective hydraulic conductivities. Baseflow, or flow through the soil matrix, is best described by Richards' equation (Darcy's law) and the matric hydraulic conductivities.

6.5 CONCLUSIONS

An analysis of the data collected at the Robinson Forest test plot

was conducted, including estimation of runoff for four selected events. This analysis suggests that the hillslope responds rapidly to precipitation and that the shallow soils which are interlaced with macropores are the primary reason. Lateral subsurface flow along roots and through soil pipes was observed in soil pits dug on the test plot.

The kinematic wave and kinematic storage mdoels were applied to all the selected events, and Nieber's 1-D finite element model was applied to two events. For each model three hydraulic conductivities were tested to find the effect of using effective hydraulic conductivities in describing subsurface stormflow. The kinematic storage model gave the best results because it was conceptually the more correct, allowing for quick subsurface stormflow through macropores. The 1-D model, conversely, can predict baseflow correctly because it uses Richards' equation for laminar flow, which is correct for flow through the soil matrix, but not through the macropores.

CHAPTER 7

SUMMARY AND CONCLUSIONS

7.1 SUMMARY

A simple conceptual, daily-based, rainfall-runoff model was developed for predicting runoff from small, steep-sloped, forested Appalachian watersheds. The model is based on the variable source area concept and requires only daily precipitation and an estimate of daily potential evapotranspiration, such as pan evaporation, as the basic hydrologic and meteorological inputs. The model was tested with 6½ years of observed discharge and meteorological records from the 81.7 ha undisturbed Little Millseat watershed in eastern Kentucky. Three and a half years of records were used for calibrating the model and 3 years were used for validation. There was good agreement between the observed and predicted daily discharges, and the results demonstrate the ability of the model to simulate the "flashy" hydrologic response of this type of watershed.

Five subsurface flow models were compared using existing data measured by Hewlett (1961) and Hewlett and Hibbert (1963). The experimental set-up consisted of a soil trough filled with a recompacted forest soil. The drainage hydrograph for this soil trough represents what would be expected from a steep-sloped reconstructed homogeneous forest soil. The soil was compacted so no soil pipes were present and all flow was through the soil matrix. Darcy's law would then be expected to hold throughout the profile and numerical models based on Darcy's law should work well under such conditions.

The five physically based models tested varied from a 2-D finite element model based on Richards' equation to simple storage models. The complexity of the model had no relationship to how well the measured hydrograph was simulated, and all did fairly well. For this homogeneous soil trough the coupled infiltration model had a large effect on the simulation results.

Three of the numerical models were then tested using precipitation and soil-water data collected from a small test plot in Robinson

Forest in eastern Kentucky. The coupled infiltration relationship for the model based on the 1-D Richards' equation and for the kinematic storage model was not used after it was found to produce excessive lags in the timing of runoff. It was apparent from the runoff data that the high surface hydraulic conductivities and macropores allowed quick infiltration, and lateral movement of water downslope began almost immediately following a precipitation event. Increasing the effective hydraulic conductivity improved the simulations, showing that the overall response of the hillslope was increased significantly by the presence of macropores and soil pipes.

The simple kinematic storage model gave the best results with the high effective hydraulic conductivities. So, not only are simple storage models less expensive and easier to run than the more complex subsurface flow models based on Richards' equation and using finite elements, but they can also give better results. The kinematic subsurface flow assumption is more accurate for stormflow through macropores and soil pipes than Richards' equation, which is based on Darcian flow.

7.2 CONCLUSIONS

Two general conclusions can be drawn from the field study and computer modeling studies reported herein:

(1) The primary process involved in runoff generation on undisturbed steep-sloped forested watersheds similar to those in Robinson Forest is subsurface stormflow as a component in the variable source area concept, and

(2) Simple physically based models can adequately simulate runoff from steep-sloped forested watersheds and are the most economical to use because of the great heterogeneity, the complexity involved in describing a natural watershed, and the cost of running computer programs of complex models.

Additional conclusions stemming from this study include:

(1) Observations in the field (subsurface flow along roots and in animal burrows) and computer simulations showed the importance of macropore flow in generating storm runoff for steep-sloped forested watersheds. The high effective hydraulic conductivities determined by the numerical analysis demonstrate that rapid water movement through macropores does occur (i.e. non-Darcian flow).

(2) The rainfall-runoff analysis and simulations showed that there are two components of subsurface flow:

a) Macropore water flow, which is responsible for stormflow response on the Robinson Forest watersheds, and

b) Soil matrix water flow, which is responsible for baseflow response.

(3) When the decision is made to use a model based on an effective hydraulic conductivity for steep forested watersheds, simple models, such as the kinematic wave or kinematic storage models, are the most effective.

(4) Results of the simulation comparisons raise questions about the process of validating subsurface flow models. Complex models are frequently verified by setting up a trough in the laboratory and filling it with sand, which is an idealized case. Evaluation of the different models on the Coweeta data and Robinson Forest data shows that the appropriateness of some of the complex Darcian flow based models may not extend beyond the laboratory at the present time. The complex finite element and finite difference models are often cited as being a standard against which simpler models can be compared. In the field of hillslope hydrology these complex models may not be a very good standard for testing or validating other models, since they themselves are quite idealized, and may not be any more accurate than the simple models. The basic assumption of Darcian flow used to formulate these complex models appears to be questionable for subsurface stormflow.

7.3 SUGGESTIONS FOR FURTHER RESEARCH

(1) Much work has been done recently dealing with hillslope subsurface flow models based on Darcy's law. Since it has become widely known that soil pipes and macropores are very important on forested watersheds, more theoretical work is needed to develop physically accurate models which include non-Darcian subsurface stormflow.

(2) When dealing with subsurface stormflow on steep hillslopes some direct method of measuring runoff is more appropriate than using soil water content and tension instrumentation, and relying on a water balance to calculate runoff.

(3) Models based on Darcy's law, such as those discussed in this study, may be more appropriate for reclaimed lands, which are more homogeneous than natural watersheds. Field measurements should be made to test various models for their appropriateness in estimating post mining (disturbance) runoff.

(4) Following from Conclusion 4, a data base of measured rainfall and runoff from hillslopes should be developed for hillslope model verification, rather than validating by comparing among models.

(5) Since the kinematic storage model was effective in simulating runoff from a forest test plot, the next step would be to incorporate it into a watershed model similar to that described in Chapter 4. The watershed could be divided into subwatersheds according to slope and soil characteristics. The kinematic storage model would be applied to each, and stream discharge at the outlet would then be estimated by using a routing technique.

NOMENCLATURE

A, a, B, b, c, g, m, N, r	constants
A_1	saturated area along channels where water exfiltrates to the stream (VSAS model)
A_2	Horizontal projected area of saturated areas (VSAS model)
A_3	Virtually impervious area where Hortonian flow occurs (VSAS model)
α	Slope of impermeable bed to the horizontal
β	Slope of the watertable to the horizontal
C	Specific water capacity $\left(=\frac{\partial \theta}{\partial h}\right)$
CEPMAX	Maximum interception capacity
CMAX	Actual interception capacity
D	Soil depth
e	Gravity head
E	Evaporation volume
ERATE	Evapotranspiration rate coefficient
FCAN	Canopy development function
FS	Groundwater exponent
FSTR	Fraction of watershed always contributing to direct runoff
FU	Soil water conductivity coefficient
H	Hydraulic head (= h + e)
h	Pressure head
h_c	Critical pressure head
I	Infiltration rate
i	Precipitation or rainfall rate
K	Hydraulic conductivity
K_s	Saturated hydraulic conductivity
K_r	Relative hydraulic conductivity $\left(=\frac{K}{K_s}\right)$
KS	Groundwater recession constant

Nomenclature (continued)

KU	Soil water conductivity exponent
K1	Fraction of Soil Zone drainage becoming interflow
K2	Fraction of groundwater flow becoming baseflow
λ	
L	Hillslope length
L_s	Saturated hillslope length
	Dimensionless parameter $\left(=\frac{4i\cos\alpha}{K_s \sin^2\alpha}\right)$
P	Precipitation volume
PAC	Source area exponent
PB	Fraction of watershed contributing to direct runoff
PC	Source area coefficient
Q	Drainage rate
q	Seepage velocity, and Discharge per unit area
R	Runoff volume
S'	Slope of calibration curve for the nuclear moisture probe
S	Drainable volume of water stored in the saturated zone
SSIN	Actual groundwater volume
t	Time
t_d	Time input to the water table ceases
t_r	Time rainfall input ceases
θ	Volumetric water content
θ_f	Offset of calibration curve for the nuclear moisture probe
θ_{res}	Residual water content
θ_s	Saturated water content
θ_{us}	Water content in the unsaturated zone
USIN	Actual soil water volume
USMAX	Soil Zone thickness
USWP	Wilting point water content

Nomenclature (continued)

V,v	Discharge per unit cross sectional area, and Rate of advance of the wetting front
V_{us}	Volume of the unsaturated zone
X	Ratio of count to standard count of the nuclear moisture probe
x	Horizontal distance
y	Fraction of precipitation converted to direct runoff
z	Vertical distance

REFERENCES

Aitken, A. P. 1973. Assessing systematic errors in rainfall-runoff models. J. Hydrol. 20:121-136.

Atkinson, T. C. 1978. Techniques for measuring subsurface flow in hillslopes. In: M.J. Kirkby (Ed.), Hillslope Hydrology, John Wiley, New York, NY, pp. 73-120.

Barcelo, M. D., and J. L. Nieber. 1982. Influence of a soil pipe network on catchment hydrology. Amer. Soc. Agri. Engrs., Paper No. 82-2027, St. Joseph, MI.

Beasley, R. S. 1976. Contribution of subsurface flow from the upper slopes of forested watersheds to channel flow. Soil Sci. Amer. Proc. 40:955-957.

Betson, R. P. 1964. What is watershed runoff? J. Geophy. Res. 69(8): 1541-1552.

Betson, R. P. and J. B. Marius. 1969. Source areas of storm runoff. Water Resour. Res. 5(3):574-582.

Beven, K. 1981. Kinematic subsurface stormflow. Water Resour. Res. 17(5):1419-1424.

Beven, K. and P. Germann. 1982. Macropores and water flow in soils. Water Resour. Res. 18(5):1311-1325.

Beven, K. 1982. On subsurface stormflow: Predictions with simple kinematic theory for saturated and unsaturated flows. Water Resour. Res. 18(6):1627-1633.

Bison. 1974. Instruction manual. Bison Instruments, Minneapolis, MN, 36 p.

Black, T. A., W. R. Gardner, and C. B. Tanner. 1970. Water storage and drainage under a row crop on a sandy soil. Agron. J. 62:48-51.

Boughton, W. C. 1966. A mathematical model for relating rainfall to runoff with daily data. Civil Engr. Trans., Instit. Engrs. (Australia) CE8:83-93.

Boughton, W. C. 1968. Evaluating the variables in a mathematical catchment model. Civil Engr. Trans., Instit. Engrs. (Australia) CE10: 31-39.

Bowen, I. S. 1926. The ratio of heat loss by conduction and by evaporation from any water surface. Phys. Rev. 27:779-787.

Campbell, G. S. 1974. A simple method for determining unsaturated conductivity from moisture retention data. Soil Sci. 117(6);311-314.

Carpenter, S. B. and R. L. Rumsey. 1976. Trees and shrubs of Robinson Forest, Breathitt County, Kentucky. Castanea 41:227-282.

Childs, E. C. 1971. Drainage of groundwater resting on a sloping bed. Water Resour. Res. 7(5):1256-1263.

Clarke, R. T. 1973. Mathematical models in hydrology. Food and Agri. Org. of the United Nations, FAO Irrigation and Drainage Paper No. 19. 282 p.

Corbett, E. S. 1979. Hydrological evaluation of the stormflow generation process on a forested watershed. Ph.D. Thesis. Office of Water Res. and Tech., Washington, D.C., NTIS: PB80-129133, 125 p.

Crawford, N. H. and R. K. Linsley. 1966. Digital simulation in hydrology: Stanford Watershed Model IV. Tech. Rept. No. 39, Dept. Civil Engr., Stanford Univ., CA. 210 p.

Curtis, W. R. 1972. Strip-mining increases flood potential of mountain watersheds. In: Watersheds in Transition, Amer. Water Resour. Assoc., pp. 357-360.

Davidson, T. M., L. R. Stone, D. R. Nielson, and M. E. Larue. 1969. Field measurement and use of soil properties. Water Resour. Res. 5:1312-1321.

Dobrin, M. B. 1960. Introduction to Geophysical Methods. McGraw-Hill, New York, NY. 446 p.

Dunne, T., and R. D. Black. 1970. Partial area contributions to storm runoff in a small New England watershed. Water Resour. Res. 6(5):1296-1311.

Federer, C. A. 1982. Frequency and intensity of drought in New Hampshire forests: Evaluation by the BROOK model. In: V. P. Singh (Ed.) Applied Modeling in Catchment Hydrology. Water Resour. Pub., Littleton, CO, pp. 459-470.

Federer, C. A. and D. Lash. 1978. BROOK: A hydrologic simulation model for eastern forests. Res. Rept. No. 19, Water Resour. Res. Center, Univ. New Hampshire, Durham, NH. 84 p.

Fleming, G. 1979. Deterministic models in hydrology. Food and Agri. Org. of the United Nations, FAO Irrigation and Drainage Paper No. 32. 80 p.

Freeze, R. A. 1971. Three-dimensional, transient, saturated-unsaturated flow in a groundwater basin. Water Resour. Res. 7(2):347-366.

Freeze, R. A. 1972. Role of subsurface flow in generating surface runoff: 2. Upstream source areas. Water Resour. Res. 8(5):1272-1283.

Gardner, W. R., D. Hillel, and Y. Benyamini. 1970. Post irrigation movement of soil water to plant roots. I. Redistribution. Water Resour. Res. 6:851-861.

Green, R. E. and J. C. Corey. 1971. Calculation of hydraulic conductivity: A further evaluation of some predictive methods. Proc. Soil Sci. Soc. Amer. 35:3-8.

Haan, C. T. 1972. A water yield model for small watersheds. Water Resour. Res. 8:58-69.

Haan, C. T. 1976. Evaluation of a monthly water yield model. Trans. Amer. Soc. Agri. Eng. 19:55-60.

Haef, F. 1981. Can we model the rainfall-runoff process today? Hydrolog. Sci. - Bull. - Sci. Hydrolog. 26, 3, 9/1981.

Hamon, W. R. 1963. Computation of direct runoff amounts from storm rainfall. Int. Assoc. Sci. Hydrol. 63:52-62.

Hanson, C. T. 1977. Relationship of soil and site characteristics to soil moisture regimes in a forested watershed. Unpub. M. S. Thesis, University of Kentucky, Lexington, KY.

Helvey, J. D. and J. H. Patric. 1965. Canopy and litter interception of rainfall by hardwoods of Eastern United States. Water Resour. Res. 1(2):193-206.

Henderson, F. M. and R. A. Wooding. 1964. Overland flow and groundwater flow from a steady rainfall of finite duration. J. Geophy. Res. 69(8):1531-1540.

Hewlett, J. D. 1961. Soil moisture as a source of base flow from steep mountain watersheds. Southeastern Forest Experiment Station Paper No. 132. USDA-Forest Service, Asheville, NC. 11 p.

Hewlett, J. D. and A. R. Hibbert. 1963. Moisture and energy conditions within a sloping soil mass during drainage. J. Geophy. Res. 68(4): 1081-1087.

Hewlett, J. D. and A. R. Hibbert. 1967. Factors affecting the response of small watersheds to precipitation in humid areas. Proc. Int. Symp. on Forest Hydrology, Pennsylvania State Univ., University Park, PA, pp. 275-290.

Hobson, G. D. 1970. Seismic methods in mining and groundwater exploration. Canada Geol. Survey, Econ. Geol. Rept. No. 26, pp. 148-176.

Horton, R. E. 1933. The role of infiltration in the hydrologic cycle. Trans. Amer. Geophy. Union 14:460-466.

Hursh, C. R. 1936. Storm-water and absorption. Trans. Amer. Geophy. Union 17(2):301-302.

Hutchins, R. B., R. L. Blevins, J. H. Hill, and E. H. White. 1976. The influence of soils and microclimate on vegetation of forested slopes in eastern Kentucky. Soil Sci. 12(4):239-341.

Jamieson, D. G. and C. R. Amerman. 1969. Quick-return subsurface flow. J. Hydrol. 8:122-136.

Jenson, M. E. and H. R. Haise. 1963. Estimating evapotranspiration from solar radiation. J. Irrigation and Drainage Div., Amer. Soc. Civil Eng. 89(IR1):15-41.

Jones, J. A. 1975. Soil piping and the subsurface initiation of stream channel networks. Unpub. Ph.D. Thesis. Univ. Cambridge, England, 467 p.

Kirkby, M. J. and R. J. Chorley. 1967. Throughflow, overland flow and erosion. Int. Assoc. Sci. Hydrol. Bull. 12(3):5-21.

Mangum, M. A., W. G. Kunze, and J. P. Szabo. 1981. Seismic refraction of a buried valley near Penisula, Summit County, Ohio. J. Sci. 81:69-73.

Mohsenisaravi, M. 1981. Forecasting subsurface water flow and storage on forested slopes using a finite element model. Ph.D. Thesis, Univ. Idaho. Univ. Microfilms International, Ann Arbor, MI, 162 p.

Moore, I. D. 1981. Effects of surface sealing on infiltration. Trans. Amer. Soc. Agri. Engrs. 24(6):1546-1552.

Moore, I. D. and R. G. Mein. 1976. Evaluating rainfall-runoff model performance. J. Hydraulics Div., Amer. Soc. Civil Engr. 102(HY9): 1390-1395.

Mosley, M. P. 1979. Streamflow generation in a forested watershed, New Zealand. Water Resour. Res. 15(4):795-806.

Neuman, S. P. 1973. Saturated-unsaturated seepage by finite elements. J. Hydraulics Div., Amer. Soc. Civil Engrs. 99(HY12):2233-2250.

Nieber, J. L. 1979. Hillslope runoff characteristics. Ph.D. Thesis, Cornell Univ., Ithaca, NY. University Microfilms International, Ann Arbor, MI. 260 p.

Nieber, J. L. and M. F. Walter. 1981. Two-dimensional soil moisture flow in a sloping rectangular region: experimental and numerical studies. Water Resour. Res. 17(6):1722-1730.

Nieber, J. L. 1982. Hillslope soil moisture flow, approximation by a one-dimensional formulation. Amer. Soc. Agri. Engrs. Paper No. 82-2026, St. Joseph, MI.

Nuckols, J. R. 1982. The influence of atmospheric nitrogen influx upon the stream nitrogen profile of two relatively undisturbed forested watersheds in the Cumberland Plateau of the eastern United States. Unpub. Ph.D. Dissertation, Univ. of Kentucky, Lexington, KY. 264 p.

Nuckols, J. R. and C. T. Haan. 1979. Evaluation of TVA streamflow model on small Kentucky watersheds. Trans. Amer. Soc. Agri. Engrs. 22:1097-1105.

Penman, H. L. 1963. Vegetation and hydrology. Commonwealth Bur. Soils, Harpenden, England. Tech. Comm. 53, 125 p.

Pilgrim, D. H. and D. D. Huff. 1978. A field evaluation of subsurface and surface runoff. I. Tracer Studies. J. Hydrol. 38:299-318.

Pilgrim, D. H., D. D. Huff, and T. D. Steele. 1978. A field evaluation of subsurface and surface runoff. II. Runoff processes. J. Hydrol. 38:319-341.

Porter, J. W. and T. A. McMahon. 1971. A model for the simulation of streamflow data from climatic records. J. Hydrol. 13:297-324.

Porter, J. W. and T. A. McMahon. 1976. The Monash model: User manual for daily program HYDROLOG. Dept. Civil Engr., Monash Univ., Res. Rept. 2/76, 41 p.

Reeves, M. and J. O. Duguid. 1975. Water movement through saturated-unsaturated porous media: a finite element galerkin model. Oak Ridge National Laboratory, Oak Ridge, TN. NTIS:ORNL-4927. 232 p.

Retzer, J. L. 1963. Soil formation and classification of forested mountain lands in the United States. Soil Sci. 96(1):68-74.

Ross, G. A. 1970. The Stanford watershed model: The correlation of parameter values selected by a computerized procedure with measurable physical characteristics of the watershed. Res. Rept. No. 35, Kentucky Water Resour. Inst., Univ. Kentucky, Lexington, KY.

Scheidegger, A. E. 1957. The Physics of Flow Through Porous Media. Macmillan, New York, NY.

Scholl, D. G. and A. R. Hibbert. 1973. Unsaturated flow properties used to predict outflow and evapotranspiration from a sloping lysimeter. Water Resour. Res. 9(6):1645-1655.

Shearer, M. T. 1976. Distribution of nitrate-nitrogen in forest soil following ammonium-nitrate fertilization. Unpub. M.S. Thesis, Univ. Kentucky, Lexington, KY. 132 p.

Sherman, L. K. 1932. Streamflow from rainfall by unit-graph method. Engineering News-Record, April 7, 1932, pp. 501-505.

Smith, W. D. 1982. The physical and hydrological processes of soils on Field Branch watershed. Unpub. M.S. Thesis, Univ. Kentucky, Lexington, KY. 107 p.

Springer, E. P. 1978. Calibration and analysis of three Robinson Forest watersheds. Unpub. M.S. Thesis, Univ. Kentucky, Lexington, KY. 65 p.

Springer, E. P. and G. B. Coltharp. 1978. Some hydrologic characteristics of a small forested watershed in eastern Kentucky. Trans. Kentucky Acad. Sci. 39(1-2):31-38.

Tennessee Valley Authority. 1972. A continuous daily streamflow model. T. V. A. Res. Paper No. 8.

Thornthwaite, C. W. 1948. An approach toward a rational classification of a climate. Geogr. Rev. 38:55-94.

Tischendorf, W. G. 1969. Tracing stormflow to varying source areas in a small forested watershed in the southeastern Piedmont. Unpub. Ph.D. Dissertation. Univ. Georgia, Athens, GA. 114 p.

Troendle, C. A. 1979. A variable source area model for storm flow prediction on first order forested watersheds. Unpub. Ph.D. Dissertation. Univ. Georgia, Athens, GA. 114 p.

Troendle, C. A. and J. D. Hewlett. 1979. A variable source area hydrograph simulator (VSAS) for small forested watersheds. Unpub. paper, Univ. Georgia, Athens, GA. 38 p.

United States Department of Agriculture. 1965. Soil reports for fourteen counties in eastern Kentucky. USDA, Washington, D.C.

United States Geological Survey. 1981. Water resources data for Kentucky, water year 1980. U.S. Geol. Surv., Water-Data Rept. KY-80-1, pp. 1-3.

Verma, R. D. and W. Brutsaert. 1971. Similitude criteria for flow from unconfined aquifers. J. Hydraulics Div., Amer. Soc. Civil Engrs., 97(HY9):1493-1509.

Weeks, W. D. and R. H. B. Hebbert. 1980. A comparison of rainfall-runoff models. Nordic Hydrol. 11:7-24.

Weyman, D. R. 1970. Throughflow on hillslopes and its relation to the stream hydrograph. Bull. Assoc. Sci. Hydrol. 15(3):25-33.

Weyman, D. R. 1973. Measurement of the downslope flow of water in a soil. J. Hydrol. 20:267-288.

Whipkey, R. Z. 1965. Subsurface stormflow from forested slopes. Int. Assoc. Sci. Hydrol. Bull. 10(2):74-85.

Whipkey, R. Z. 1967. Theory and mechanics of subsurface stormflow. Proc. Int. Symp. on Forest Hydrology, Pennsylvania State Univ., University Park, PA, pp. 255-260.

World Meteorological Organization. 1974. Intercomparison of conceptual models used in operational hydrological forecasting. Geneva, Switzerland.

Zaslavsky, D. and G. Sinai. 1981. Surface hydrology: I. Explanation of phenomena, II. Distribution of raindrops, III. Causes of lateral flow, IV. Flow in sloping layered soil, V. In-surface transient flow. J. Hydraulics Div., Amer. Soc. Civil Engrs. 107(HY1):1-93.

APPENDIX A

CONTINUOUS DAILY MODEL FOR PREDICTING RUNOFF FROM SMALL APPALACHIAN WATERSHEDS

Appendix A–1 Sample Input Data for the Application of the Daily Watershed Model to the Little Millseat Watershed - Test Period.

```
LITTLE MILLSEAT WATERSHED - ROBINSON FOREST KY - TEST PERIOD

-------------------------------------------------------------------------------
   MONTH    1     2     3     4     5     6     7     8     9    10    11    12
PAN COEF. 0.60  0.60  0.60  0.60  0.60  0.70  0.80  0.80  0.80  0.70  0.65  0.60
-------------------------------------------------------------------------------

RUN BEGINS JAN  1,1975     RUN ENDS DEC  31,1977

    TOTAL WATERSHED AREA =     61.67 HECTARE

           WATERSHED MODEL INPUT PARAMETERS
CEPMAX =    2.02    USMAX = 1087.40    USWP =  11.44 (PERCENT BY VOL.)
FU =  0.149E 08    KU =  11.810    FS =  0.000E 00    KS =   0.000
K1 =  1.000    K2 =  0.000
ERATE =  0.274E 02
PAC = 39.2950    PC =  0.411E-05
R = 0.01
           CANOPY EXPANSION FACTORS
DAY   0 TO  110. CANOPY FACTOR = 0.15
DAY 151. TO  273. CANOPY FACTOR = 1.00
DAY 304. TO 366. CANOPY FACTOR = 0.15
CONST1 =  0.000E 00   FSTR = 0.050

           INITIAL CONDITIONS
INCEP =   0.000   USIN = 324.000   SSIN =   0.000
```

Appendix A-2 Sample Output from the Watershed Model for 1976: Little Millseat Watershed - Test Period.

ANNUAL FLOW SUMMARY FOR - LITTLE MILLSEAT WATERSHED - DUNLINSON FOREST 4T - TEST PERIOD

YEAR 1976

MEAN DAILY DISCHARGE SUMMARY (M3/S*10-3)

DAY	JAN	FEB	MARCH	APRIL	MAY	JUNE	JULY	AUGUST	SEPT	OCT	NOV	DEC	ANNUAL
1S/F	44,337	56,036	16,460	46,572	5,996	6,268	5,981	5,662	1,295	19,446	25,551	15,746	
A/F	87,679	43,393	8,929	56,314	4,157	2,143	2,457	12,766	0,603	19,016	25,069	8,125	
2S/F	35,318	26,728	14,909	38,715	1,032	19,145	4,918	0,782	4,985	13,439	22,997	10,375	
A/F	86,161	21,339	8,125	41,429	6,018	14,018	2,143	4,375	3,571	8,304	21,339	9,822	
3S/F	82,841	25,201	13,652	31,061	9,229	1,243	31,096	3,408	1,725	11,031	20,393	9,785	
A/F	75,447	16,482	7,411	32,183	6,107	12,232	16,804	2,500	2,143	5,446	17,057	10,268	
4S/F	40,480	21,196	12,529	26,619	6,961	1,179	4,063	3,571	1,596	11,139	19,138	9,101	
A/F	51,161	16,786	6,696	25,089	3,304	6,250	10,536	1,696	1,964	4,018	14,911	10,268	
5S/F	34,895	41,791	12,990	19,095	8,751	1,107	5,096	2,738	1,512	4,157	17,634	8,556	
A/F	36,965	17,252	7,411	19,911	5,036	4,018	5,804	1,250	1,786	3,125	11,697	10,268	
6S/F	36,583	27,298	11,059	19,141	1,573	1,040	3,455	21,949	1,365	22,223	16,547	56,926	
A/F	31,872	27,500	6,696	16,607	3,125	3,125	4,286	7,232	1,607	5,304	9,522	85,962	
7S/F	54,742	22,776	10,359	13,778	8,692	8,959	4,056	4,926	1,168	24,663	15,229	42,309	
A/F	27,232	25,699	5,982	14,286	3,442	2,500	3,571	6,071	0,982	10,089	8,929	164,019	
8S/F	35,366	29,789	10,827	11,930	8,994	8,789	11,911	4,175	8,956	25,266	14,249	24,543	
A/F	25,069	21,964	5,714	12,679	3,125	2,143	5,989	3,571	0,714	9,286	4,571	66,786	
9S/F	28,849	18,476	48,286	10,126	8,556	8,693	5,718	4,049	8,946	176,033	13,384	32,441	
A/F	22,252	19,197	16,429	11,161	2,679	1,786	4,375	2,679	1,429	291,669	8,571	36,072	
10S/F	35,313	17,501	17,174	8,415	8,474	8,574	4,853	3,346	1,104	44,319	12,615	22,396	
A/F	20,893	17,252	21,258	9,822	2,500	1,518	2,500	1,964	2,321	34,752	8,571	33,965	
11S/F	49,224	25,361	17,456	11,345	3,271	8,771	5,867	2,672	0,969	54,769	11,926	31,449	
A/F	22,322	15,268	19,197	10,089	3,929	1,339	1,786	1,339	1,161	16,259	8,571	38,098	
12S/F	35,139	17,148	14,791	7,175	8,456	8,412	3,142	2,610	8,813	28,497	20,260	50,209	
A/F	25,804	12,679	17,252	8,571	3,125	1,339	1,518	1,071	8,893	10,557	7,411	34,554	
13S/F	67,166	42,723	25,212	6,176	8,399	8,352	2,501	2,049	8,781	23,664	16,357	22,168	
A/F	45,893	27,322	21,072	7,768	2,500	0,982	1,161	0,982	0,804	7,768	5,714	36,911	
14S/F	30,215	28,744	15,639	5,567	8,336	8,287	2,019	3,073	8,581	21,759	12,788	20,262	
A/F	58,465	57,766	17,857	7,411	2,321	8,808	8,808	1,429	8,718	8,071	5,357	30,098	
15S/F	51,700	25,574	14,246	6,872	7,913	8,251	6,112	10,268	8,747	17,551	11,831	23,659	
A/F	42,679	39,197	17,252	7,054	6,786	0,625	0,982	4,018	1,429	6,821	5,714	26,697	
16S/F	27,911	23,817	20,869	4,188	1,681	8,887	4,192	44,698	8,441	15,144	12,389	18,572	
A/F	33,929	30,268	16,786	6,696	4,643	0,714	2,589	88,197	1,339	9,286	5,714	22,058	
17S/F	24,908	137,652	11,906	5,520	2,224	8,196	1,508	11,197	8,382	13,357	10,604	17,155	
A/F	27,679	182,323	14,286	6,339	8,821	0,982	1,339	10,447	1,518	8,018	5,357	17,232	
18S/F	22,471	195,896	12,758	2,995	6,929	8,829	1,468	4,605	8,531	12,402	9,899	15,932	
A/F	30,625	132,987	12,679	5,714	11,607	1,339	8,536	5,536	1,339	8,614	5,089	14,822	
19S/F	28,495	58,872	13,197	2,525	8,946	16,807	1,192	6,528	8,384	10,986	8,253	17,878	
A/F	28,825	75,268	12,679	5,089	8,214	7,143	8,268	3,571	8,895	4,018	8,921	13,214	
20S/F	18,768	44,967	56,960	2,848	8,894	38,852	8,976	5,564	1,213	30,928	8,679	20,315	
A/F	15,467	44,556	14,739	5,089	6,071	50,487	8,869	2,679	3,982	5,446	4,558	14,375	
21S/F	19,736	46,147	173,965	6,186	8,755	29,036	8,485	4,515	8,257	12,628	8,159	17,567	
A/F	13,758	34,643	450,628	6,339	4,558	53,215	8,868	2,143	1,339	5,089	4,558	14,286	
22S/F	18,758	38,782	59,476	2,183	8,636	11,033	8,669	3,701	8,233	11,648	11,982	17,215	
A/F	12,679	26,964	72,327	5,357	1,754	43,572	8,179	2,143	1,071	4,911	8,558	13,214	
23S/F	20,164	35,836	46,992	1,694	8,569	10,558	8,555	2,918	8,195	10,116	9,586	17,698	
A/F	12,143	19,911	42,054	5,089	3,304	16,161	8,757	2,143	8,893	3,304	8,286	13,214	
24S/F	14,132	28,271	36,414	1,459	8,458	9,032	27,928	2,439	8,178	31,044	8,145	17,278	
A/F	12,143	16,786	31,259	4,821	3,036	4,661	14,462	1,964	8,625	5,179	4,286	13,214	
25S/F	37,579	27,087	30,521	1,525	8,446	25,909	2,886	2,092	8,148	117,612	7,536	19,141	
A/F	17,500	14,822	28,793	4,554	2,457	9,196	4,982	1,786	8,446	150,359	8,554	19,214	
26S/F	31,739	23,217	36,314	1,696	8,367	12,187	2,983	5,229	14,562	91,938	9,536	21,829	
A/F	60,467	13,214	21,492	4,286	2,321	10,447	2,321	1,875	5,536	59,016	4,375	13,740	
27S/F	36,613	21,076	29,736	0,848	8,295	10,159	1,850	5,492	23,301	35,813	10,105	17,399	
A/F	57,213	11,697	19,256	3,750	2,143	6,429	1,607	3,571	17,500	30,986	5,089	14,286	
28S/F	19,020	14,295	25,439	0,820	1,924	8,641	1,538	2,490	3,272	31,873	16,211	15,290	
A/F	47,611	10,714	15,982	3,482	2,500	4,554	1,161	2,143	6,250	18,661	6,071	16,518	
29S/F	29,464	17,753	155,454	0,703	1,923	16,857	1,962	2,260	21,064	23,393	13,065	17,193	
A/F	37,143	9,822	193,464	3,304	3,393	5,839	1,875	1,746	8,750	14,822	4,482	19,197	
30S/F	26,450		55,488	0,623	8,304	7,784	19,545	1,868	36,609	94,150	10,340	18,273	
A/F	28,462		189,822	3,036	2,321	4,643	10,088	1,339	44,167	17,589	7,768	18,442	
31S/F	23,729		62,023		1,321		20,243	1,595		34,479		13,405	
A/F	22,768		66,786		2,500		6,875	0,893		27,413		18,442	
TOTAL	1107,744	1037,461	1122,536	292,560	58,708	251,661	199,508	191,296	131,089	910,144	406,961	639,094	6324,672 CMSDH
	117,191	109,755	115,754	30,952	5,364	26,542	21,106	20,235	13,963	96,749	43,051	67,611	669,101 MM.
ACT.	1089,112	956,381	1301,864	353,442	121,829	296,162	105,715	161,162	115,001	782,329	287,688	749,338	6317,699 CMSDH
	115,220	104,188	137,729	37,396	12,446	31,332	11,180	17,050	12,166	78,536	26,203	84,568	668,364 MM.

FLOW BREAKDOWN (MM)

SURFACE = 210.988 SUBSURF1 = 893.581 SUBSURF2 = 0.000 DIRECT INPUT TO STREAM = 60.508

LOSSES EVAP1 = 106.049 EVAP2 = 574.301 DEEPSEEPAGE = 0.000

INPUTS PRECIP = 1314.213

SUMMARY STATISTICS FOR THE YEAR 1976

	MEAN DAILY FLOW	MEAN MONTHLY FLOW	STANDARD DEVIATION OF DAILY FLOWS	STANDARD DEVIATION OF MONTHLY FLOWS	CORRELATION COEFF. OF DAILY FLOWS	CORRELATION COEFF. OF MONTHLY FLOWS
SIMULATED	17,281	527,056	31,230	412,475		
ACTUAL	17,291	526,495	34,717	432,027		
					0.9510	0.9657

Appendix A-3 Listing of the Main Computational Algorithms of the Daily Model for Predicting Runoff from Small Appalachian Watersheds.

```
      SUBROUTINE CANOPY(DAY)
      COMMON/CANOP1/D1,D2,D3,D4,CAN1,CAN2,CONST1
      COMMON/DIVIS/FCAN,FSTR,FFLOR
      IF(DAY.LE.D1)GO TO 5
      IF(DAY.LE.D2)GO TO 10
      IF(DAY.LE.D3)GO TO 15
      IF(DAY.LE.D4)GO TO 20
5     FCAN=CAN1
      GO TO 25
10    FCAN=CAN1+(CAN2-CAN1)*(DAY-D1)/(D2-D1)
      GO TO 25
15    FCAN=CAN2
      GO TO 25
20    FCAN=CAN1+(CAN2-CAN1)*(D4-DAY)/(D4-D3)
25    FFLOR=1.0-FCAN-FSTR
      RETURN
      END
```

```
      SUBROUTINE WATER(RAINF,ETRAN)
      COMMON/DIVIS/FCAN,FSTR,FFLOR
      COMMON/PARAM1/INCEP,USIN,SSIN,INCEPI,USINI,SSINI
      COMMON/PARAM2/CEPMAX,USMAX,USWP,FU,KU,FS,KS,K1,K2,
     1ERATE,PAC,PC
      COMMON/PARAM3/RFALL1,RUNF,QSOIL1,QSOIL2,QSOIL,
     1AEVAP1,AEVAP2,TROFF,DROFF,GW
      REAL INCEP,KU,KS,K1,K2,INCEPI
      RFALL1=0.0
      DROFF=0.0
      RUNO2=0.0
      RUNO1=0.0
      PRECIP=RAINF
      EVAP=ETRAN
C     ***** WETTING CYCLE-INTERCEPTION *****
      IF(PRECIP.EQ.0.0)GO TO 5
      INCEP=INCEP+PRECIP
      PRECIP=0.0
      CMAX=CEPMAX*FCAN
      IF(CMAX.GE.INCEP)GO TO 5
      PRECIP=INCEP-CMAX
      INCEP=CMAX
      RFALL1=PRECIP
5     AINC=0.2
      PRECIP=PRECIP*AINC
      RUNO1=0.0
      RUNO2=0.0
      QSOIL1=0.0
```

Appendix A-3 (Cont.)

```
      QSOIL2=0.0
      GW=0.0
      DO 50 I=1,5
      IF(PRECIP.LE.0.0)GO TO 40
C     *****PARTIAL AREA RUNOFF*****
      PA=PC*EXP(PAC*USIN/USMAX)
      PB=PA+FSTR
      PB=AMIN1(PB,1.0)
      PA=PB-FSTR
      RUNO1=RUNO1+PA*PRECIP
      RUNO2=FSTR*PRECIP+RUNO2
C     *****WETTING CYCLE-UPPER SOIL ZONE*****
      USIN=USIN+PRECIP*(1.0-PB)
C     *****DRAINAGE CYCLE*****
40    FFU=0.0
      IF(USIN.LE.1.0)GO TO 42
      FFU=FU*((USIN/USMAX)**KU)*AINC
42    IF(USIN.LE.FFU)FFU=USIN
      QSOIL1=QSOIL1+FFU*K1
      RFALL=FFU*(1.0-K1)
      USIN=USIN-FFU
      IF(K1.EQ.1.0)GO TO 50
      SSIN=SSIN+RFALL
      FFS=0.0
      IF(SSIN.LE.1.0)GO TO 43
      FFS=FS*(SSIN**KS)*AINC
43    IF(SSIN.LE.FFS)FFS=SSIN
      QSOIL2=QSOIL2+FFS*K2
      GW=GW+FFS*(1.0-K2)
      SSIN=SSIN-FFS
50    CONTINUE
C     ***** EVAPORATION-TRANSPIRATION CYCLE *****
C     ***** INTERCEPTION EVAPORATION AT POTENTIAL RATE *****
8     AEVAP1=0.0
      INCEP=INCEP-EVAP
      IF(INCEP.LT.0.0)GO TO 10
      AEVAP1=EVAP
      GO TO 15
10    AEVAP1=EVAP+INCEP
      INCEP=0.0
C     ***** EVAPOTRASPIRATION FROM UPPER SOIL STORE *****
15    AVW=USIN-USWP
      C1=0.0
      IF(AVW.LE.0.0)GO TO 25
      C1=AVW/ERATE
      IF(C1.GE.EVAP)C1=EVAP
25    USIN=USIN-C1
      AEVAP2=C1
C     ***** SUMMARY AND ACOUNTING *****
      DROFF=RUNO2
      RUNF=RUNO1
      QSOIL=QSOIL1+QSOIL2
      TROFF=RUNF+QSOIL+DROFF
      RETURN
      END
```